Stony Brook University

Computational Studies of the Effect of Nanofillers in Polymeric Matrices

A Dissertation Presented

by

Joseph Nathaniel Ortiz

to

The Graduate School

in Partial Fulfillment of the

Requirements

for the Degree of

Doctor of Philosophy

in

Materials Science & Engineering

Stony Brook University

August 2013

Stony Brook University

The Graduate School

Joseph Nathaniel Ortiz

We, the dissertation committee for the above candidate for the

Doctor of Philosophy degree, hereby recommend

acceptance of this dissertation.

Professor Dilip Gersappe, Advisor
Department of Materials Science & Engineering

Professor Miriam Rafailovich - Chairperson of Defense
Department of Materials Science & Engineering

Professor Jonathan Sokolov
Department of Materials Science & Engineering

Assistant Professor Chad Korach
Department of Mechanical Engineering, Stony Brook University

This dissertation is accepted by the Graduate School

Charles Taber
Interim Dean of the Graduate School

Abstract of the Dissertation

Computational Studies of the Effect of Nanofillers in Polymeric Matrices

by

Joseph Nathaniel Ortiz

Doctor of Philosophy

in

Materials Science & Engineering

Stony Brook University

2013

Nanofiller particles are often added to polymeric matrices in order to create a new class of materials, polymeric nanocomposites. In these nanocomposites, the idea is that the large surface area offered by the nanofillers will result in vastly improved properties, such as increased mechanical strength and thermal conductivity. While much work has been done on adding nanofillers to homopolymers, there is a fundamental gap in understanding how the addition of nanofillers to a polymeric blend enhances the strength of the blend. Further, the role of nanofillers in improving the thermal conductivity of polymer matrices is poorly understood. In this dissertation, Molecular Dynamics and Lattice-Boltzmann simulations are used to determine the role of nanofillers in improving the mechanical integrity of polymer blend and the enhanced thermal conductivity of polymers.

The work presented is divided into three main sections. In the first, the role of nanofillers in strengthening the interfaces of polymeric blends is examined. In the second, the results

presented are compared to those by a blend containing diblock compatibilizers, while also exploring the mechanisms by which strengthening is achieved. Finally, the study of property enhancement is extended into that of flame retardancy and thermal conductivity of polymeric blends.

These studies reveal that nanofillers can be used to strengthen polymeric blends and – in filler concentrations of less than five percent – work better than diblock compatibilizers under the influence of external shear. Results show that this strengthening occurs through the formation of small spanning networks of polymer chains and nanofillers within the interfacial region. Finally, the introduction of nanofillers with high heat capacities was found to enhance the total heat tolerance of the nanocomposite, leaving the polymer more flame-retardant by decreasing the time to ignition of these composites.

For my best friend & wife,

LorY,

The Girl Who Waited

Table of Contents

Abstract iii

Dedication v

Table of Contents vi

List of Tables x

List of Figures xi

Acknowledgements xvii

Chapter 1 – Introduction 1

1.1 The Rise of Nanomaterials 1

1.2 Simulations as a Tool for Examining Nanocomposites 2

1.3 Nanofiller Particles as Compatibilizers for Strength Enhancement Within Polymer Blends 3

1.4 Nanofiller Particles as Flame Retardants Within Nanocomposites 5

1.5 References 7

Chapter 2 – Background and Motivation 12

2.1 Composite Materials 12

2.2 Polymer Blends and Composites 13

2.3 Polymer Nanocomposites 16

2.4 Ignition and Combustion of Polymeric Materials 19

2.5 Nanocomposites as Flame Retardant Materials 20

2.6 References 23

Chapter 3 – Molecular Dynamics Simulations and System Parameters 30

3.1 Molecular Dynamics Simulations 30

3.2 Newtonian Motion 31

3.3 The Verlet Algorithm 33

3.4 The Gear's Predictor-Corrector Algorithm 35

3.5 Equilibrium States 36

3.6 Polymeric Interactions Within Molecular Dynamics Simulations 37

3.7 Nanofiller Creation 39

3.8 Interfacial Separation 40

3.9 Viscosity and Interfacial Width Calculations Within Molecular Dynamics Simulations ... 42

3.10 *In Situ* Internal Structures 43

3.11 Chain Orientation Within Sheared Systems 44

3.12 References 46

3.13 Tables 49

3.14 Figures 50

Chapter 4 – Nanoparticles as Compatibilizers and the Internal Structure of Nanocomposites 51

4.1 The Homopolymer System 51

4.2 The Blended System 52

4.3 Nanocomposites Under Shear 54

4.4 A Comparison of Nanofiller Particles and Diblock Composites 58
4.5 Defining and Understanding Internal Structural Development Within Nanocomposites ... 63
4.6 Interfacial Tension in Compatibilized Blends 65
4.7 Chain Orientation Within Sheared Nanocomposites 67
4.8 Examining *In Situ* Structures Within Nanocomposites 69
4.9 A Summary of Conclusions 73
4.10 References 75
4.11 Tables 77
4.12 Figures 81

Chapter 5 – Nanoparticles as Thermal Diffusers in Flame Retardant Polymeric Materials 124
5.1 Modeling Heat Transport and Lattice-Boltzmann Methods 124
5.2 Lattice-Boltzmann Discretization in Time 127
5.3 Lattice-Boltzmann Discretization in Space 128
5.4 Parallel Computing as a Research Tool 130
5.5 The Parallel Lattice-Boltzmann Solver (Palabos) 132
5.6 Proof of Concept Preliminary Model 133
5.7 The Insulating Filler Model 134
5.8 The Enhanced Heat-Resistant Filler Model 137
5.9 Extension into Three Dimensions 140
5.10 Validation and Results of the Three-Dimensional Model 141
5.11 Summary and Conclusions 143
5.12 References 145

5.13 Figures 147

Chapter 6 – Summaries, Conclusions, and Future Work 156

6.1 Summary and Conclusions – Nanoparticles as Compatibilizers in Polymer Blends 156

6.2 Future Work – Mixed Nanofiller Systems 157

6.3 Future Work – Phase-Preferential Nanofiller Manipulation Within Polymer Blends 158

6.4 Summary and Conclusions – The Effectiveness of Nanofillers as Flame Retardant Nodes Within Polymer Blends 160

6.5 Future Work – Predicting Better Thermally Resistant Materials via the Lattice-Boltzmann Methodology 161

6.7 Closing Statements 162

Collected References 163

List of Tables

Table 3.1 Values of miscibility factor, filler size, compatibilizer concentration and shear rate used in this experiment.

Table 4.1 Equilibrated pre-shear interfacial tension for all available systems.

Table 4.2 Slip lengths for systems sans nanofillers or diblocks at various levels of miscibility and shear.

Table 4.3 Velocity independent slip length ratios of compatibilized systems versus systems lacking compatibilizers.

Table 4.4 Velocity independent slip magnitude ratios of compatibilized systems versus systems lacking compatibilizers.

List of Figures

Figure 3.1 A cartoon representation of the extrapolation method for calculating slip as put forth by DeGennes and Brochard.

Figure 4.1 Velocity profile of a homopolymer system containing large nanofillers at very high shear.

Figure 4.2 Snapshots of system with (left to right) slightly miscible, moderately miscible, and highly miscible interfaces at equilibrium.

Figure 4.3 Equilibrium nanofiller distribution in a system containing small nanofillers and a slightly miscible interface.

Figure 4.4 Equilibrium nanofiller distribution in a system containing large nanofillers and a moderately miscible interface.

Figure 4.5 Nanofiller distribution under shear in a system containing small nanofillers at two percent concentration and a slightly miscible interface.

Figure 4.6 Nanofiller distribution under shear in a system containing large nanofillers at five percent concentration and a moderately miscible interface.

Figure 4.7 Velocity profile for a system containing small nanofillers and a slightly miscible interface, undergoing very high shear.

Figure 4.8 Velocity profile for a system containing small nanofillers and a highly miscible, undergoing very low shear.

Figure 4.9 Interfacial slip lengths in systems containing small nanofillers and a slightly miscible interface.

Figure 4.10 Ratio of the interfacial slip length of a system containing small nanofillers and a slightly miscible interface to that of a system lacking filler particles.

Figure 4.11 Ratio of the interfacial slip length of a system containing small nanofillers and a moderately miscible interface to that of a system lacking filler particles.

Figure 4.12 Ratio of the interfacial slip length of a system containing small nanofillers and a highly miscible interface to that of a system lacking filler particles.

Figure 4.13 Velocity profile for a system containing large nanofillers and a slightly miscible interface, undergoing high shear.

Figure 4.14 Velocity profile for a system containing large nanofillers and a moderately miscible interface, undergoing moderate shear.

Figure 4.15 Interfacial slip lengths in systems containing large nanofillers and a slightly miscible interface.

Figure 4.16 Ratio of the interfacial slip length of a system containing large nanofillers and a slightly miscible interface to that of a system lacking filler particles.

Figure 4.17 Ratio of the interfacial slip length of a system containing large nanofillers and a moderately miscible interface to that of a system lacking filler particles.

Figure 4.18 Ratio of the interfacial slip length of a system containing large nanofillers and a highly miscible interface to that of a system lacking filler particles.

Figure 4.19 Interfacial slip lengths in systems containing diblock compatibilizers and a moderately miscible interface.

Figure 4.20 Ratio of the interfacial slip length of a system containing diblock compatibilizers and a slightly miscible interface to that of a system lacking filler particles.

Figure 4.21 Ratio of the interfacial slip length of a system containing diblock compatibilizers and a moderately miscible interface to that of a system lacking filler particles.

Figure 4.22 Ratio of the interfacial slip length of a system containing diblock compatibilizers and a highly miscible interface to that of a system lacking filler particles.

Figure 4.23 Velocity profile for a system containing diblock compatibilizers and a moderately miscible interface, undergoing high shear.

Figure 4.24 Velocity profile for a system containing diblock compatibilizers and a highly miscible interface, undergoing very high shear.

Figure 4.25 Velocity profile for a system containing large nanofillers and a highly miscible interface, undergoing very high shear.

Figure 4.26 Derivative of the velocity profile for a system containing small nanofillers and a moderately miscible interface, undergoing moderate shear.

Figure 4.27 Derivative of the velocity profile for a system containing small nanofillers and a moderately miscible interface, undergoing low shear.

Figure 4.28 Interfacial slip magnitude in systems containing large nanofillers and a slightly miscible interface.

Figure 4.29 Interfacial slip magnitude in systems containing small nanofillers and a highly miscible interface.

Figure 4.30 Ratio of the interfacial slip magnitude of a system containing small nanofillers and a slightly miscible interface to that of a system lacking filler particles.

Figure 4.31 Ratio of the interfacial slip magnitude of a system containing large nanofillers and a slightly miscible interface to that of a system lacking filler particles.

Figure 4.32 Ratio of the interfacial slip magnitude of a system containing large nanofillers and a moderately miscible interface to that of a system lacking filler particles.

Figure 4.33 Ratio of the interfacial slip magnitude of a system containing large nanofillers and a highly miscible interface to that of a system lacking filler particles.

Figure 4.34 Derivative of the velocity profile for a system containing diblock compatibilizers and a slightly miscible interface, undergoing very high shear.

Figure 4.35 Interfacial tension in systems containing diblock compatibilizers and a highly miscible interface.

Figure 4.36 Interfacial tension in systems containing small nanofillers and a highly miscible interface.

Figure 4.37 Interfacial tension in systems containing large nanofillers and a slightly miscible interface.

Figure 4.38 Ratio of the orientation tensor of a system containing small nanofillers and a slightly miscible interface to that of a system lacking filler particles.

Figure 4.39 Ratio of the orientation tensor of a system containing small nanofillers and a highly miscible interface to that of a system lacking filler particles.

Figure 4.40 Ratio of the orientation tensor of a system containing large nanofillers and a slightly miscible interface to that of a system lacking filler particles.

Figure 4.41 Ratio of the orientation tensor of a system containing large nanofillers and a highly miscible interface to that of a system lacking filler particles.

Figure 4.42 Network groups within the interfacial region of systems containing small nanofillers and a highly miscible interface.

Figure 4.43 Network groups within the interfacial region of systems containing large nanofillers and a highly miscible interface.

Figure 5.1 Cluster formation maps produced by the percolation algorithm (left) and corresponding thermal maps produced by the advection-diffusion lattice Boltzmann method. Rows are 38, 39, 40, and 41 percent filler concentration, respectively.

Figure 5.2 Ratio of number of clusters to number of conductive particles by non-conductive filler concentration

Figure 5.3 Heat propagation in systems containing (from left to right): 10%, 20%, and 30% non-conductive point fillers.

Figure 5.4 The effects of increased point filler concentration on average bulk node temperature within the system.

Figure 5.5 The effects of increased point filler concentration on average filler node temperature within the system.

Figure 5.6 The effects of filler thermal diffusivity on average bulk node temperature within the system.

Figure 5.7 The effects of filler thermal diffusivity on average filler node temperature within the system.

Figure 5.8 The effects of filler morphology and orientation on average bulk node temperature within the system.

Figure 5.9 The effects of filler morphology and orientation on average filler node temperature within the system.

Acknowledgments

I have been fortunate enough to have a multitude of fantastic mentors, friends, and family; this work is as much theirs as it is mine.

I would like to first express my gratitude to my advisor, Dilip Gersappe, for his encouragement and support throughout the research and dissertation process. The late Miguel Paredes gave me the push I needed to pursue a graduate career and introducing me to Stony Brook University. Eihab Jaber provided me with an ever-listening ear and a smile while guiding me though the early pitfalls of graduate school while thousands of miles from home and for that I am eternally grateful. Gary Halada showed me how to be a better teacher for students of all ages. David Ferguson helped to prepare me for life after graduate school while providing me with the opportunity to get others interested in science as well.

All of my friends had a hand in the creation of this work but I would like to recognize two particularly important individuals, Christopher Young and José Colmenares, without whom this journey would have seemed even longer. I would also like to thank my parents for making education a priority in our household and for their unwavering support in this process.

Finally, this dissertation is dedicated to my wife, LorY, for keeping me calm when everything seemed to fall apart and for keeping me focused when my mind began to trail off. Thank you, always.

Chapter 1 – Introduction

1.1 The Rise of Nanomaterials

Over the last twenty years, the ability to explore the nanoscale has increased exponentially. More powerful microscopes allow a view of the nanoscale world that is sharper and clearer than ever before[1]. With the creation of carbon nanotubes and other nanoscale structures, the ability to manipulate and engineer within this miniscule world a precision that could not have existed less than a generation ago is now common in experimental usage. Even newer niches within the overarching umbrella of nanomaterials have grown just as quickly, if not faster, as the field as a whole.

The study of polymer nanocomposites holds particular interest to materials scientists. Polymer nanocomposites arise when nanofiller particles of various materials are added to polymer matrices in order to enhance the properties of the material. Due to their small scale, nanofiller particles are usually within the same order of magnitude as an individual polymer chain, which allows them to diffuse nearly uninhibited throughout the system. The addition of nanofiller particles has been used to create polymer nanocomposites that are stronger, more durable, tougher polymers at a fraction of cost of the bulk material[2-13]. Nanocomposites have also been used to decrease flammability and combustibility and create electronic networks within polymers[14-21].

However, even as our instrumentation has allowed us to better understand the nanoscale world, the field as a whole is still in its relative infancy. Because of this, there are still gaps in what we know about nanoscale interactions and the mechanisms by which the nanofiller particles within polymer nanocomposites provide mechanical property enhancement. A better

understanding of these phenomena and more accurate development of the underlying theory can provide an even better guideline for developing the technology even further. As the technology necessary for creating new nanoscale materials continues to improve, the practicality of nanomaterials has grown accordingly. Nanomaterials such as graphene have been hailed as miracle materials, capable of self-healing and possessing incredible strength[22-29]. These materials are also thought of as the gateway to molecular computing, a holy grail sought after by computer engineers. Other nanomaterials have been proposed for a wide range of utility from changing the way we think about drug delivery, to how we move data across small spaces, and to how we charge our everyday electronic gadgets that have so quickly and thoroughly pervaded our everyday lives[30-34].

1.2 Simulations as a Tool for Examining Nanocomposites

In this thesis, the role of nanofillers as compatibilizers within polymer blends is examined so as to better understand the means by which they enhance mechanical and thermoreactive properties. To study these two distinct and separate phenomena, two forms of simulations were used by which the benefits best fit each situation. Molecular dynamics (MD) simulations were used to determine how adding nanofillers to a composite blend would strengthen the blend at the interface and protect against slip and utilized the Lattice-Boltzmann (LB) methodology to observe how nanofillers could be used to enhance flame retardancy.

Molecular dynamics simulations allow the user to simulate the motion of many particles all at once through pairwise interactions in order to understand how their exchanges govern and

react to the energy within the system[35,36]. By employing the Verlet and Gear's Predictor-Corrector algorithms into simulations, one can incorporate the potential and kinetic energy of each particle into an algorithm with the goal of solving Newton's primary equation of motion: $F=ma$.

Chapter Three discusses the use of intermolecular potentials used in MD simulations. Also examined in detail are the methodologies behind the Verlet and Gear's Predictor-Corrector algorithms. Additionally, the ability to gauge when a system has reached equilibrium was determined. Furthermore, focus has been given to intermolecular potentials as they relate to polymer chains and their interactions between or within phases. Chapter Three also considers the variable parameters used to govern the simulation, as well as the creation of nanofiller particles within an MD simulation, and engineering an interface with the purpose of creating a dual-phase system. Finally, we assess the possibility of *in situ* microstructures that could allow for strength enhancement, how to define these structures, what makes them mechanically relevant, and what role they play in overall chain alignment within the system.

1.3 Nanofiller Particles as Compatibilizers for Strength Enhancement Within Polymer Blends

In the presence of shear forces, a material risks deformation or failure at its weakest point. In the case of polymer blends, the highest risk of deformation occurs at the interface that exists between phases. While homopolymers exhibit shear thinning, wherein very high shear stresses result in decreasing viscosities, possibly due to chain alignment, polymer blends with low levels of miscibility already tend to have low viscosities at the interface. This low viscosity

allows the phases to slide along one another, at times completely unencumbered, depending on how low interfacial viscosity may be.

Diblocks have already been used as compatibilizers to strengthen blends but are cost-prohibitive and difficult to control[37-39]. Thus, a series of questions is raised. What if diblocks, or a mechanism that presents properties closely resembling those of a diblock compatibilizer, could be formed *in situ*? How much strength enhancement would be needed to claim economic benefit? If this mechanism could be created or observed, what drives it and how does it work? Is this solution cost-effective? Nanocomposites have already been used to compatibilize blends but it as yet unknown, how, if at all, they affect strengthening at the interface and the mechanisms by which this occurs.

Chapter Four attempts to answer all these questions. It begins by verifying that the proposed system correctly models the homopolymer system under shear. Once verified, the use of engineered interfaces to create dual-phase systems allows for the creation of systems that can then be subjected to external shear stresses. This results in an uncompatibilized blend to use as a basis for comparison. Nanofilled blends are processed and then placed under shear and the results are then compared to those presented by the unfilled systems. A set of systems containing diblocks are then created after hypothesizing that the strength enhancements displayed by the nanofilled systems could possibly be due to the formation of *in situ* diblocks. This allows for the direct comparison of the effectiveness of nanofiller-compatibilized blends against those of known compatibilized systems. Finally, the possibility of *in situ* diblock formation and their role on chain orientation and alignment is examined.

1.4 Nanofiller Particles as Flame Retardants Within Nanocomposites

Due to their cost-efficiency, ability to conform well to prefabricated molds, and general ease of use, polymers have become the material of choice in many cases. However, their relatively low melting points prevent their use in high temperature situations. While polymers will never have quite the melting point of most metals, experimentalists have already shown that the addition of nanoparticles can increase the melting point and thermal stability of many polymers[40-42]. By increasing the point of ignition for polymeric materials, we can increase their viability in high temperature situations.

The Lattice-Boltzmann (LB) method allows the Boltzmann equations for gas behavior to be fixed at a lattice, making it ideal for simulation[43,44]. While molecular dynamics simulations allow us to study the motion of each individual particle within in a system, LB allows us to simulate a fluid as it moves through a material system of our creation. Thus, the concern and focus of the experiment lays not with the movement within the system but rather the thermal permeability of the system itself. Through the utilization of third-party libraries written to account for the lattice Boltzmann methodology, a model was constructed to examine the changes in flame retardancy as the morphology of the system is evolved.

In Chapter Five, the Lattice-Boltzmann methodology is discussed in far more detail, as well as the governing ideas behind the fluid dynamics used to guide the motion of fluid through the system. The physics of bounceback, or the ability of our nanofillers to absorb or repel heat, is also considered. Chapter Five also includes a brief overview of Palabos, the third-party library that was utilized to create these simulations. Likewise, discussed within are verifications of proposed filler concentration thresholds that allow for fully percolated networks to span throughout the system. Finally, an examination of heat transfer through many evolutions of the

modeled system, including several morphologies of nanofiller as well as varying the specific heats of the materials present, is presented in order to understand how to more quickly and adeptly disperse heat throughout the system thus increasing flame retardancy.

Nanofiller particles as compatibilizers; *in situ* microstructure formation; chain orientation; reduced flammability; the dependence of heat transfer on the morphology of nanofillers – Chapter Six summarizes and reiterates the conclusions brought about by the work presented in this thesis and attempts to recognize its value within the larger scope of polymer theory. Chapter Six also discusses the natural evolution of the research at hand and how it may be developed in order to continue to examine other issues within and just beyond the scope of the research presented in this thesis.

1.5 References

1 Drexler, K. E., Peterson, C. & Pergamit, G. *Unbounding the future: the nanotechnology revolution*. (Morrow, 1991).

2 Nielsen, L. E. & Landel, R. F. *Mechanical Properties of Polymers and Composites*. (M. Dekker, 1994).

3 Dufresne, A. Processing of Polymer Nanocomposites Reinforced with Polysaccharide Nanocrystals. *Molecules* 15, 4111-4128 (2010).

4 Reynaud, E., Jouen, T., Gauthier, C., Vigier, G. & Varlet, J. Nanofillers in polymeric matrix: a study on silica reinforced PA6. *Polymer* 42, 8759-8768 (2001).

5 Kim, K. J. & White, J. L. Rheological investigations of suspensions of talc, calcium carbonate, and their mixtures in a polystyrene melt. *Polym Eng Sci* 39, 2189-2198, doi:Doi 10.1002/Pen.11608 (1999).

6 Flores, A., Cagiao, M. E., Ezquerra, T. A. & Calleja, F. J. B. Influence of filler structure on microhardness of carbon black-polymer composites. *J Appl Polym Sci* 79, 90-95, doi:Doi 10.1002/1097-4628(20010103)79:1<90::Aid-App110>3.0.Co;2-F (2001).

7 Yin, D., Horiuchi, S. & Masuoka, T. Lateral assembly of metal nanoparticles directed by nanodomain control in block copolymer thin films. *Chem Mater* 17, 463-469, doi:Doi 10.1021/Cm048695g (2005).

8 Yin, D. H., Horiuchi, S., Morita, M. & Takahara, A. Tunable metallization by assembly of metal nanoparticles in polymer thin films by photo- or electron beam lithography. *Langmuir* 21, 9352-9358, doi:Doi 10.1021/La0511485 (2005).

9 Gersappe, D. Molecular mechanisms of failure in polymer nanocomposites. *Phys Rev Lett* 89, doi:Artn 058301 Doi 10.1103/Physrevlett.89.058301 (2002).

10 Lobe, V. M. & White, J. L. Experimental-Study of the Influence of Carbon-Black on the Rheological Properties of a Polystyrene Melt. *Polym Eng Sci* 19, 617-624, doi:Doi 10.1002/Pen.760190905 (1979).

11 Minagawa, N. & White, J. L. Influence of Titanium-Dioxide on Rheological and Extrusion Properties of Polymer Melts. *J Appl Polym Sci* 20, 501-523, doi:Doi 10.1002/App.1976.070200222 (1976).

12 Yurekli, K. *et al.* Structure and dynamics of carbon black-filled elastomers. *Journal of Polymer Science Part B: Polymer Physics* 39, 256-275, doi:10.1002/1099-0488(20010115)39:2<256::aid-polb80>3.0.co;2-z (2001).

13 Balberg, I. A comprehensive picture of the electrical phenomena in carbon black–polymer composites. *Carbon* 40, 139-143 (2002).

14 Kim, K., Utracki, L. A. & Kamal, M. R. Numerical simulation of polymer nanocomposites using self-consistent mean-field model. *J Chem Phys* 121, 10766-10777, doi:Doi 10.1063/1.1794636 (2004).

15 Vaia, R. A. & Maguire, J. F. Polymer nanocomposites with prescribed morphology: Going beyond nanoparticle-filled polymers. *Chem Mater* 19, 2736-2751, doi:Doi 10.1021/Cm062693+ (2007).

16 Zhang, W. *et al.* The use of functionalized nanoparticles as non-specific compatibilizers for polymer blends. *Polym Advan Technol* 22, 65-71, doi:Doi 10.1002/Pat.1875 (2011).

17 Bubenhofer, S. B. *et al.* Large-Scale Synthesis of PbS-TiO2 Heterojunction Nanoparticles in a Single Step for Solar Cell Application. *J Phys Chem C* 116, 16264-16270, doi:Doi 10.1021/Jp3036814 (2012).

18 Buzea, C., Pacheco, II & Robbie, K. Nanomaterials and nanoparticles: sources and toxicity. *Biointerphases* 2, MR17-71 (2007).

19 Kumar, V. R. & Prasad, V. S. Synthesis, Characterization and Photocatalytic Activities of Ba2ybzro5.5 Nanoparticles under Solar Irradiation. *Nano* 6, 279-286, doi:Doi 10.1142/S1793292011002585 (2011).

20 Tsekouras, G. *et al.* Charge Transport in Dye-Sensitized Solar Cells Based on Flame-made TiO2 Nanoparticles. *Ieee J Sel Top Quant* 16, 1641-1648, doi:Doi 10.1109/Jstqe.2010.2049734 (2010).

21 Xiao, Q., Zhang, J., Xiao, C., Si, Z. C. & Tan, X. O. Solar photocatalytic degradation of methylene blue in carbon-doped TiO2 nanoparticles suspension. *Sol Energy* 82, 706-713, doi:Doi 10.1016/J.Solener.2008.02.006 (2008).

22 Calandra, P., Calogero, G., Sinopoli, A. & Gucciardi, P. G. Metal Nanoparticles and Carbon-Based Nanostructures as Advanced Materials for Cathode Application in Dye-Sensitized Solar Cells. *Int J Photoenergy*, doi:Artn 109495 Doi 10.1155/2010/109495 (2010).

23 Chen, X. H. *et al.* Ionic liquid-functionalized carbon nanoparticles-modified cathode for efficiency enhancement in polymer solar cells. *Appl Phys Lett* 95, doi:Artn 133305 Doi 10.1063/1.3237161 (2009).

24 Gong, F., Li, Z. Q., Wang, H. & Wang, Z. S. Enhanced electrocatalytic performance of graphene via incorporation of SiO2 nanoparticles for dye-sensitized solar cells. *J Mater Chem* 22, 17321-17327, doi:Doi 10.1039/C2jm33483f (2012).

25 Jia, R. R. *et al.* Synthesis of highly nitrogen-doped hollow carbon nanoparticles and their excellent electrocatalytic properties in dye-sensitized solar cells. *J Mater Chem* 20, 10829-10834, doi:Doi 10.1039/C0jm01799j (2010).

26 Kim, H. I., Moon, G. H., Monllor-Satoca, D., Park, Y. & Choi, W. Solar Photoconversion Using Graphene/TiO2 Composites: Nanographene Shell on TiO2 Core versus TiO2 Nanoparticles on Graphene Sheet. *J Phys Chem C* 116, 1535-1543, doi:Doi 10.1021/Jp209035e (2012).

27 Narayanan, R., Deepa, M. & Srivastava, A. K. Nanoscale connectivity in a TiO2/CdSe quantum dots/functionalized graphene oxide nanosheets/Au nanoparticles composite for enhanced photoelectrochemical solar cell performance. *Phys Chem Chem Phys* 14, 767-778, doi:Doi 10.1039/C1cp22548k (2012).

28 Sun, S. R., Gao, L. A., Liu, Y. Q. & Sun, J. Assembly of CdSe nanoparticles on graphene for low-temperature fabrication of quantum dot sensitized solar cell. *Appl Phys Lett* 98, doi:Artn 093112 Doi 10.1063/1.3558732 (2011).

29 Yen, M. Y. *et al.* Platinum nanoparticles/graphene composite catalyst as a novel composite counter electrode for high performance dye-sensitized solar cells. *J Mater Chem* 21, 12880-12888, doi:Doi 10.1039/C1jm11850a (2011).

30 Ghosh, P., Han, G., De, M., Kim, C. K. & Rotello, V. M. Gold nanoparticles in delivery applications. *Advanced drug delivery reviews* 60, 1307-1315, doi:10.1016/j.addr.2008.03.016 (2008).

31 Han, G., Ghosh, P. & Rotello, V. M. Multi-functional gold nanoparticles for drug delivery. *Advances in experimental medicine and biology* 620, 48-56 (2007).

32 Han, G., Ghosh, P. & Rotello, V. M. Functionalized gold nanoparticles for drug delivery. *Nanomedicine (Lond)* 2, 113-123, doi:10.2217/17435889.2.1.113 (2007).

33 Kim, C. K., Ghosh, P. & Rotello, V. M. Multimodal drug delivery using gold nanoparticles. *Nanoscale* 1, 61-67, doi:10.1039/b9nr00112c (2009).

34 Morimoto, Y. [Pulmonary toxicity of manufactured nanomaterials]. *Nihon eiseigaku zasshi. Japanese journal of hygiene* 67, 396-400 (2012).

35 Alder, B. J. & Wainwright, T. E. Studies in Molecular Dynamics .1. General Method. *J Chem Phys* 31, 459-466, doi:Doi 10.1063/1.1730376 (1959).

36 Hoover, W. G. Nonequilibrium Molecular Dynamics. *Annual Review of Physical Chemistry* 34, 103-127, doi:doi:10.1146/annurev.pc.34.100183.000535 (1983).

37 Buxton, G. A. & Balazs, A. C. Simulating the morphology and mechanical properties of filled diblock copolymers. *Phys Rev E* 67, -, doi:Artn 031802 Doi 10.1103/Physreve.67.031802 (2003).

38 Buxton, G. A., Lee, J. Y. & Balazs, A. C. Computer simulation of morphologies and optical properties of filled diblock copolymers. *Macromolecules* 36, 9631-9637, doi:Doi 10.1021/Ma034322+ (2003).

39 Lyatskaya, Y., Gersappe, D., Gross, N. A. & Balazs, A. C. Designing compatibilizers to reduce interfacial tension in polymer blends. *J Phys Chem-Us* 100, 1449-1458, doi:Doi 10.1021/Jp952422e (1996).

40 Li, S. Y., Niklasson, G. A. & Granqvist, C. G. Nanothermochromics: Calculations for VO2 nanoparticles in dielectric hosts show much improved luminous transmittance and solar energy transmittance modulation. *J Appl Phys* 108, doi:Artn 063525 Doi 10.1063/1.3487980 (2010).

41 Qin, Z. *et al.* Influences of low temperature thermal treatment on ZnO nanowire arrays and nanoparticles based flexible dye-sensitized solar cells. *Colloid Surface A* 402, 127-131, doi:Doi 10.1016/J.Colsurfa.2012.03.037 (2012).

42 Won, J. *et al.* Photothermal fixation of laser-trapped polymer microparticles on polymer substrates. *Appl Phys Lett* 75, 1506-1508, doi:Doi 10.1063/1.124737 (1999).

43 Buxton, G. A., Verberg, R., Jasnow, D. & Balazs, A. C. Newtonian fluid meets an elastic solid: Coupling lattice Boltzmann and lattice-spring models. *Phys Rev E* 71, -, doi:Artn 056707 Doi 10.1103/Physreve.71.056707 (2005).

44 Zeng, Q. H., Yu, A. B. & Lu, G. Q. Multiscale modeling and simulation of polymer nanocomposites. *Prog Polym Sci* 33, 191-269, doi:Doi 10.1016/J.Progpolymsci.2007.09.002 (2008).

Chapter 2 – Background and Motivation

2.1 Composite Materials

Composite materials – combining two or more materials to result in a novel material – are not new technology; they have existed since the ancient Egyptians mixed straw and mud, applied heat, and made bricks[1]. Polymers are not necessarily novel technology either; the ancient Mesoamericans had learned to utilize rubber millenia before the conquistadores arrived in the New World[2,3]. However, it was not until the mid-nineteenth century when Charles Goodyear and Thomas Hancock developed vulcanization by curing rubber in a sulfurous bath in order to enhance the hardness and toughness of the rubber (by instigating crosslinking) that polymer science and the development of polymer composites really began[4].

At the dawn of the twentieth century, the first true polymer composites were discovered. Developed by Leo Baekeland in 1905, Bakelite (or phenol formaldehyde or phenolic), was the first fiber-reinforced polymer, wherein fibers of a secondary material are enveloped by a polymer matrix, and as such is considered to be the first standard polymer composite[3]. As new synthetic polymers were discovered and utilized, polymer science continued to grow throughout the twentieth century. Eventually, polymer composites would move past fiber reinforcement to other materials, such as spheres of carbon black filler dispersed within a polystyrene matrix.

As technology progressed more quickly, particularly at the dawn of the twenty-first century, the ability to see, access, and manipulate things at the nanoscale gave rise to nanomaterials[5]. The promise offered by nanomaterials – that of more efficient solar energy capture; cell-specific drug-delivery; and even smaller transistors to mimic neurons – is driving much of nanomaterials research today[6-8]. Yet for all the focus on the rise of nanomaterials in

emergent technologies and processes, there are several long-practiced processes that are also benefitting from the discoveries that the nanoscale has presented. These processes may benefit by creating, stronger, cheaper, smaller, more easily manufactured products and materials. One such process is the creation of polymer composites, and it is this process that is the focus of this thesis.

2.2 Polymer Blends and Composites

Polymer blends occur when two homopolymers are mixed together in order to incur the benefits of either polymer. Although properly created polymer blends allow for the new material to possess the desired traits of both polymers, polymer blends are more susceptible to strain, fracture, and fatigue, particularly at the interface. Homopolymers under high shear forces may be subject to shear thinning, a decrease in viscosity within the bulk of the polymer that may eventually lead to fracture[9-11]. While polymer blends are not usually in peril of shear thinning, lower viscosity leads to instability within the material. The existence of the interface and the miscibility, or lack thereof, at said interface produces a region wherein viscosity is already lower than the surrounding bulk[12,13].

When the viscosity within the interfacial region is significantly lower than the surrounding bulk, the polymers glide past one another unencumbered while subjected to external shear stresses – a phenomenon known as interfacial slip[12]. Complementing a blend with a compatibilizer in order to combat the effects of interfacial slip results in a composite blend. Much like a blend assumes the traits of the polymers that comprise it, a composite blend also

encompasses the beneficial traits of the filler material. A successful compatibilizer must optimize systemic interfacial tension; stabilize the system; and enhance adhesion between phases[14]. Compatibilization may be traced to two methodologies: addition and reaction. In the former method, compatibilization is achieved via the inclusion of an additive that may be miscible between both phases. Should the additive be preferential to a single phase, a second additive preferential to the remaining phase and the first additive may also be an option. Meanwhile, the reaction method of compatibilization is focused solely on using chemical reactions and their byproducts to force blend adhesion[15]. Compatibilization within this thesis refers to the additive method, where that additive may be nanofiller particulates or diblock copolymer chains.

The addition of diblock copolymer chains allows for more adhesion within the system due to the miscibility inherent in their makeup[16]. As a chain composed of monomers of each phase, the diblock is inherently attractive to both phases, and is thus able to span the interface. However, interfacial spanning may only occur when the diblock chains are already located at or near the interface. Diblocks within the bulk run the risk of micellization, a phenomenon that may occur when diblocks are attracted to one another, forming small aggregate structures within the bulk[17,18]. These structures, randomized throughout the bulk, produce more interfaces within the system, creating more opportunities for decreased viscosity. In order to prevent micellization and promote interfacial adhesion, the copolymer must be placed within the interfacial region, a process that, while easy enough to do via simulation, is expensive and tedious in practice. Laun and Sundararaj also found that the addition of copolymer, whether in diblock or micelle form, could lead to additional instability within the blend[19-22]. Schultz confirmed, via simulation, the idea of instability being caused by increased complexity within the blend in systems which included nanofiller particles[23].

Given the difficulty and cost of compatibilization via diblock copolymer, filler particulates of other materials have also been used as an additive to enhance adhesion[24]. The addition of filler particles does not create additional interfaces between phases, and since these fillers are amenable to one or both polymer phases, this generally leads to less instability within the system. While there are many materials that have been used as compatibilizing fillers, carbon black – a filler material used to create a conducting polymer composite – is used as the basis for the spherical filler materials within the simulations conducted in later chapters[25]. Previously, these filler materials have been much larger than the surrounding monomers and their ability to compatibilize blends has been accrued to surface area interactions with the surrounding polymer chains[26]. These surface area interactions are given as a product of size, as a chain cannot easily circumvent a filler particle that is larger than the chain's own radius of gyration. Consequently, Zhang concluded that polymer-filler interactions ultimately influence transport dynamics within the system[27].

Groups led by Si and Hu both found that Cloisite platelet fillers in a polystyrene/polymethylmethacrylate blend (PS/PMMA) under shear remained within the PMMA phase and did not segregate to the interface[28,29]. These studies also showed that those systems also exhibited a severe increase in viscosity within the PMMA phase while no change in viscosity was observed within the polystyrene phase. While these fillers did not display interfacial segregation, this is evidence that should migration toward the interface occur, viscosity at the interfacial region can be expected to increase as well. Groups headed by Tang and Thompson found that larger fillers tended to aggregate due to van der Waal's forces[30,31]. Aggregated fillers may not enhance strength uniformly, leaving the composite susceptible to

weak points that may be exploited by external shear forces[32]. In essence, aggregated fillers create a new phase and with it, new interfaces, thus introducing further instability into the system.

Although large fillers have effectively been used to compatibilize blends, the size scale on which they operate hinders mobility throughout the bulk, as smaller particles move throughout the melt more easily than large particles would. This creates an issue where, similar to diblock copolymer chains, the large fillers must be placed at or near the interface or risk both segregating within a bulk phase and providing no enhancement in blend adhesion. Finally, filler aggregation brings its own issues that may further weaken the blend.

2.3 Polymer Nanocomposites

However, as materials at the nanoscale and the methods by which to study them become more readily available, the addition of nanofillers – filler materials within the nanoscale – have been added to blends in order to form a new class of composite polymer, the nanocomposite[33]. With filler size within the nanoscale, the new fillers are on the same size scale as the surrounding monomers, allowing for free filler movement throughout the bulk. This newfound range of motion often results in segregation to the interface, though this is not necessarily the case.

Chung, *et al*, found that segregation to the interface was dependent on the needs of the internal system: should a system risk fracture at the interface, fillers would segregate to strengthen the blend; otherwise, fillers tended to stay in whatever phase was preferred[34]. Meanwhile, Buxton and Balazs confirmed filler segregration was necessity-dependent via simulation[35]. This suggests that nanocomposites are, to a point, self-healing; in other words, up

until the point where fracture occurs, the nanofillers are free to move around the system to reinforce structural weaknesses within the system. Lipatov posits that filler segregation to the interface is dependent on the Gibbs free energy of the system and the minimization of Equation 2.1, where ***A*** and ***B*** are the polymer phases present within the system and ***F*** is the filler phase[36-39].

$$\Delta G_{mix} = \Delta G_{AF} + \Delta G_{BF} - \Delta G_{AB} \quad \textbf{(2.1)}$$

The system is thermodynamically stable when ΔG_{mix} is less than zero. When the filler is appealing to both phases, the free energy of the system is always negative and thus thermodynamically stable. However, should the filler be attractive to only one phase, the results are then system-dependent. Lo used a self-consistent field theory model and observed that given neutral nanofiller particles slip effects did decrease[40]. Thus, given neutral fillers and using molecular dynamics simulations, such as those used in Chapters Three and Four, one would expect to observe filler segregation to the interface and a decrease in interfacial slip. The reduction of slip with no explanation of the mechanisms by which this occurs hints at the creation of *in situ* structures within the system that help counteract external shear and the investigation of such structures informs much of Chapter Four.

When examining the nanofilled homopolymer system, Tsagaropolous and Eisenberg were able to establish that strength enhancement is a function of filler concentration, size, mobility, and the filler-polymer interaction energy[22]. However, Tsagarapolous and Eisenberg stopped short of predicting whether the same guidelines would hold for blended systems; Chapter Four deals with this question directly while also investigating the mechanism by which

this occurs. Meanwhile, Jaber suggests that high concentrations of nanofillers within homopolymers lead to fully spanning percolated networks within the system and that these networks are the mechanism by which shear enhancement would occur[41]. However, the percolation threshold prescribed by Jaber resides between five and ten percent nanofiller concentration. In order to verify that percolation can, in fact, account for strength enhancement within blends, Chapters Three and Four consider filler concentrations above and below the prescribed percolation threshold.

Salaniwal and Manias – via simulation and experimentation, respectively – observed that an increase in the number of nanofillers within a system led to a decrease in chain diffusivity and increased interaction between nanofillers, given a fixed nanofiller size[42-44]. In molecular dynamics simulations, increased interaction can easily be handled with an adjustment to the ε parameter within the Lennard-Jones potential. Meanwhile, these findings can be rather easily explained as a greater concentration of fillers gives more obstacles that the chains must navigate in order to diffuse. Also, in a low concentration of neutral fillers, the fillers are free to disperse from one another if the free energy within the system allows. However, the addition of more fillers reduces the amount of volume in which to disperse, forcing the fillers to interact more with one another. This is not to say, though, that fillers are necessarily forced to aggregate but rather, that they must account for other fillers within the system.

All of this leads to several questions that guide the research covered in Chapters Three and Four.

- What filler concentration is necessary for noticeable gains in strength enhancement?
- Does filler size impact the amount of concentration necessary for these gains?
- What role do nanofillers play in strength enhancement and layer adhesion?

- Is strength enhancement guided primarily by surface area interactions or are other parameters in play?
- Are *in situ* networks being formed at or near the interface?
- If so, what are the morphology and extent of these networks?
- Can there be enough fillers added to negate slip entirely?
- Can nanofillers be used as compatibilizers that enhance strength as effectively as diblock copolymers without presenting the same problems given by the diblocks?

2.4 Ignition and Combustion of Polymeric Materials

Polymers and plastics – known for being cheaper, lighter, more flexible, and easily shapeable – have long since become ubiquitous materials within society. However, the heat and temperatures necessary for ignition are significantly low enough (only about 250 to 600 degrees Celsius) to significantly contribute to their high flammability, inhibiting their adaptability to high temperature environments[45-47]. Polymers are more prone to ignition at lower temperatures primarily due to the relatively large amount of carbon and hydrogen atoms that pervade their chemical makeup[48]. Ignited polymeric materials may result in heat, smoke, and toxic gases; when combined with the prospect of complete material failure, polymeric materials are ill suited to heat-intensive settings[49]. Although metals are usually utilized in these situations, they often lack the benefits offered by polymeric materials.

Nelson determined that polymer combustion occurs in a cycle in which heat generated by the flame reacts with the surface, causing fragmentation. As these fragments fracture off of the

surface and enter the flame, they react with oxygen, thereby producing more heat, and continuing the cycle[50]. The goal of flame retardancy is to cause an interruption within the cycle by either reducing fragmentation or suppressing the heat generated. Since fragmentation reduction is dependent on the stability of the matrix before, during, and after combustion, most flame-retardants focus on heat suppression. The process by which this is accomplished may occur via the burning of flame retardant particles, wherein the inert gases formed by their ignition dilutes the concentration of combustible gases surrounding the polymer[51]. Polymeric materials are also susceptible to piloted ignition, in which the gases released by the quickly melted matrix also combust, effectively speeding up the reaction[45,52]. This indicates that not only must piloted ignition be accounted for within any method created to model polymer combustion but that flame retardant materials must also account for the gases that could potentially result from combustion.

2.5 Nanocomposites as Flame-Retardant Materials

In order to adapt polymeric materials into high temperature environments, flame-retardant filler materials are added to increase heat resistance. However, traditional flame-retardant materials have been found to be toxic and/or carcinogenic, thus precipitating the need for newer, safer materials[53,54]. Since filler materials have already demonstrated toxicity changes at the nanoscale, it is possible (though unlikely) that particulates of previously carcinogenic materials would not present carcinogenic effects at the nanoscale, thus providing a new perspective on effective but outdated materials[55-58]. Traditional materials may also require a significant amount of inclusion in order to reach retardancy, thus decreasing the cost-

effectiveness of their inclusion while also significantly reducing any weight benefits proposed by the use of polymers[59,60].

Nanocomposites show promise as flame-retardants due to the formation of an insulating layer of char as well as low permeability of the byproducts of combustion that would accelerate the reaction[51,61,62]. Nanocomposites created via organoclay inclusion at low concentrations form a protective char layer upon ignition that helps prevent catastrophic degradation[51,63,64]. However, the future of thermal materials research resides not with nanoscale samples of old materials, but with novel nanomaterials, such as graphene and carbon nanotubes; but more specifically, how these new materials can be used to create more efficient heat sinks[65-68]. While device and component size has steadily decreased over the last thirty years, the ability to more efficiently diffuse and/or transport heat within these components has not been able to keep pace. Advances in heat diffusion and transport would reduce costs as well as the amount of energy wasted as heat, resulting in more energy efficient devices at a time when environmental energy costs are at a premium.

Research in heat-resistant and flame retardant polymers has thus far been largely experimental. Upon examining single-walled carbon nanotubes' relevance to flame retardancy, Kashiwagi noted that even a very low (less than two percent) concentration of nanotubes was a more effective heat sink than a ten percent concentration of organoclay nanofillers[69]. A second set of experiments found that heat resistance is dependent on nanotube aspect ratio and dispersion within the polymer matrix[70]. Furthermore, the study showed that nanocomposites containing carbon nanotubes produced char surfaces that were less prone to cracking than surfaces created by the organoclay fillers. Meanwhile, Pack found that a combination of multi-walled nanotubes and organoclay nanofillers created a situation where the nanofillers segregated

to the walls of the nanotubes and provided better heat suppression than just the nanotubes alone[71].

However, research concerning the physics and dynamics of heat transport within these nanocomposite materials is still lacking. This hinders the efficiency and efficacy of designed novel materials and slows their development. Modeling and simulation would allow for less costly means of optimization and testing of these materials' thermal properties. However, modeling multiphase systems is inherently more difficult than monophase systems since the heat capacities, ignition temperatures, and overall thermal dynamics differ at the interfaces between materials, adding inherent complexity. Therefore, any model that is developed herein must meet the criteria listed below and this gives focus to Chapter Five. The model must:

- Accurately model heat transport, exchange, propagation, and absorption in a filled polymer matrix with an applied flame;
- Account for multiple distinct heat capacities and transport dynamics between phases;
- Simulate heat transport and propagation in three dimensions, along with the examination of the filler morphologies possible with the addition of the third dimension;
- Forecast localized ignition, as well as piloted ignition, if possible.

2.6 References

1 Nicholson, P. T. & Shaw, I. *Ancient Egyptian materials and technology*. (Cambridge University Press, 2000).

2 Hosler, D., Burkett, S. L. & Tarkanian, M. J. Prehistoric polymers: Rubber processing in ancient Mesoamerica. *Science* **284**, 1988-1991, doi:Doi 10.1126/Science.284.5422.1988 (1999).

3 Osswald, T. A. & Menges, G. *Materials science of polymers for engineers*. 2nd edn, (Hanser Publishers ; Cincinnati : Hanser Gardner Publications, 2003).

4 Flinn, R. A. & Trojan, P. K. *Engineering materials and their applications*. 2nd edn, (Houghton Mifflin, 1981).

5 Drexler, K. E., Peterson, C. & Pergamit, G. *Unbounding the future: the nanotechnology revolution*. (Morrow, 1991).

6 Abbasian, K., Rostami, A. & Pourkhorshidi, S. Design of Hybrid Solar Cell Based on Dye-Sensitized TiO2 Nanoparticles with Conjugated Polymer. *Acta Phys Pol A* **121**, 10-12 (2012).

7 Ghosh, P., Han, G., De, M., Kim, C. K. & Rotello, V. M. Gold nanoparticles in delivery applications. *Advanced drug delivery reviews* **60**, 1307-1315, doi:10.1016/j.addr.2008.03.016 (2008).

8 Bichler, O. *et al.* Functional Model of a Nanoparticle Organic Memory Transistor for Use as a Spiking Synapse. *Ieee T Electron Dev* **57**, 3115-3122, doi:Doi 10.1109/Ted.2010.2065951 (2010).

9 Goveas, J. L. & Fredrickson, G. H. Apparent slip at a polymer-polymer interface. *Eur Phys J B* **2**, 79-92 (1998).

10 Barsky, S. & Robbins, M. O. Molecular dynamics study of slip at the interface between immiscible polymers. *Phys Rev E* **6302**, -, doi:Artn 021801 (2001).

11 Narayanan, B., Pryamitsyn, V. A. & Ganesan, V. Interfacial phenomena in polymer blends: A self-consistent brownian dynamics study. *Macromolecules* **37**, 10180-10194, doi:Doi 10.1021/Ma048986a (2004).

12 Larson, R. G. *The structure and rheology of complex fluids*. (Oxford University Press, 1999).

13 Barsky, S. & Robbins, M. O. Bulk and interfacial shear thinning of immiscible polymers. *Phys Rev E* **65**, -, doi:Artn 021808 Doi 10.1103/Physreve.65.021808 (2002).

14 Utracki, L. A. Compatibilization of polymer blends. *The Canadian Journal of Chemical Engineering* **80**, 1008-1016 (2002).

15 Deanin, R. D. & Manion, M. A. Compatibilization of polymer blends. *PLASTICS ENGINEERING-NEW YORK*- **52**, 1-22 (1999).

16 Macosko, C. W. *et al.* Compatibilizers for melt blending: Premade block copolymers. *Macromolecules* **29**, 5590-5598 (1996).

17 Semenov, A. Microphase separation in diblock-copolymer melts: ordering of micelles. *Macromolecules* **22**, 2849-2851 (1989).

18 Bütün, V., Billingham, N. & Armes, S. Unusual aggregation behavior of a novel tertiary amine methacrylate-based diblock copolymer: formation of micelles and reverse micelles in aqueous solution. *J Am Chem Soc* **120**, 11818-11819 (1998).

19 Laun, H. M. *et al.* Rheological and Small-Angle Neutron-Scattering Investigation of Shear-Induced Particle Structures of Concentrated Polymer Dispersions Submitted to Plane Poiseuille and Couette-Flow. *J Rheol* **36**, 743-&, doi:Doi 10.1122/1.550314 (1992).

20 Sundararaj, U. & Macosko, C. W. Drop Breakup and Coalescence in Polymer Blends - the Effects of Concentration and Compatibilization. *Macromolecules* **28**, 2647-2657, doi:Doi 10.1021/Ma00112a009 (1995).

21 Tsai, S. C., Botts, D. & Plouff, J. Effects of Particle Properties on the Rheology of Concentrated Noncolloidal Suspensions. *J Rheol* **36**, 1291-1305, doi:Doi 10.1122/1.550260 (1992).

22 Tsagaropoulos, G. & Eisenberg, A. Direct Observation of 2 Glass Transitions in Silica-Filled Polymers - Implications for the Morphology of Random Ionomers. *Macromolecules* **28**, 396-398, doi:Doi 10.1021/Ma00105a059 (1995).

23 Schultz, A. J., Hall, C. K. & Genzer, J. Computer simulation of block copolymer/nanoparticle composites. *Macromolecules* **38**, 3007-3016, doi:Doi 10.1021/Ma0496910 (2005).

24 Koning, C., van Duin, M., Pagnoulle, C. & Jerome, R. Strategies for compatibilization of polymer blends. *Prog Polym Sci* **23**, 707-757, doi:Doi 10.1016/S0079-6700(97)00054-3 (1998).

25 Gubbels, F. *et al.* Design of Electrical Conductive Composites - Key Role of the Morphology on the Electrical-Properties of Carbon-Black Filled Polymer Blends. *Macromolecules* **28**, 1559-1566, doi:Doi 10.1021/Ma00109a030 (1995).

26 Beatty, C. L. Evidence of Interaction of Fillers with Matrix Polymers Via Transition Maps. *Polym Composite* **5**, 319-326, doi:Doi 10.1002/Pc.750050412 (1984).

27 Zhang, J. B., Cole, P. J., Nagpal, U., Macosko, C. W. & Lodge, T. P. Direct correlation between adhesion promotion and coupling reaction at immiscible polymer-polymer interfaces. *J Adhesion* **82**, 887-902, doi:Doi 10.1080/00218460600875847 (2006).

28 Si, M. *et al.* Compatibilizing bulk polymer blends by using organoclays. *Macromolecules* **39**, 4793-4801 (2006).

29 Hu, X. *et al.* Dynamics of Polymers in Organosilicate Nanocomposites. *Macromolecules* **36**, 823-829, doi:10.1021/ma020937f (2003).

30 Tang, H., Chen, X. F. & Luo, Y. X. Electrical and dynamic mechanical behavior of carbon black filled polymer composites. *Eur Polym J* **32**, 963-966, doi:Doi 10.1016/0014-3057(96)00026-2 (1996).

31 Thompson, C. M., Besuden, T. W. & Beumel, L. L. Resistivity of Rubber as a Function of Mold Pressure. *Rubber Chem Technol* **61**, 828-841, doi:Doi 10.5254/1.3536221 (1988).

32 Willey, S. J. & Macosko, C. W. Steady Shear Rheological Behavior of Pvc Plastisols. *J Rheol* **22**, 525-545, doi:Doi 10.1122/1.549487 (1978).

33 Alexandre, M. & Dubois, P. Polymer-layered silicate nanocomposites: preparation, properties and uses of a new class of materials. *Materials Science and Engineering: R: Reports* **28**, 1-63, doi:http://dx.doi.org/10.1016/S0927-796X(00)00012-7 (2000).

34 Chung, H., Ohno, K., Fukuda, T. & Composto, R. J. Self-regulated structures in nanocomposites by directed nanoparticle assembly. *Nano Lett* **5**, 1878-1882, doi:Doi 10.1021/Nl051079e (2005).

35 Buxton, G. A. & Balazs, A. C. Lattice spring model of filled polymers and nanocomposites. *J Chem Phys* **117**, 7649-7658, doi:Doi 10.1063/1.1509447 (2002).

36 Lipatov, Y. S. Polymer blends and interpenetrating polymer networks at the interface with solids. *Prog Polym Sci* **27**, 1721-1801 (2002).

37 Nesterov, A., Lipatov, Y. S. & Ignatova, T. Effect of an interface with solid on the component distribution in separated phases of binary polymer mixtures. *Eur Polym J* **37**, 281-285 (2001).

38 Lipatov, Y. S., Nesterov, A. E., Ignatova, T. D. & Nesterov, D. A. Effect of polymer-filler surface interactions on the phase separation in polymer blends. *Polymer* **43**, 875-880, doi:Doi 10.1016/S0032-3861(01)00632-2 (2002).

39 Nesterov, A. E. & Lipatov, Y. S. Compatibilizing effect of a filler in binary polymer mixtures. *Polymer* **40**, 1347-1349, doi:Doi 10.1016/S0032-3861(98)00277-8 (1999).

40 Lo, T. S., Mihajlovic, M., Shnidman, Y., Li, W. T. & Gersappe, D. Interfacial slip in sheared polymer blends. *Phys Rev E* **72**, -, doi:Artn 040801 Doi 10.1103/Physreve.72.040801 (2005).

41 Jaber, E., Luo, H. B., Li, W. T. & Gersappe, D. Network formation in polymer nanocomposites under shear. *Soft Matter* **7**, 3852-3860, doi:Doi 10.1039/C0sm00990c (2011).

42 Salaniwal, S., Kant, R., Colby, R. H. & Kumar, S. K. Computer simulations of local concentration variations in miscible polymer blends. *Macromolecules* **35**, 9211-9218, doi:Doi 10.1021/Ma020624k (2002).

43 Salaniwal, S., Kumar, S. K. & Douglas, J. F. Amorphous solidification in polymer-platelet nanocomposites. *Phys Rev Lett* **89**, doi:Artn 258301 Doi 10.1103/Physrevlett.89.258301 (2002).

44 Manias, E. *et al.* Intercalation kinetics of long polymers in 2 nm confinements. *Macromolecules* **33**, 7955-7966, doi:Doi 10.1021/Ma0009552 (2000).

45 Lyon, R. E. & Quintiere, J. G. Criteria for piloted ignition of combustible solids. *Combustion and Flame* **151**, 551-559, doi:http://dx.doi.org/10.1016/j.combustflame.2007.07.020 (2007).

46 Walters, R. N., Hackett, S. M. & Lyon, R. E. Heats of combustion of high temperature polymers. *Fire and materials* **24**, 245-252 (2000).

47 Mouritz, A. P. & Gibson, A. G. *Fire Properties of Polymer Composite Materials*. (Springer London, Limited, 2006).

48 Macskásy, H. & Palyi, G. *Plastics: Their Behaviour in Fires*. (Elsevier Science, 1991).

49 Hirschler, M. M. Fire hazard and toxic potency of the smoke from burning materials. *Journal of fire sciences* **5**, 289-307 (1987).

50 Nelson Gordon, L. in *Fire and Polymers II* Vol. 599 *ACS Symposium Series* Ch. 1, 1-26 (American Chemical Society, 1995).

51 Laoutid, F., Bonnaud, L., Alexandre, M., Lopez-Cuesta, J. M. & Dubois, P. New prospects in flame retardant polymer materials: From fundamentals to nanocomposites. *Materials Science and Engineering: R: Reports* **63**, 100-125, doi:http://dx.doi.org/10.1016/j.mser.2008.09.002 (2009).

52 Fereres, S., Lautenberger, C., Fernandez-Pello, A. C., Urban, D. L. & Ruff, G. A. Understanding ambient pressure effects on piloted ignition through numerical modeling. *Combustion and Flame* **159**, 3544-3553, doi:http://dx.doi.org/10.1016/j.combustflame.2012.08.006 (2012).

53 Blum, A. & Ames, B. N. Flame-Retardant Additives as Possible Cancer Hazards. *Science* **195**, 17-23, doi:Doi 10.1126/Science.831254 (1977).

54 Darnerud, P. O. Toxic effects of brominated flame retardants in man and in wildlife. *Environment International* **29**, 841-853, doi:http://dx.doi.org/10.1016/S0160-4120(03)00107-7 (2003).

55 Dhawan, A. & Sharma, V. Toxicity assessment of nanomaterials: methods and challenges. *Analytical and bioanalytical chemistry* **398**, 589-605, doi:10.1007/s00216-010-3996-x (2010).

56 Sharifi, S. *et al.* Toxicity of nanomaterials. *Chem Soc Rev* **41**, 2323-2343, doi:10.1039/c1cs15188f (2012).

57 Schrand, A. M., Dai, L., Schlager, J. J. & Hussain, S. M. Toxicity testing of nanomaterials. *Advances in experimental medicine and biology* **745**, 58-75, doi:10.1007/978-1-4614-3055-1_5 (2012).

58 Dhawan, A., Pandey, A. & Sharma, V. Toxicity assessment of engineered nanomaterials: resolving the challenges. *Journal of biomedical nanotechnology* **7**, 6-7 (2011).

59 Beyer, G. Nanocomposites — a new class of flame retardants. *Plastics, Additives and Compounding* **11**, 16-21, doi:http://dx.doi.org/10.1016/S1464-391X(09)70048-0 (2009).

60 Beyer, G. Nanocomposites: a new class of flame retardants for polymers. *Plastics, Additives and Compounding* **4**, 22-28, doi:http://dx.doi.org/10.1016/S1464-391X(02)80151-9 (2002).

61 Beyer, G. Flame retardant properties of EVA-nanocomposites and improvements by combination of nanofillers with aluminium trihydrate. *Fire and Materials* **25**, 193-197, doi:10.1002/fam.776 (2001).

62 Beyer, G. Short communication: Carbon nanotubes as flame retardants for polymers. *Fire and Materials* **26**, 291-293, doi:10.1002/fam.805 (2002).

63 Lewin, M. Reflections on migration of clay and structural changes in nanocomposites. *Polym Advan Technol* **17**, 758-763 (2006).

64 Zanetti, M., Kashiwagi, T., Falqui, L. & Camino, G. Cone calorimeter combustion and gasification studies of polymer layered silicate nanocomposites. *Chem Mater* **14**, 881-887 (2002).

65 Berber, S., Kwon, Y. K. & Tomanek, D. Unusually high thermal conductivity of carbon nanotubes. *Phys Rev Lett* **84**, 4613-4616, doi:Doi 10.1103/Physrevlett.84.4613 (2000).

66 Balandin, A. A. *et al.* Superior thermal conductivity of single-layer graphene. *Nano Lett* **8**, 902-907, doi:Doi 10.1021/Nl0731872 (2008).

67 Balandin, A. A., Shamsa, M., Liu, W. L., Casiraghi, C. & Ferrari, A. C. Thermal conductivity of ultrathin tetrahedral amorphous carbon films. *Appl Phys Lett* **93**, doi:Artn 043115 Doi 10.1063/1.2957041 (2008).

68 Shamsa, M. *et al.* Thermal conductivity of nitrogenated ultrananocrystalline diamond films on silicon. *J Appl Phys* **103**, doi:Artn 083538 Doi 10.1063/1.2907865 (2008).

69 Kashiwagi, T. *et al.* Relation between the viscoelastic and flammability properties of polymer nanocomposites. *Polymer* **49**, 4358-4368, doi:http://dx.doi.org/10.1016/j.polymer.2008.07.054 (2008).

70 Kashiwagi, T. *et al.* Flammability properties of polymer nanocomposites with single-walled carbon nanotubes: effects of nanotube dispersion and concentration. *Polymer* **46**, 471-481, doi:http://dx.doi.org/10.1016/j.polymer.2004.10.087 (2005).

71 Pack, S. *et al.* Segregation of Carbon Nanotubes/Organoclays Rendering Polymer Blends Self-Extinguishing. *Macromolecules* **42**, 6698-6709, doi:10.1021/ma900966k (2009).

Chapter 3 – Molecular Dynamics Simulations and System Parameters

3.1 Molecular Dynamics Simulations

Computer simulations allow for the examination of the physical properties of individual molecules as well as how external forces and stresses affect them. Molecular dynamics simulations, in particular, allow us to examine these molecules' positions, velocities, accelerations, and orientations within the system as they develop over time[1-3]. Since the system is allowed to evolve as time passes, a more gestalt view of the inner workings of the system than can be garnered than what is possible with the limitations in instrumentation currently available. This also allows us to create a variety of systems that can vary several parameters, which may be impossible to do in a lab due to instrumentation or synthetic limitations.

Polymer interactions are particularly well suited to be examined by molecular dynamics simulations since we can initialize and manipulate a set of information with precision, while keeping track of several sets of data regarding the motion and reaction of each molecule within the system[4]. As computer systems grow larger and faster, and as we are able to chain cheaper and speedier processors together via parallelization, molecular dynamics simulations will become a faster, more efficient, and more useful in the exploration of polymer interactions. However, the underlying tradeoff remains in which as system size grows – even in large computing systems with several hundreds or thousands of processors – the equilibration times and runtimes grow exponentially with them[5]. And while hard disk space and random access memory is cheaper and more plentiful than it has ever been, systems pushing millions of

particles can be a strain to memory resources. Given the particular computing setup used, the selected systems created herein were kept relatively small.

Molecular dynamics can be used to examine equilibrium and nonequilibrium systems. In an equilibrium system, an isolated system of molecules (*N*) exists at fixed volume (*V*) and pressure (*P*). Since no external forces are applied to the system, the energy of the system (*E*) is determined by the sums of kinetic and potential energies of each individual particle[1,6]. This leaves the energy constant within the system at any given time. When the system is no longer isolated, external forces may vary volume and pressure, moving the system away from equilibrium. The internal energy of the system becomes dependent on the forces that exist outside of the system.

By making changes to an equilibrium system and moving it away from equilibrium, one can measure the effect of these changes qualitatively and quantitatively, allowing the user to easily gauge any rheological changes that may occur. Since molecular dynamics is based on pairwise interactions, the introduction of a new species, such as nanofillers, into a system is directly observable as long as the actions of the new species are well defined. Thus, it becomes essential that the user fully understand the equations and theory that govern molecular modeling and simulations.

3.2 Newtonian Motion

Molecular dynamics simulations involve the solution of the Newtonian force equation, $F(t)=m\times a(t)$, rewritten in order to more accurately describe polymer interactions[1,6]. Simple

physics has shown us that the position of anything can be found by twice integrating its acceleration function, and so we can use $F(t)=m\times a(t)$ to determine the position, $r(t)$, of a particle by measuring the force acting upon it by all other particles within the system. Equation 3.1 shows the relationship between these factors where F is the force acting upon a particle, i; m is the molecular mass of the particle; a is its acceleration; r is its position with the system; and U is the intermolecular potential energy of the system on molecule i.

$$F_i(t) = m \cdot a_i(t) = m \cdot \ddot{r}_i(t) = -\frac{\partial \bar{U}(r^N)}{\partial r_i} \quad \textbf{(3.1)}$$

However, since the calculation of all the forces acting on a particle due to all other particles can be computationally expensive, a cut-off distance was used to designate a radius for the sphere of influence to determine which forces directly acting on a particle determine its position[7,8]. This coarse-grained model saves on computing time and memory resources. Though a more accurate picture of the system could be accomplished from verifying the forces acting upon each particle by every other particle in the system, the differences would be so minimal and the computing costs so great that molecular dynamics would probably no longer be an efficient method for examining these systems. The addition of the cutoff distance allows for operation under the assumption that outside the sphere of influence, the forces being applied to a particle are balanced and their sum is effectively zero. In a system in which all molecules are allowed interaction with one another, computation time increases exponentially. This is justified since the Lennard-Jones potential (Equation 3.12) used to calculate molecular interactions stipulates that the potential, U, is inversely proportional to molecular distance, thus approaching zero as intermolecular distance approaches infinity (3.2).

$$U(r) \propto \left(\frac{1}{r}\right)^N \rightarrow \lim_{r\to\infty} U(r) \propto \lim_{r\to\infty}\left(\frac{1}{r}\right)^N = 0, \text{ for N>0.} \quad \textbf{(3.2)}$$

The cutoff distance, r_c, was selected at r_c=2.5σ, leading to *U(r)* being calculated normally if $r \leq r_c$, and zero otherwise. Repeating the position calculations for each time step allows for the examination ofthe trajectory and path of each particle, which can then be averaged over time to allow for an evaluation of the macroscopic properties of the entire system.

3.3 The Verlet Algorithm

Although Equation 3.1 is based off simple Newtonian physics, it assumes that the system is initialized with acceleration or velocity values. The acceleration is calculated in regards to a given position and uses that known position to estimate the next position value. Initially the Verlet algorithm is used to define positions within the system using a Taylor expansion series[9]. Though the Taylor expansion series has infinitely many terms, the primary concern lays within the first three terms, which deal with position, velocity, and acceleration, respectively (3.3.a-3.3.c).

$$r(t+\Delta t) = r(t) + \dot{r}(t)\,\Delta t + \frac{1}{2}\ddot{r}(t)(\Delta t)^2 + \frac{1}{6}\dddot{r}(t)(\Delta t)^3 + \ldots \quad \textbf{(3.3.a)}$$

$$v(t+\Delta t) = \dot{r}(t+\Delta t) = \dot{r}(t) + \ddot{r}(t)\,\Delta t + \frac{1}{2}\dddot{r}(t)(\Delta t)^2 + \ldots \quad \textbf{(3.3.b)}$$

$$a(t+\Delta t) = \ddot{r}(t+\Delta t) = \ddot{r}(t) + \dddot{r}(t)\,\Delta t + \cdots \quad \textbf{(3.3.c)}$$

Having defined these physical parameters allows us to predict the positions at times, (*t+Δt)* and (*t-Δt)*, as seen in Equations 3.4.a and 3.4.b.

$$r(t + \Delta t) = r(t) + \dot{r}(t)\,\Delta t + \frac{1}{2}\ddot{r}(t)(\Delta t)^2 + \ldots \quad \textbf{(3.4.a)}$$

$$r(t - \Delta t) = r(t) - \dot{r}(t)\,\Delta t + \frac{1}{2}\ddot{r}(t)(\Delta t)^2 + \ldots \quad \textbf{(3.4.b)}$$

Adding these two positions leaves an equation that eliminates the velocity term (3.5).

$$r(t + \Delta t) = 2r(t) - r(t - \Delta t) + \ddot{r}(t)(\Delta t)^2 + \cdots \quad \textbf{(3.5)}$$

While the Verlet algorithm can be used to calculate molecular positions, velocities, and accelerations, it is limited insofar that it cannot calculate both the position and velocity of a given molecule at the same timestep. This leads to a half-step calculation of velocity (3.6) that must then be corrected later (since positions are calculated for (*t+Δt)* rather than (*t+Δt/2*)), lest the error created by not doing so balloons quickly, thereby corrupting the effectiveness of the method.

$$\dot{r}\left(t + \frac{\Delta t}{2}\right) = \dot{r}(t) + \frac{1}{2}\ddot{r}(t)\,\Delta t \quad \textbf{(3.6)}$$

3.4 The Gear's Predictor-Corrector Algorithm

Molecular Dynamics simulations primarily use Gear's Predictor-Corrector algorithm in order to correct for the error pervasive within the Verlet algorithm. This method uses the values of *r(t)* and *r(t-h)* to predict the value of *r(t+h)*[10]. It does so by first attempting to solve the ordinary second order differential equation that follow (3.7.a, 3.7.b).

$$\ddot{r}_i = f_i(r_i, \dot{r}_i, t) \quad \textbf{(3.7.a)}$$

$$f(t) \equiv f(r, \dot{r}, t) \quad \textbf{(3.7.b)}$$

First, the value of *r(t+h)* is estimated using a fifth-order Taylor series that is centered at the particle's position and its positional derivatives at *t*. Equations 3.8.a and 3.8.b illustrate the general calculations for predicting position and velocity, respectively.

$$r(t+h) = r(t) + \dot{r}(t)h + h^2 \sum_{i=1}^{k-1} \alpha_i \cdot f(t + (i-1)h) \quad \textbf{(3.8.a)}$$

$$\dot{r}(t+h) = \frac{r(t+h) - r(t)}{h} + h \sum_{i=1}^{k-1} \alpha_i^{'} \cdot f(t + (i-1)h) \quad \textbf{(3.8.b)}$$

The force is then calculated on each particle at *(t+h)* using the positions estimated by the Taylor series as illustrated by Equation 3.9.

$$f(t+h) \equiv f(r(t,h)) \quad \textbf{(3.9)}$$

Individual positions and velocities are then corrected by minimizing the difference between the predicted accelerations and the intermolecular forces calculated at *(t+h)* (3.10.a, 3.10.b).

$$r(t+h) = r(t) + \dot{r}(t) + h^2 \sum_{i=1}^{k-1} \beta_i \cdot f(t + (2-i)h) \quad \textbf{(3.10.a)}$$

$$\dot{r}(t+h) = \frac{r(t+h)-r(t)}{h} + h \sum_{i=1}^{k-1} \beta_i^{'} \cdot f(t + (2-i)h) \quad \textbf{(3.10.b)}$$

The coefficients, α_I, β_I, α_I', and β_I', are dependent on k; in this case, k is set at five as a result of having chosen a fifth-order Taylor expansion. These coefficients were chosen by Gear in order to create numerical stability within the system and minimize error. This was done using the predictor-corrector method on linear equations with known solutions and analyzing stability throughout. The coefficients chosen by Gear give stability coeffcients of α={3/16; 251/360; 1; 11/18; 1/6; 1/60}[4,10]. While Gear's initial value for α_0 was set at 3/20, it was eventually discovered that α_0=3/16 produced a more stable system and hence was eventually adopted as the standard value for a fifth-order expansion of the predictor-corrector algorithm.

3.5 Equilibrium States

Only once a given system has reached steady-state equilibrium can external forces be exerted upon it. This frees the system up from any residual stresses that may affect desired results, such as internal or interfacial pressure, stresses at the interface or at the walls, or environmental heat exchange. This guarantees that the values determined from the system upon finalization are results of the external forces acting upon the system rather than remnants of initialization[11]. Since this step is so critical, systems were allowed to remain at equilibrium for several million timesteps before external forces were applied. On average, a given system

required about five million timesteps to reach equilibrium but was run for upwards of ten million just to guarantee that equilibrium had been achieved.

Systems were created as bulk homopolymer residing between two walls. Once those systems had been brought to equilibrium, nanofillers were added and the system was brought to equilibrium once again. As systems tended toward steady-state equilibrium, the walls were allowed to expand and contract so as to allow pressure to escape the system. By examining the pressure acting upon the walls of the system, any external stresses that may have precluded results henceforth could be identified. Thus when the pressure on the walls had effectively reached zero for several hundred thousand timesteps, it could be ascertained that all internal stresses not directly related to the formation of the interface had been relieved. This also meant that any pressure applied to the wall after the creation of the interface was due to interfacial tension within the system and allowed for the study of the effect of introducing nanofillers to a blend on interfacial tension.

3.6 Polymeric Interactions Within Molecular Dynamics Simulations

Each polymer chain in the system was modeled using the bead-spring method presented by Kremer and Grest[12,13]. Each chain consisted of N=64 spherical monomers held together by the finite-elastic nonlinear extendable (FENE) potential (3.11),

$$U_{CH}(r) = -\frac{1}{2}KR_0^2 \ln\left[1 - \left(\frac{r}{R_0}\right)^2\right] \quad \textbf{(3.11)}$$

where r is the distance between two monomers on the chain, K=30ε and R_0=1.5σ. The FENE potential guarantees that the bonds that keep monomers together within a chain are not allowed stretching beyond their limits, thus keeping chains at a fixed length. All monomer interactions within a chain or with the wall particles were guided by the Lennard-Jones 12-6 potential (3.12)[14].

$$U(r) = 4\varepsilon\left[\left(\frac{\sigma}{r}\right)^{12} - \left(\frac{\sigma}{r}\right)^{6}\right] \quad \textbf{(3.12)}$$

All nanofiller particle interactions with monomer and wall particles were governed by a modification of the Lennard-Jones potential (3.13)

$$U(r) = 4\varepsilon_{fp}\left[\left(\frac{\sigma}{r-s}\right)^{12} - \left(\frac{\sigma}{r-s}\right)^{6}\right] \quad \textbf{(3.13)}$$

where ε_{fp} is the interaction energy between polymer and filler and s is a function of filler size as seen in Equation 3.14.

$$s = \frac{1}{2}(\sigma_f - \sigma) \quad \textbf{(3.14)}$$

σ and σ_f are the sizes of monomer and filler particles respectively and larger values of s indicate a larger filler size. The system is constrained with $(r\text{-}s) \leq r_c = 2.5\sigma$. Filler sizes were adjusted by varying s rather than σ_f. The interaction energy, ε_{fp}, was held constant at 2.0 in order to suppress cluster formation among the filler particles. The interaction energy between the polymer and the

wall particles, ε_{fw}, as well as the interaction energy between the filler and wall, ε_{pw}, was held constant at 4.0.

3.7 Nanofiller Creation

The system was created as an equilibrated pure bulk polymer system with 128 chains ($N=64$) fitted between rigid walls. The chain length used was well above the entanglement length proposed by Kremer and Grest (N=35)[12]. While the system obeyed periodic boundary conditions in the x and y directions ($L_x=L_y=16\sigma$), the rigid walls bounding the system ($L_z=32\sigma$) did not allow the same conditions in the z direction. Each wall contained 400 atoms giving a total system size of 9792 particles. Each wall consisted of $2*L_x*L_y$ atoms residing in two layers so as to be impermeable by monomers or fillers. Molecules forming the wall were also guided by the Lennard-Jones potential with ε_{ww}=4.0. The internal temperature of the system was dissipated with a heat bath that held the temperature constant at 1.1 (ε/k_B), well above the theoretical glass transition temperature, 0.5 (ε/k_B).

In order to create nanofiller particles, random chains were broken into monomers to allow for the creation of fillers at two, five, and ten percent of total volume, ϕ_f. Once the correct ratio of fillers was fulfilled and any extras dropped, the fillers were slowly grown within the system using the size parameter, s, described previously.

Creating the diblocks within the control system was far easier. Chains located within two σ-lengths of the interface were selected and converted into diblocks by allowing one half of the chain to be of type ***A*** and the other of type ***B***. Since the FENE potential is much stronger than the

Lennard-Jones potential, the chains were able to withstand the repulsion exhorted by the δ term within the modified Lennard-Jones potential. Although both phases are repulsed by one another, all other constraints of the system were exactly the same for each phase. This resulted in the ***A***-type half of the diblocks being more attracted to the ***A*** phase within the system with similar results in the ***B*** phase.

3.8 Interfacial Separation

Upon bringing the internal pressure of the system to zero by allowing the walls to expand and then contract slowly, an interface was created at the midpoint between the walls. This allows for the ability to track the interfacial tension produced when the homopolymer systems were split after having reached equilibrium. Chains with a center of mass above this engineered interface were labeled ***A*** while those below were labeled ***B***, thus creating a bulk homopolymer blend. At this point, ***A*** and ***B*** were fundamentally equivalent except that a general dislike for chains of differing type was created, resulting in immiscibility at the interface. A further modified version of the Lennard-Jones potential (3.15) was used to guarantee separation of both phases, thus making the polymers immiscible.

$$U(r) = 4\varepsilon\left[\left(\frac{\sigma}{r}\right)^{12} - \delta\left(\frac{\sigma}{r}\right)^{6}\right] \quad \textbf{(3.15)}$$

Since δ was introduced as a coefficient to the attractive term of the Lennard-Jones potential, lower values of δ indicate increased repulsion between the two phases, resulting in

sharper interfaces. δ was given several values, but the majority of this paper will focus on the δ=0.75 and δ=0.90 cases unless stated otherwise. Higher values of δ were selected in order to allow for some miscibility at the interface, though in earlier studies the effect of selecting even lower values for δ was examined. However, these earlier studies showed that there was a limiting factor in the utility of selecting these values that begins soon after δ=0.75. By using δ to determine miscibility between the polymers, the system was provided with a simulation analogue to the Flory-Huggins parameter, χ. Flory-Huggins analogues, such as ε_{AB}^{*}, have been used to delineate phase separation by several groups while fitting nicely into the context presented by the Lennard-Jones potential[15-17].

Although both phases are repulsed by one another, all other constraints of the system were exactly the same for each phase. The interactions between polymer ***A*** and the fillers were the same as those between ***B*** and the fillers. In the case of polymer-filler interactions, fillers were neutral to both phases and thus were neither attracted nor repulsed by either phase. This assured that the fillers are not partial to a single phase and remain mobile – able to roam freely throughout the system.

Since the chains that were selected to create the diblocks were already within the interfacial region, the diblocks were encouraged to align themselves by phase at the interface. This resulted in the diblocks effectively being locked into the interface and thus unlikely to micellize within the bulk. Had the diblocks been allowed to disperse throughout the bulk, chains of like phases would have been attractive to each other within the opposite phase; thus, the formation of micelles, or small groups of one phase within another, results in multiple interfaces rather than just one[18-20]. However, this is an artifice created by the simulation and not something likely to be found without direct interference in an experimental setting. It did, nevertheless,

allow for the use of direct comparison between the nanocomposite structures suggested by the nanofiller systems and diblock copolymers within a bulk system.

3.9 Viscosity and Interfacial Width Calculations Within Molecular Dynamics Simulations

Using a fifth-order predictor-corrector algorithm and a time step of Δt=0.005τ, the systems were allowed to equilibrate for 20,000τ. Upon equilibration, the systems were sheared at various constant shear rates, υ, for 250,000τ and their velocity profiles calculated upon three separate regions. The process for calculating interfacial slip was provided by Brochard and de Gennes, who proposed that the shear profiles could be broken up into three regions[21]. The first and third regions examined the velocity within the bulks of ***A*** and ***B***, respectively, while the second examined the velocity at and around the interface. For a normal curve, the regions outside of the interface would have the same slope, while the interfacial region would have a slope much higher than those. By extrapolating the roots of the lines created by the first and third regions and then subtracting the difference, the length of interfacial slip occurring within the system could be measured. Figure 3.1 is an illustration of Brouchard and de Genne's method. Utilizing this method, enables the measurement of regional viscosity, μ (3.16)[14,21]. If slip were indeed present within systems, it would be due to a decreased viscosity at the interface; conversely, if slip were to improve upon the introduction of fillers, it could be attributed to improved interfacial viscosity[22].

$$\tau = \frac{F}{A} = \mu \frac{du}{dy} \quad \textbf{(3.16)}$$

The interfacial width was determined using a discretization of the integral presented by Equations 3.17.a and 3.17.b[23]. In each system, the interfacial width was calculated to be very near 2σ.

$$w_I = 4 \int_{-\infty}^{\infty} (\phi_A)(1 - \phi_A) dz \quad \textbf{(3.17.a)}$$

$$w_I = 4 \sum \left(\frac{n_A}{N}\right) \left(1 - \frac{n_A}{N}\right) \Delta z \quad \textbf{(3.17.b)}$$

Table 3.1 illustrates the various systems that were created using the presented methodology.

3.10 *In Situ* Internal Structures

Operating under the hypothesis that the *in situ* internal structures being formed within the nanofilled systems were actually *in situ* diblocks (ISDs) being formed between chains of opposing type with a nanofiller mediator, an exploration of the implications of this hypothesis was necessary. An ISD was defined as any cluster of chains in which chains of opposing type resided within ($2^{1/6}$ + *s*) of a given nanofiller particle. $2^{1/6}$ fits well with the model presented by Jaber, *et al*, that detailed the potential tail in systems with differing values of δ, while the *s* factor allowed us to account for the various nanofiller particle sizes found within the system[24,25].

An ISD was designated as mechanically relevant if it resided within the interfacial region before shear and remained within this region throughout the shear process. While clusters were allowed to form and detach as demanded by the system, mechanical relevance was further restricted by tracking only those clusters which had one chain of each type remain "attached" to that given nanofiller throughout the entirety of the shear process. By tracking ISDs throughout the process, it could be ascertained that a mechanically relevant ISD would factor into the system the same way the diblocks had prior. Finally, the orientation of each ISD was tracked at the interface in order to determine how much stretching these ISDs incurred in attempting to strengthen their respective blends.

3.11 Chain Orientation Within Sheared Systems

In order to conceive a firm idea of the reaction of our microstructures within the system under shear, the orientation of the chains before and after shear must be examined. In a normally flowing system, one would expect the chain direction to align itself in the direction of shear[14]. In the case of interfacial slip in our systems, the upper phase travels in the direction of shear in the top wall while the lower phase moves in the direction of the bottom wall. While the distance at which the interface exists relative to the wall diminishes shear effects, these effects are still present at the interface, thus leading to the upper phase sliding over the lower phase, thereby creating slip[14,26-28].

However, if slip is to be reduced, then it follows that something within the system must be providing resistance to these external forces. If the proposed *in situ* diblocks are creating

resistant forces to counteract shear, one can assume that their post-shear orientation should mirror the chain orientation of actual diblocks within the system. Conversely, since the length of the ISDs is twice as long as the proper diblocks that are being examined, ISD orientation may not mirror diblock orientation exactly but should be similar among the affected areas near the interface.

In order to study chain angle orientation and alignment, the overall structure order tensor in the x-direction, P_x, is examined (3.18).

$$P_x = \langle \tfrac{1}{2}(3(\cos\bar{\theta}_x)^2 - 1)\rangle \quad \textbf{(3.18)}$$

This function is commonly used to determine orientation in liquid crystal display terminals, among other applications[29,30]. Three layers in each system are considered: the interfacial layer and the bulk layers on either side of it. The angle, $\theta_{x,}$ is calculated on a per-bond basis and then averaged over the total chain for each chain in a given layer. The structure tensor, P_x, averaged over the entire layer, may range from -0.5 to 1, but a value, P_h^*, is selected as a baseline value using a given system's homopolymer analogue and uses the ratio, $P_R = P_x/P_h^*$, to communicate the relative amount of orientation exhibited.

In the next chapter, the previously outlined methods are used to examine the role nanoparticles play in the strengthening of a polymer blend. The degree to which nanoparticles can compete with diblock compatibilizers at filling that role is also considered.

3.12 References

1 Haile, J. M. *Molecular Dynamics Simulation: Elementary Methods*. (Wiley, 1997).

2 Allen, P. & D. J. Tildesley, M. P. A. *Computer Simulation of Liquids*. (Clarendon Press, 1989).

3 Roe, R. J. & Chemistry, A. C. S. D. o. P. *Computer Simulation of Polymers*. (Prentice Hall, 1991).

4 Wilkins, M. L. *Computer Simulation of Dynamic Phenomena*. (Springer, 1999).

5 Mattson, T. G., Chemistry, A. C. S. D. o. C. i. & Meeting, A. C. S. *Parallel computing in computational chemistry*. (American Chemical Society, 1995).

6 Hoover, W. G. Nonequilibrium Molecular Dynamics. *Annual Review of Physical Chemistry* **34**, 103-127, doi:doi:10.1146/annurev.pc.34.100183.000535 (1983).

7 Huang, C., Li, C., Choi, P. Y. K., Nandakumar, K. & Kostiuk, L. W. Effect of cut-off distance used in molecular dynamics simulations on fluid properties. *Mol Simulat* **36**, 856-864, doi:10.1080/08927022.2010.489556 (2010).

8 Rapaport, D. C. *The Art of Molecular Dynamics Simulation*. (Cambridge University Press, 2004).

9 Verlet, L. Computer "Experiments" on Classical Fluids. I. Thermodynamical Properties of Lennard-Jones Molecules. *Physical Review* **159**, 98-103 (1967).

10 Gear, C. W. *Numerical initial value problems in ordinary differential equations*. (Prentice-Hall, 1971).

11 Nosé, S. A molecular dynamics method for simulations in the canonical ensemble. *Mol Phys* **52**, 255-268, doi:10.1080/00268978400101201 (1984).

12 Kremer, K. & Grest, G. S. Dynamics of Entangled Linear Polymer Melts - a Molecular-Dynamics Simulation. *J Chem Phys* **92**, 5057-5086 (1990).

13 Grest, G. S. & Kremer, K. Molecular dynamics simulation for polymers in the presence of a heat bath. *Phys Rev A* **33**, 3628-3631 (1986).

14 Larson, R. G. *The structure and rheology of complex fluids*. (Oxford University Press, 1999).

15 Grest, G. S., Lacasse, M. D., Kremer, K. & Gupta, A. M. Efficient continuum model for simulating polymer blends and copolymers. *J Chem Phys* **105**, 10583-10594 (1996).

16 Barsky, S. & Robbins, M. O. Bulk and interfacial shear thinning of immiscible polymers. *Phys Rev E* **65**, -, doi:Artn 021808 Doi 10.1103/Physreve.65.021808 (2002).

17 Barsky, S. & Robbins, M. O. Molecular dynamics study of slip at the interface between immiscible polymers. *Phys Rev E* **6302**, -, doi:Artn 021801 (2001).

18 Riess, G. Micellization of block copolymers. *Prog Polym Sci* **28**, 1107-1170, doi:http://dx.doi.org/10.1016/S0079-6700(03)00015-7 (2003).

19 Rodríguez-Hernández, J. & Lecommandoux, S. Reversible Inside−Out Micellization of pH-responsive and Water-Soluble Vesicles Based on Polypeptide Diblock Copolymers. *J Am Chem Soc* **127**, 2026-2027, doi:10.1021/ja043920g (2005).

20 Gohy, J.-F. in *Block Copolymers II* Vol. 190 *Advances in Polymer Science* (ed Volker Abetz) Ch. 48, 65-136 (Springer Berlin Heidelberg, 2005).

21 Brochard, F. & Degennes, P. G. Shear-Dependent Slippage at a Polymer Solid Interface. *Langmuir* **8**, 3033-3037, doi:Doi 10.1021/La00048a030 (1992).

22 Adhikari, N. P. & Goveas, J. L. Effects of slip on the viscosity of polymer melts. *J Polym Sci Pol Phys* **42**, 1888-1904, doi:Doi 10.1002/Polb.20066 (2004).

23 Li, W. *Modeling the Static and Dynamic Properties of Polymers at Interfaces*. (State University of New York at Stony Brook, 2001).

24 Jaber, E. *Rheology and dynamics in polymeric nano-composites*. (Stony Brook University, 2005).

25 Jaber, E., Luo, H. B., Li, W. T. & Gersappe, D. Network formation in polymer nanocomposites under shear. *Soft Matter* **7**, 3852-3860, doi:Doi 10.1039/C0sm00990c (2011).

26 Goveas, J. L. & Fredrickson, G. H. Apparent slip at a polymer-polymer interface. *Eur Phys J B* **2**, 79-92 (1998).

27 Macosko, C. W. *et al.* Compatibilizers for melt blending: Premade block copolymers. *Macromolecules* **29**, 5590-5598 (1996).

28 Winey, K. I., Patel, S. S., Larson, R. G. & Watanabe, H. Interdependence of Shear Deformations and Block Copolymer Morphology. *Macromolecules* **26**, 2542-2549 (1993).

29 Lee, E. C., Solomon, M. J. & Muller, S. J. Molecular orientation and deformation of polymer solutions under shear: A flow light scattering study. *Macromolecules* **30**, 7313-7321, doi:Doi 10.1021/Ma9706945 (1997).

30 Wilson, M. R. Molecular dynamics simulations of flexible liquid crystal molecules using a Gay-Berne/Lennard-Jones model. *J Chem Phys* **107**, 8654-8663 (1997).

3.13 Tables

δ	s	ϕ	υ
0.75	0.25	0.02	0.03
0.80	1.0	0.05	0.06
0.90		0.10	0.12
			0.24
			0.48

Table 3.1. Values of miscibility factor, filler size, compatibilizer concentration and shear rate used in this experiment.

3.14 Figures

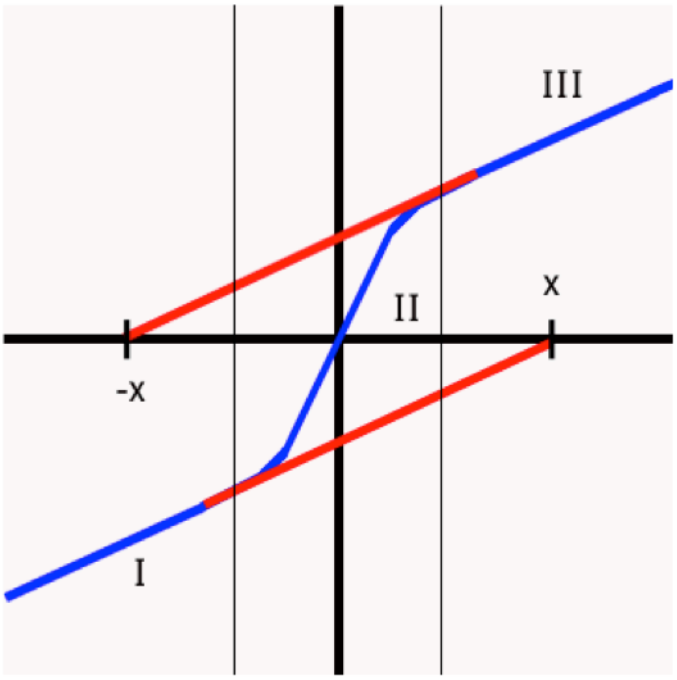

Figure 3.1. A cartoon representation of the extrapolation method for calculating slip as put forth by DeGennes and Brochard.

Chapter 4 – Nanoparticles as Compatibilizers and the Internal Structure of Nanocomposites

4.1 The Homopolymer System

The simulation was begun by first testing the model's efficiency under simple constraints. In the homopolymer case, only a single polymer phase exists, and without the presence of fillers of any size, the polymer chains are capable of moving throughout the system unimpeded. In a simple system under normal shear velocities, viscosity in the system is consistent throughout the bulk; thus, an examination of the velocity profile for such a system should produce a constant, straight-line profile throughout the system while allowing for stick at the wall layers.

Wall stick occurs when the attraction between the wall and the polymer is large enough to prevent slippage[1-3]. While the upper wall is allowed to fluctuate in the z-direction in order to eliminate residual stresses during equilibration runs, the walls are held fixed in the z-direction once the system has reached equilibrium. For a fixed wall system, such as the one presented here, the wall stick phenomena usually persists for any monomer within 2σ of either wall, though that presence is highly dependent on the values of ε_{fw} and ε_{pw}, which for these systems are always equal.

The system was run with imposes velocities ranging from very low (υ=0.03) to very high (υ=0.48), equivalent to those that would later be used upon the dual-phase systems. Figure 4.1 shows the velocity profile of a homopolymer system containing large nanofillers at very high shear (s=1.0, υ=0.48) producing consistent, straight-line profiles as expected. The figure shown displays values from z=-10 to z=10 so as to be consistent with later graphs where the aim is to

concentrate the investigation on the interfacial region and surrounding areas within the bulk. We note that this behavior is very similar to what has been observed in earlier simulations[4].

4.2 The Blended System

The introduction of the attractive coefficient, δ, as a simulative analogue to the Flory-Huggins miscibility parameter, χ, was utilized in order to create the interface within the homopolymer, resulting in phase separation between two types of polymers[5-7]. In this system, the two polymers are otherwise identical, with chain length and monomer size equivalent along both chain types. Since this coefficient is attached to the attractive term within the Lennard-Jones potential, decreasing it increases the phase repulsion within the system.

$$U(r) = 4\varepsilon\left[\left(\frac{\sigma}{r}\right)^{12} - \delta\left(\frac{\sigma}{r}\right)^{6}\right] \quad \textbf{(4.1)}$$

By allowing the two polymers to repel one another, the system will result in a state with two distinct layers, each consisting of only one type of polymer.

For high values of this coefficient ($\delta \geq 0.90$), these layers are distinct with some miscibility still apparent within the interfacial region. These systems are heretofore known throughout the chapter as systems with a well-mixed interface. As the attractive coefficient was decreased, miscibility was decreased along the interface, which led to the formation of small but noticeable gaps along the affected region. For δ=0.80, these gaps are minute but are far more pronounced in the δ=0.75 case, indicating that the miscibility threshold must exist somewhere

between these two values. The δ=0.80 and δ=0.75 systems will be referred to as the partially mixed and sharp interface systems, respectively, so as to allow for clearer verbal demarcations of the various systems produced and described throughout the chapter. Figure 4.2 illustrates the gaps created by phase separation in a few of the blended systems. Snapshot figures were created via the Visual Molecular Dynamics (VMD) software suite[8].

Early test cases in this study indicated that for $0.50<\delta<0.75$, interfacial mixing remains relatively unchanged as the interfacial gaps seem to reach a limit within this region; this realization led to δ={0.50, 0.65, 0.70} being discarded as redundant experiments and values below δ=0.50 not being examined at all. While it may be reasonable to assume that the gaps created are not actually approaching a limit, it is also reasonable to assume that systems at these levels of mixing are best represented by the sharp interface systems.

Since all internal stresses had been eliminated via systemic equilibration, this meant that any additional pressure within the system after phase separation and gap formation could be accounted for by interfacial tension. What is of particular interest to note is how the addition of nanofillers and diblock compatibilizers affect interfacial tension within the system and Table 4.1 shows the baseline interfacial tensions for all systems prior to undergoing shear forces.

The first thing that becomes apparent is that systems containing diblock compatibilizers generally adhere very closely to the interfacial tension within systems with no compatibilizers at all. This stems from the fact that there is no second variety of particles competing for available volume at the interface and thus the system does not have to adjust itself in that regard, leaving any changes in interfacial tension solely up to phase separation. It also becomes evident that the interfacial tension response presented by a given nanofilled system is miscibility-dependent. In systems with a sharp interface, the inclusion of filler, regardless of size, produces a hefty

increase in interfacial tension. However, in systems with higher miscibility factors, the addition of five percent or more large fillers actually decreases initial interfacial tension. Further examination shows that interfacial tension is also more consistent across all values of δ when large fillers are added. The interfacial tension readings for systems with small nanofillers show no such consistency.

4.3 Nanocomposites Under Shear

The introduction of shear forces upon the blended systems indicated that low interfacial miscibility is a large factor in creating interfacial slip. In a binary phase-separated system, slip lengths were measured at values approaching or surpassing the width of the system, the real-world upper limit for slip measurement. Should the slip length surpass the overall width of the system, it indicates that slip along the interface in these systems is relatively infinite with the phases allowed to slide past one another with little to no impedance. The lack of any viable miscibility in systems with a lower value of δ has also decreased the viscosity to such a degree that the two phases slide past one another. This concurs with the results presented by Adhikari in which slip is directly correlated to a drop in viscosity[9]. In the case of the partially mixed systems, slip lengths remain well below the width of the system and thus indicate that some mixing is indeed occurring at the interface. Table 4.2 contains the interfacial slip values for systems lacking nanofillers at all levels of mixing and shear, averaged over several initial states.

The addition of nanofiller particles to the blended systems should increase mixing within the interfacial region. In fact, after discovering the gaps created by low attractive coefficients, it

is natural to assume that some of this space would be occupied by these nanofillers. However, in order to prevent incorrect results based on a faulty assumption, nanofillers were added to a homopolymer system and then allowed to fully disperse, thus creating the nanocomposites. Only after the systems had reached equilibrium were the interfaces introduced and the system equilibrated yet again. In every case, nanofillers were found to segregate to the interface while the gaps seen in the blended system were still persistent though not as pronounced, thereby fulfilling the assumption that the fillers would occupy the empty space created within the interfacial region. Segregation of nanoparticles to the interface was more pronounced in systems with lower attractive coefficients, but nanoparticle segregation was observable even in systems with no visible interfacial gaps. Figures 4.3 and 4.4 show filler concentrations within the areas directly surrounding the interfacial region for select systems.

After the shear process had been completed on each system, it was found that there were only negligible changes in filler and polymer concentrations at any layer within the system as can be seen in Figures 4.5 and 4.6. This suggests that once fillers had infiltrated the interfacial region, they were likely to remain therein unless a more direct force acted upon them. Rather, since the nanofillers were neutral to one another, there was no driving force for coalescence. Also, since the fillers were also neutral to each polymer, neither was there a limit on the motility of these particles other than volumetric restrictions; that is to say that a filler could only move as long as the surrounding polymers allowed it ample space to occupy. Finally, since the only non-intermolecular forces acting upon the system occurred well away from the interface, the nanofiller particles reacted to only a small fraction of the shear forces.

Nevertheless, an examination of the velocity profiles using the method proffered by DeGennes and Brochard indicates that the presence of any volume fraction of nanofiller particles

reduces interfacial slip[10]. While Figures 4.7 and 4.8 illustrate the relationship between small filler addition and slip decrease, a cursory glance at these velocity profiles would indicate that the sharp drops within these profiles get unilaterally smaller as the fillers increase in concentration. Although both large and small fillers are shown to decrease slip length, their efficiency at doing so is different enough so as to warrant separate discussions. This phenomenon appears to have a greater effect as miscibility decreases.

Figure 4.9 shows that for sharp interface systems containing small fillers (δ=0.75, s=0.25), interfacial slip measurements continually decrease as more filler is added. Figure 4.10 is indicative of the ratio when examined against initial slip length. In this form, it indicates over a fifty percent decrease across the board at only two percent concentration. As more fillers are added, slip length steadily decreases – at five percent concentration of small fillers, this decrease is closer to seventy percent and at ten percent concentration, closer to seventy-five percent. What is most striking about this, however, is how consistent the slip reduction factor is in spite of shear velocity. This indicates that in an interfacially phase-separated system, slip reduction can be confidently predicted and yet remains independent of the amount of external stress it may undergo, indicating that these nanofillers can indeed be used as compatibilizers in the future.

However, as δ approaches one, these effects become less pronounced. While the partially mixed systems closely mirror the sharp interface systems, in systems with higher miscibility (δ=0.90), the efficacy of small filler inclusion is reduced (Figures 4.11, 4.12). Despite this revelation, there is a distinct reduction in slip length for most filler concentrations, even at high levels of miscibility. In the moderately interfacially mixed system containing small fillers, we see reductions of about 45% at for two percent concentration, 65% at five percent concentration, and 74% at ten percent while in the mixed phase system, slip decreases rate at only 22, 31, and

54 percent, respectively. At this point, the reader should be aware that in the two percent concentration well-mixed systems (ϕ_f=0.02, δ=0.90), the twenty-two percent reduction is not nearly as consistent as those granted by the sharp interface or partially mixed systems. Overall, this indicates that the inclusion of any amount of filler precipitates a drop in interfacial slip length, regardless of filler size or miscibility. This also suggests that for small fillers, increased concentration results in reduced slip lengths.

However, data from the large filler systems (s=1.0) presents a somewhat different picture (Figures 4.13, 4.14). Although the presence of large fillers does indeed decrease slip length (Figure 4.15), in a sharp interface system, a two percent concentration of large fillers is just as effective as a ten percent concentration of small fillers. It may, in fact, actually be more effective than the ten percent system given that it provides the about the same efficiency in slip reduction on a more consistent basis. In small filler systems, enhancement increases along with filler concentration; this remains true in large filler systems with five percent filler concentration. However, once filler concentration reaches ten percent, slip length reduction begins to decrease. For systems involving large nanofiller particles, the five percent nanofiller systems consistently produce better results than any other large nanofiller system, independent of miscibility (Figures 4.16 - 4.18).

To this end, however, an oddity becomes apparent within the systems with a well-mixed interface: the ten percent filler systems perform consistently worse than both the two and five percent systems except at very low shear. This brings to mind a distinct possibility: for large fillers, the addition of too many fillers forces a spatial issue at the interface, crowding out polymer chains and thus actually reducing polymer chain miscibility while still increasing viscosity at the interface. This also suggests that there may be a limiting concentration threshold

at which slip length reduction turns upward again that is dependent on both filler concentration and blend miscibility. For large filler systems, this threshold, if it exists, resides somewhere between five and ten percent. It should be noted that the percolation threshold as postulated by Jaber also resides within this range; however, it is unclear as yet whether one has anything to do with the other[4,11]. While the existence of such a threshold is not apparent in the small filler systems that are examined within this thesis, it is also possible that the threshold resides above ten percent in such systems.

Overall, the data reflects a few noteworthy ideas. Most importantly, the addition of any amount of nanofillers as compatibilizers is enough to induce slip length reductions and for immiscible blends this reduction is consistent and stable. Secondly, the addition of nanofillers into a blended system with forced repulsion between phases promotes nanofiller segregation to the interface. However, this seems to be limited by available free volume within the region since large-scale aggregation at the interface by nanofiller particles was not readily apparent. Finally, while some support from nanofillers is important to overall slip reduction, the ability for polymer chains to also occupy the region (thus increasing overall miscibility) is equally important for accomplishing slip minimization.

4.4 A Comparison of Nanofiller Particles and Diblock Composites

As this project's primary purpose is to explore whether nanofillers could be used to strengthen polymer blends as effectively as the inclusion of diblocks, a comparative set of diblock-compatibilized blends was created. By selecting preexisting chains within the interfacial

region and relegating half of each chain to that of the opposing phase, the diblocks that were created were less prone to micellization within the bulk[12-14].

Low to moderate concentrations of diblocks were consistently outperformed by the nanofiller systems, regardless of miscibility or shear rate (Figure 4.19, Table 4.3). While nanofiller reduction tended to stay relatively consistent irrespective of shear rate, reduction caused by diblock introduction was far more shear-dependent. In fact, diblock systems tended to perform well in low shear situations but declined as shear rate increased – a trend that continued despite miscibility changes (Figures 4.20 – 4.22). The efficacy of diblock systems was also far more dependent on miscibility. The diblocks' miscibility dependence is intuitive since the diblock is, in essence, a forced miscibility control upon a single chain. While the attractive term of the Lennard-Jones equation has been reduced via the coefficient, δ, the chain remains intact due to the FENE potential within the chain having a much stronger local effect. However, since chain selection and manipulation does not take into account chain orientation in the z-direction, it is possible to have a diblock oriented within the phases opposite its own. This should be self-corrected rather quickly within the system and should only be a factor briefly after creation, but it does shed some light on the diblocks being far more dependent on their own place within the blend and thus more reactive to shear forces acting upon that blend.

In the sharp interface environ, a low concentration of diblocks was able to reduce slip length by at least twenty-five percent, even at high shear; yet, the same concentrations in high miscibility surroundings did not afford any benefit at all, having been rendered a nonfactor. While the five percent diblock systems performed more admirably, offering nearly a twenty percent enhancement at high shear, they were still far outstripped by all of the nanofiller systems, which provided nearly twice the enhancement for nearly every shear rate.

All of this is, inevitably, rendered moot by one factor: the inclusion of high diblock concentrations. Regardless of miscibility or shear rate, all binary polymer systems containing a ten percent diblock concentration resulted in interfacial stick. While some systems including large nanofillers were able to diminish slip by nearly eighty percent, particularly those undergoing low shear rates, none were able to completely counteract shear. A cursory examination of the velocity profiles for diblock systems shows that for ten percent concentrations, a kink forms within the interfacial region (Figures 4.23, 4.24). This kink, under most circumstances, is an area within the velocity profile that acts as an inflection point, but in other cases may manifest itself as a saddle point as well. Regardless of the calculus behind the velocity profile curves, the existence of such a point signifies that at this point the phases – despite their given levels of miscibility – have become fully mixed and inseparable.

What the shape and existence of the kink suggests is that while the methodology provided by DeGennes and Brochard is invaluable for calculating slip length, it works only under the conditions that slip has obviously occurred. Consider, for instance, an example in which the lines that make up Regions I and III in this methodology have a very shallow slope and are separated by a Region II which is, in this case, very small and possesses only a minimal increase in slope as compared to the surrounding regions. In essence, as the velocity profile moves closer and closer to the homopolymer ideal, the regions that define the methodology become more and more indistinguishable. In this case, the extrapolation-subtraction method for determining slip returns a slip length much greater than the actual slip length. A second examination of large filler velocity profiles (Figure 4.25) indicates that at ten percent concentration, such a situation may indeed be presented. Therefore, in a situation such as this, another method must be considered in addition to extrapolation.

Fluid mechanics and calculus provide one possible solution. In the case of flow between two parallel plates, fluid dynamics indicates that velocity of the flow is both indirectly proportional to viscosity and proportional to the pressure gradient[15]. Thus, differentiating the velocity profile would leave a second profile that is also indirectly proportional to viscosity. Since a homopolymer system produces a linear velocity profile, the new curve produced would be a horizontal line equivalent to the slope of the profile. However, it has already been established that in a polymer blend, viscosity decreases along the interfacial region, thus creating slip; a peak in the new curve would indicate a viscous decrease (Figures 4.26, 4.27). Measuring the distance from the peak to the baseline of the new curve produces the slip magnitude, M_s.

A cursory examination of this new measurement indicates a strong, positive linear relationship between slip magnitude and shear velocity (Figures 4.28, 4.29). This is in direct contrast to the curves produced by the slip length in which slip length seemed to decrease as velocity increased; there is, however, a reason for this. As was previously mentioned, the slip length measurements, especially in the case of the pure blended systems, are not in the realm of the existing systems, as they are much larger than the total width of the systems. Due to the very low viscosity at the interface, the blended layers slide past one another with little to no impedance, resulting in infinite slip. Although the extrapolation method has become the accepted measurement of slip length, we have demonstrated that the methodology has a limited scope. As velocity increases, one would expect more, not less, slip to occur; hence, slip magnitude might give a better indicator of what is actually occurring within the system.

Examining the ratio of slip magnitude in filled systems to unfilled systems suggests yet again that the benefit provided by the addition of nanoparticles is consistent and predictable (Figures 4.30 - 4.33, Table 4.4). This is a byproduct of the linearity between velocity and slip

magnitude. Additionally, the new methodology suggests that this consistency extends past the interfacially phase-separated systems and into the moderately interfacially mixed systems as well. It also indicates that with the exception of the mixed phase systems, predictability in diblock-compatibilized systems likewise exists.

Inspecting the differentiated velocity profiles for diblocks incurs two notable observations (Figure 4.34). The most obvious is that at ten percent diblock inclusion, the differentiated velocity profile transforms from one peak to two peaks and a valley. This new area is consistent with the increased viscosity one would expect with a kink, indicating stick. This also suggests that the viscosity immediately outside of the kink possesses a lower viscosity than the surrounding area but does not cause an issue for slip or fracture within any of the observed conditions. The second observation is that at five percent diblock inclusion, the differentiated velocity profile also contains a transformed peak. While a wider peak is observed in the interfacially phase-separated systems, as miscibility increases, the peak begins to plateau. Additionally, the peaks have widened, regardless of miscibility, which indicates that diblock inclusion is potentially increasing the reach of the interfacial region. Similar effects are not seen at two percent diblock inclusion or in any of the arrangements that contain nanofiller particles. This same interfacial expansion is also seen at the ten percent condition but is overshadowed by the valley indicative of stick.

While these observations may influence bias when selecting compatibilizers, it is worth remembering that diblocks within the bulk are prone to micellization, in addition to being expensive and difficult to control. Tables 4.3 and 4.4 reemphasize the slip length and slip magnitude enhancements provided by all systems, divided by miscibility, by way of efficiency percentages; thus, a rating of 0.21 indicates that the slip length of that system reduces slip length

to twenty-one percent of its non-compatibilized counterpart. After reexamining the data in this format, and considering the difficulties presented by the inclusion of diblocks, we can conclude that the large filler systems at five percent concentration or more (s=1.0, ϕ_f=0.05 or 0.10), provide the most consistent, cost-effective method of reducing slip, independent of miscibility or shear rates. It should be noted here, though, that the data trends of the small nanofiller addition (s=0.25) indicate that perhaps the addition of even more nanofillers would be just as beneficial. However, the conditions examined within this study do not fit these parameters and such an examination warrants its own separate study to determine whether there are limiting factors such as interfacial crowding or nanofiller aggregation that may curb slip enhancement.

4.5 Defining and Understanding Internal Structural Development Within Nanocomposites

Yet knowing that nanofillers contribute to strength enhancement in blends does not begin to describe how, in fact, strengthening occurs; and, that was a question worth exploring that became the focus of this research. In systems with fillers not on the nanoscale, most strengthening benefits presented can be attributed to surface area interactions[16]. However, this is something that can be ruled out as a ten percent concentration of small fillers has nearly six and a half times as much surface area as a two percent concentration of large fillers and yet performance in either system is quite similar, regardless of shear rate or miscibility. It is then safe to assume that if surface area interactions are responsible for reducing slip, they must only account for a portion of reduction with the remainder attributable to other as yet unidentified means. But what are these other means? It is at this point that we postulate that there must be

some sort of internal microstructure within the interfacial region acting as a counterbalance to the shear forces. Since diblocks had already been used to compatibilize blends and as the control group for examining the efficacy of nanofillers as compatibilizers, it became necessary to investigate the possibility that the structures being created *in situ* were actually something resembling a diblock.

In order to examine the possibility of these *in situ* diblocks, the first step was to define in what form such a diblock would take and what would qualify such a structure as mechanically relevant to preventing shear. An *in situ* diblock – heretofore known as an ISD so as to categorically separate them from the actual diblocks that were used as our control group – is defined as at least two chains of opposing phase that remain "attached" to a given nanofiller throughout the shear process. Next, attachment was defined by a cutoff distance, r_c, which was set at $2^{1/6}\sigma$, the distance at which the Lennard-Jones potential reaches its minimum. In addition, the ISD was regarded as mechanically relevant if and only if: at least two chains of opposing phase were attached to the same given nanofiller; the structure was present prior to shear and remained connected throughout the shear process; and, the structure remained within the interfacial region throughout the shear process. In essence, a mechanically relevant ISD had to remain an ISD within the interfacial region throughout shear.

By focusing on the interfacial region, knowing that the systems being examined resided below the percolation threshold, the focus could be kept on the region directly affected by slip. Before investigating these potential formations directly, it was first necessary to determine their feasibility by looking at the interfacial tension and chain orientation within the nanofilled systems in order to compare them to the diblock-compatibilized systems.

4.6 Interfacial Tension in Compatibilized Blends

As was discussed in Chapter Three, the nanofilled blends began as nanofilled homopolymers in which the nanofillers were first allowed to disperse throughout, governed by neutrality to the polymer chains surrounding them. Since these filled homopolymer systems were then allowed to come to full equilibrium, no internal pressure remained within the systems. As such, once the attractive coefficient, δ, was introduced and the blend created, all remaining pressure within the system was indicative of the interfacial tension.

Understanding the nanofillers' contribution to interfacial tension could be the key to finding that ideal system wherein nanoparticle configurations resist shear by acting like diblock copolymers. Examining the diblock response to interfacial tension offers a few guidelines for what characteristics such a nanofilled system should possess (Figure 4.35). Generally, increases in miscibility or decreases in velocity both lead to increases in interfacial tension. Specifically, systems containing diblock copolymer hew closely to the unfilled blended environments, with only slight increases under larger shear forces. Interfacial tension in the diblock systems is also directly tied to increases in compatibilizer concentration. Having already examined and discussed the changes presented by the differentiated velocity profiles of higher-concentration diblock systems, it is safe to assume that this is, at the very least, related to the widening of the interfacial region.

Hence, using the diblock systems as a guideline, the ideal nanofilled blend should not drastically change the interfacial tension of a system and increase slightly as filler concentration increases. However, for systems containing small nanofiller particles (s=0.25), neither of these criteria is met (Figure 4.36). The introduction of the nanofillers results in a drastic increase of interfacial tension. This increase is also not consistent with an increase in nanofiller

concentration as the five percent systems are consistently lower than both the two and ten percent arrangements. As miscibility increases, the five percent systems also move closer to mirroring the interfacial tension of the unfilled blend. At high miscibility, the interfacial tension of the five percent systems is actually lower than that of the unfilled system though there is a fair amount of overlap. This, however, only leads to a decrease in slip on par with the two-percent diblock system, which was only somewhat effective at reducing slip.

The large nanofiller (s=1.0) systems present similar results (Figure 4.37). While large filler addition presents increases in interfacial tension that are not nearly as drastic as those seen in the smaller nanofiller systems, these escalations are still not consistent with concentration increases as the introduction of five percent large nanofillers consistently produces more interfacial tension than either the two or ten percent systems. In fact, these systems hew rather closely to that of the unfilled systems. As miscibility increases, interfacial tension in all large filler systems actually decreases, and in the high miscibility (δ=0.90) systems, the interfacial tension presented by all concentrations is lower than the baseline. It should be noted, however, that the five and ten percent large filler systems both consistently decrease slip more than the five percent diblock systems at low and moderate miscibility. This indicates that a decrease in slip length has less to do with interfacial tension than it does with miscibility and filler mobility.

4.7 Chain Orientation Within Sheared Nanocomposites

As a homopolymer system undergoes shear, the system must react appropriately to keep from deforming to the point of fracture. The chains in such a system align themselves in the direction of shear until the force is great enough to force a break in the bulk. Alignment can most easily be measured via chain orientation. However, it should be noted that in the case of the homopolymer systems examined herein, never were any of those system put under such strain as to force fracture, so this in itself should not be cause for concern.

In a system at equilibrium, chain orientation should be more or less random and thus should precipitate an orientation angle of about forty-five degrees ($\theta_x=\pi/4$), since the chain should follow a roughly spherical path, having been not particularly extended in any direction[17]. As shear is introduced, the angle decreases proportionally to the shear force present; as such, a system undergoing very high shear would have an orientation angle near zero.

In terms of the orientation tensor, P_x, a forty-five degree angle, $\theta_x=\pi/4$, corresponds to $P_x=1/4$. Testing the limits of the tensor equation gives us a maximum of $P_x=1$ at $\theta_x=0$ and minimum of $P_x=-1/2$ at $\theta_x=\pi/2$ with a periodicity of π. This indicates that within these boundaries, the value of P_x is inversely proportional to orientation angle along these bounds, as P_x increases toward one as θ_x decreases and decreases as the angle increases. It also bears repeating that P_x is an ensemble average for all chains within a given layer, thus preventing outliers from heavily affecting the results.

However, we are primarily interested in the ratio of tensor in the interfacial layer against the tensor in the homopolymer system, $P_R=P_x/P_h^*$. As P_R approaches zero, it indicates the presence of slip since the phases are are allowed to move along one another with little resistance; however, as P_R approaches one, it indicates that the structural resistance has increased. A P_R

value of one indicates that the blended sample has reached the same structural efficiency as that of the homopolymer, essentially negating any effects caused by the creation of the interface. It can be expected that – due to the formation of diblock compatibilizers or other possible structures *in situ* – the diblock systems should return, at least for the cases in which stick appeared, a P_R value of nearly one.

Reviewing the orientation results for small nanofiller inclusion, one thing becomes clear: while the inclusion of nanoparticles does usually increase the value of P_R, inclusion at the given concentrations does not come close to replicating the orientation angles produced by their respective homopolymer systems (Figures 4.38, 4.39). It is also apparent that an increase in miscibility results in a better return of P_R. Moreover, the amount of filler added is not a consistent predictor for the orientation ratio. In spite of that, generally, the ten percent small nanofiller systems tended to give the best results. It should be noted that there are cases where nanofiller inclusion actually produces worse results, though this is likely due to fewer chains residing within the interfacial region since only chains with a center of mass within the region were considered in those cases.

Alternatively, large filler addition yielded remarkable results in respect to P_R (Figures 4.40, 4.41). In low miscibility systems under very low shear, ten percent filler inclusion yields an orientation rating of about 0.96 and as the miscibility factor grows, the rating drops only slightly to around 0.94. While this sort of response is not applicable along all shear rates, as the orientation rating drops with an increase in shear velocity, response rates generally reside at or above 0.90, marking a difference of less than five degrees. As with small filler inclusion, the orientation rating generally improves with miscibility.

However, there is no evidence to suggest that higher filler concentration would necessarily result in a higher orientation rating. While it may be appropriate in the case of the smaller nanofillers, higher numbers of large nanofiller risk crowding chains out of the interfacial region should the internal energy of the system allow for that possibility. As the nanofillers are neutral to one another and the chains, it is possible that too many fillers at the interface would increase slip, thus negating the effects this project is attempting to achieve. As it stands, very little is still known about the structures being created at the interface and an attempt to understand these possible architectures a bit better is required.

4.8 Examining *In Situ* Structures Within Nanocomposites

The initial hypothesis that there are diblocks being formed *in situ* in nanofilled blends under shear stemmed from the idea that a diblock copolymer is nothing more than forced polymer blending within a single chain. While these chains may take many forms of arrangement, the most common are alternating monomers of each type or a dual-ended chain type, the latter being the one chosen for this project. Within this chain reside two halves of opposing type held together by intermolecular forces which are far stronger than the chain interaction forces governing motion within the overall blend. Since diblock copolymers have long been used to compatibilize blends despite their limitations, once it was discovered that nanofiller particles could also be used to compatibilize blends, the search for the mechanism by which this occurs began and this led to the formation of the hypothesis that nanofillers could actually be used to form diblocks *in situ*.

The search for mechanically relevant *in situ* diblocks revealed that while ISDs are, in fact, created within the system as it undergoes shear, none fit the prescribed criteria that would qualify as mechanically relevant. By design, chains were not allowed to qualify if the center of mass resided outside of the interfacial region. While this was effective at making sure the examined chains were always relevant to the interface, this left very few chains to be inspected, even when the targeted interfacial region was expanded slightly. Generally, this led to fewer than fifteen selected chains within the interfacial region, with most of the available volume left to be occupied by the nanofillers. This decrease in the number of interfacial chains was especially evident in the systems containing large filler particles (s=1.0). While this was not the first indication of nanofiller segregation at the interface, it is the first evidence that nanofillers could be responsible for pushing chains outside of the interface by restricting the available empty volume necessary for mobility. With only a few chains available for interaction, the search for *in situ* diblocks became increasingly futile, as chains attached, detached, and reattached to nanofillers with little consistency.

Over the course of this experiment it became apparent that the proposed hypothesis is inherently flawed. As was mentioned earlier in the chapter, an *in situ* diblock was designated as being mechanically relevant if two chains of opposing type remained attached to a given nanofiller throughout the entirety of the shear process. Intermolecular forces hold diblock copolymers together and yet the nanofillers were created specifically to be neutral to either chain type. Without a preference to either type, and with ε_{fp}, the Lennard-Jones coefficient that governs fluid-particle interaction being only twice that of the particle-particle or fluid-fluid coefficients, there is no guarantee that chains have any reason to remain within the attachment region. The FENE potential that holds the diblock copolymers together is much stronger than the Lennard-

Jones potential that governs their surroundings, and this is just not the case within the nanofilled environments. So if the *in situ* diblocks can be ruled out, the mechanism by which nanofillers reduce slip must still be sought out.

As shown by Jaber, fully spanning percolated networks do not begin until after five percent nanofiller inclusion[4]. While that may factor into why the ten percent filler concentration systems perform best in the majority of situations, it does not explain why nanofiller concentrations below the percolation threshold can also reduce slip by more than sixty percent. However, Jaber took into account only percolated networks that spanned from the top wall to bottom wall within the simulation; this does not take into account any partially spanning networks that could occur in the dimensions governed by periodic boundary conditions. This leaves the possibility that while the systems being analyzed within may be operating under the percolation threshold, smaller networks may be forming within the interfacial region that can account for the slip reduction presented by these systems. Such networks would not be determined by the attachment to particular nanofillers chains like the ISDs but rather by attachment to the network as a whole. This allows flexibility within the network without destroying the integrity of said network.

By defining each nanofiller within the interfacial region as its own network and using the same attachment radius as defined by the ISDs, any chain attached to a particular nanofiller would automatically register as a member chain of that network. Should a chain find itself attached to more than one nanofiller both the chains and nanofillers would default to lowest identified network. For the purposes of this inspection, direct chain-chain and filler-filler attachments were not considered, as these would be accounted for by the chain-filler attachment while also reducing the possibility of network misidentification. In order to increase the number

of chains available for examination, it was also decided that chains need not have a center of mass residing within the interfacial region, instead needing only to have part of the chain within the targeted region, and also that the targeted region should remain slightly expanded. This idea is supported by the interfacial widening that occurs in the diblock-assisted systems as described earlier in the chapter. This opened up the investigation to about thirty to thirty-six chains per system, minimizing the effect of interfacial crowding.

Retaining the previously determined cutoff distance of $2^{1/6}$, the network results were promising. All systems had a few networks develop but all were dominated by one larger network. While smaller networks tended to consist of one or two nanofillers and the odd chain, the larger networks would consist of nearly ninety-five percent of all particles within the region. As indicated by Figures 4.42 and 4.43, systems containing smaller fillers tended to produce more networking groups though those groups were usually in the form of a dominant group and several much smaller offshoots. Systems utilizing large fillers, on the other hand, were more likely to contain only a single group. In either size, a higher concentration of filler usually resulted in a larger number of offshoot groups, though these were still relatively rare. An examination of the number of the fillers in the largest group indicated that over time these numbers fluctuated by only a couple of fillers throughout the shear process.

Thus, we can say with confidence that the mechanism by which nanofillers enhance shear thickening is via *in situ* percolated networks rather than the formation of *in situ* diblocks. While it may behoove the author to apply the more lax restrictions to the search for *in situ* diblocks that would indicate that given the prior restrictions the diblocks (should they exist) would be more important to the area directly surrounding the interfacial region, rather than the interfacial region itself. As this is highly unlikely, this line of thinking will remain a strictly hypothetical exercise.

4.9 A Summary of Conclusions

In this chapter, nanofilled homopolymers were created and tested in order to establish that the model did provide a straight-line velocity profile as expected. After determining the homopolymers' structural integrity and the utility of the simulation process used, these systems were then split into blends and reequilibrated. The new blended systems were then sheared and examined to determine the nanofillers' ability to reduce interfacial slip. The results showed that nanofillers could in fact be utilized to compatibilize blends, regardless of filler size or concentration, or blend miscibility. Generally, a higher filler concentration, larger nanofillers, and/or higher miscibility will lead to an increase in slip length reduction.

When compared to systems containing diblock copolymers as compatibilizers, the nanofiller systems outperformed their diblock counterparts at all but the highest concentrations. However, a closer examination of the velocity profiles for the nanofiller systems suggested that the extrapolation method produced by DeGennes and Brochard decreased in accuracy once the difference in the regions within the profile that are used to determine slip became more subtle. This led to using the differentiated velocity profile to determine slip magnitude, which in turn led to more reasonable results in the systems with higher miscibility. It was also determined that at low miscibility, slip reduction in nanofilled blends was consistent and predictable when compared to similar systems lacking fillers. Finally, it was shown that the development of a kink in a diblock-inclusive system was directly related to diblock concentration and an expansion of the interfacial region within these systems, a phenomenon not detected in the nanofilled systems.

In the course of examining whether the formation of *in situ* diblock structures could offer an explanation for slip decrease in nanofilled systems, the differentiated velocity profiles, chain orientation, and interfacial tension did not at all resemble those of the diblock-inclusive systems.

It was also determined that the addition of nanofillers, particularly large nanofillers, caused chain migration out of the interfacial region via interfacial crowding. As such, the idea that diblocks were being formed *in situ* was proven to be false. Further testing revealed that percolated networks of nanofillers and chains were ultimately responsible for slip reduction.

Having revealed that nanofillers can be used to strengthen polymer blends via the creation of small percolated networks, the next chapter will focus on whether nanofillers can also be used to reduce polymer flammability and ignition.

4.10 References

1 Larson, R. G. *The structure and rheology of complex fluids*. (Oxford University Press, 1999).

2 Leonov, A. I. A linear model of the stick-slip phenomena in polymer flow in rheometers. *Rheol Acta* **23**, 591-600, doi:10.1007/bf01438799 (1984).

3 Tanner, R. I. Partial Wall Slip in Polymer Flow. *Industrial & Engineering Chemistry Research* **33**, 2434-2436, doi:10.1021/ie00034a027 (1994).

4 Jaber, E. *Rheology and dynamics in polymeric nano-composites*. (Stony Brook University, 2005).

5 Grest, G. S., Lacasse, M. D., Kremer, K. & Gupta, A. M. Efficient continuum model for simulating polymer blends and copolymers. *J Chem Phys* **105**, 10583-10594 (1996).

6 Barsky, S. & Robbins, M. O. Bulk and interfacial shear thinning of immiscible polymers. *Phys Rev E* **65**, -, doi:Artn 021808Doi 10.1103/Physreve.65.021808 (2002).

7 Barsky, S. & Robbins, M. O. Molecular dynamics study of slip at the interface between immiscible polymers. *Phys Rev E* **6302**, -, doi:Artn 021801 (2001).

8 Humphrey, W., Dalke, A. & Schulten, K. VMD: Visual molecular dynamics. *J Mol Graph Model* **14**, 33-38, doi:Doi 10.1016/0263-7855(96)00018-5 (1996).

9 Adhikari, N. P. & Goveas, J. L. Effects of slip on the viscosity of polymer melts. *J Polym Sci Pol Phys* **42**, 1888-1904, doi:Doi 10.1002/Polb.20066 (2004).

10 Brochard, F. & Degennes, P. G. Shear-Dependent Slippage at a Polymer Solid Interface. *Langmuir* **8**, 3033-3037, doi:Doi 10.1021/La00048a030 (1992).

11 Jaber, E., Luo, H. B., Li, W. T. & Gersappe, D. Network formation in polymer nanocomposites under shear. *Soft Matter* **7**, 3852-3860, doi:Doi 10.1039/C0sm00990c (2011).

12 Gohy, J.-F. in *Block Copolymers II* Vol. 190 *Advances in Polymer Science* (ed Volker Abetz) Ch. 48, 65-136 (Springer Berlin Heidelberg, 2005).

13 Gnichwitz, J. F. *et al.* Efficient Synthetic Access to Cationic Dendrons and Their Application for ZnO Nanoparticles Surface Functionalization: New Building Blocks for Dye-Sensitized Solar Cells. *J Am Chem Soc* **132**, 17910-17920, doi:Doi 10.1021/Ja106076h (2010).

14 Riess, G. Micellization of block copolymers. *Prog Polym Sci* **28**, 1107-1170, doi:http://dx.doi.org/10.1016/S0079-6700(03)00015-7 (2003).

15 *A Textbook of Fluid Mechanics*. (Laxmi Publications Pvt Limited, 2005).

16 Beatty, C. L. Evidence of interaction of fillers with matrix polymers via transition maps. *Polym Composite* **5**, 319-326, doi:10.1002/pc.750050412 (1984).

17 Ilnytskyi, J. M. & Wilson, M. R. Molecular models in computer simulation of liquid crystals. *J Mol Liq* **92**, 21-28 (2001).

4.11 Tables

	ϕ_f (%)	δ=0.75	δ=0.80	δ=0.90
	0	9.5 ± 1.0	34.1 ± 0.9	83.5 ± 2.0
nfp, s=0.25	**2**	62.1 ± 1.9	78.3 ± 1.1	105.3 ± 1.1
	5	47.4 ± 3.2	53.7 ± 1.2	78.9 ± 1.8
	10	126.7 ± 0.7	134.3 ± 2.5	145.8 ± 1.6
nfp, s=1.0	**2**	70.3 ± 6.1	64.1 ± 5.9	67.9 + 3.6
	5	17.7 ± 4.1	20.3 ± 2.5	21.8 ± 2.4
	10	28.2 ± 0.7	27.7 ± 1.4	30.6 ± 2.7
diblock	**2**	9.2 ± 1.3	33.9 ± 3.3	79.8 ± 1.3
	5	11.3 ± 1.6	35.6 ± 1.2	76.7 ± 1.4
	10	14.1 ± 0.8	34.8 ± 1.6	81.0 ± 3.4

Table 4.1. Equilibrated pre-shear interfacial tension for all available systems.

υ	δ=0.75	δ=0.80	δ=0.90
0.03	37.4 ± 3.5	27.3 ± 0.7	11.6 ± 0.7
0.06	24.6 ± 1.8	15.6 ± 0.6	6.5 ± 1.2
0.12	18.1 ± 0.3	11.1 ± 0.8	4.3 ± 0.1
0.24	11.5 ± 0.6	8.2 ± 0.1	3.1 ± 0.4
0.48	9.4 ± 0.1	6.4 ± 0.3	2.4 ± 0.1

Table 4.2. Slip lengths for systems sans nanofillers or diblocks at various levels of miscibility and shear.

	ϕ_f (%)	δ=0.75	δ=0.80	δ=0.90
nfp, s=0.25	2	0.46 ± 0.02	0.54 ± 0.02	0.78 ± 0.12
	5	0.30 ± 0.02	0.35 ± 0.04	0.59 ± 0.08
	10	0.23 ± 0.02	0.27 ± 0.05	0.47 ± 0.08
nfp, s=1.0	2	0.21 ± 0.03	0.31 ± 0.04	0.50 ± 0.04
	5	0.17 ± 0.03	0.23 ± 0.04	0.38 ± 0.11
	10	0.20 ± 0.06	0.28 ± 0.11	0.59 ± 0.15
diblock	2	0.70 ± 0.10	0.78 ± 0.06	0.89 ± 0.21
	5	0.35 ± 0.09	0.45 ± 0.10	0.69 ± 0.18
	10	0 ± 0	0 ± 0	0 ± 0

Table 4.3. Velocity independent slip length ratios of compatibilized systems versus systems lacking compatibilizers.

	ϕ_f (%)	δ=0.75	δ=0.80	δ=0.90
nfp, s=0.25	2	0.54 ± 0.02	0.59 ± 0.06	0.79 ± 0.17
	5	0.35 ± 0.04	0.41 ± 0.03	0.61 ± 0.11
	10	0.26 ± 0.03	0.29 ± 0.03	0.42 ± 0.08
nfp, s=1.0	2	0.21 ± 0.04	0.31 ± 0.04	0.44 ± 0.06
	5	0.19 ± 0.03	0.19 ± 0.04	0.30 ± 0.10
	10	0.13 ± 0.06	0.13 ± 0.04	0.21 ± 0.24
diblock	2	0.56 ± 0.04	0.63 ± 0.03	0.65 ± 0.07
	5	0.54 ± 0.02	0.26 ± 0.02	0.31 ± 0.08
	10	-0.16 ± 0.03	-0.14 ± 0.08	-0.26 ± 0.19

Table 4.4. Velocity independent slip magnitude ratios of compatibilized systems versus systems lacking compatibilizers.

4.12 Figures

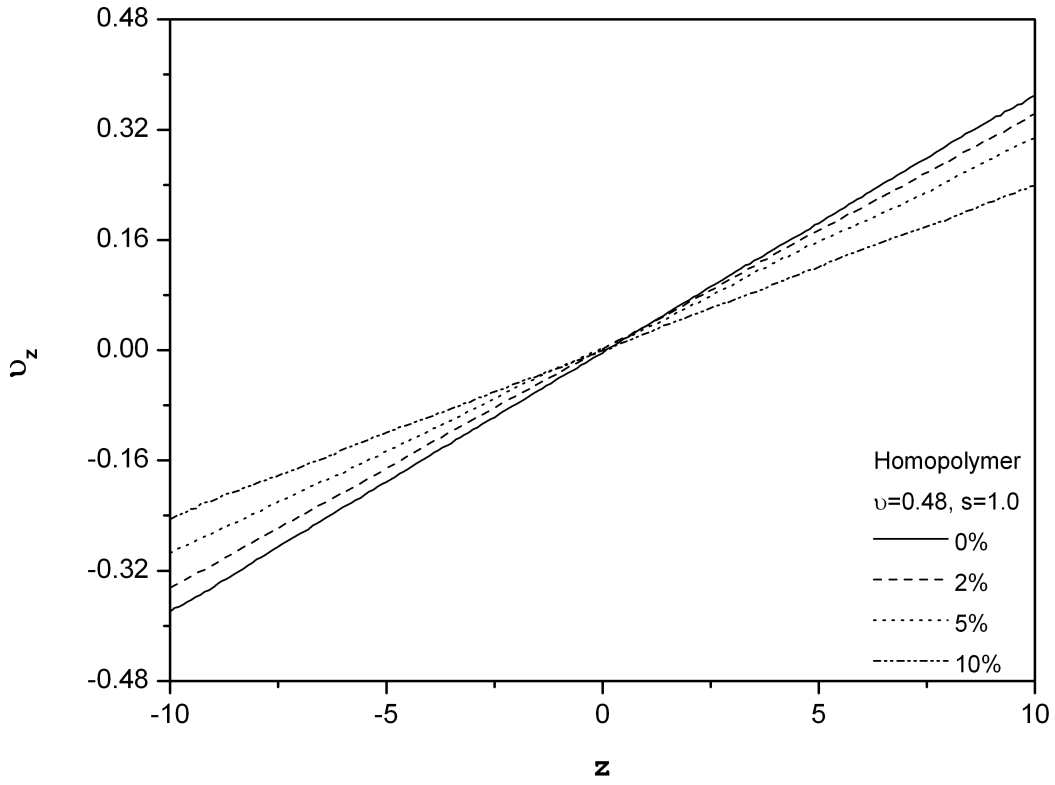

Figure 4.1. Velocity profile of a homopolymer system containing large nanofillers at very high shear.

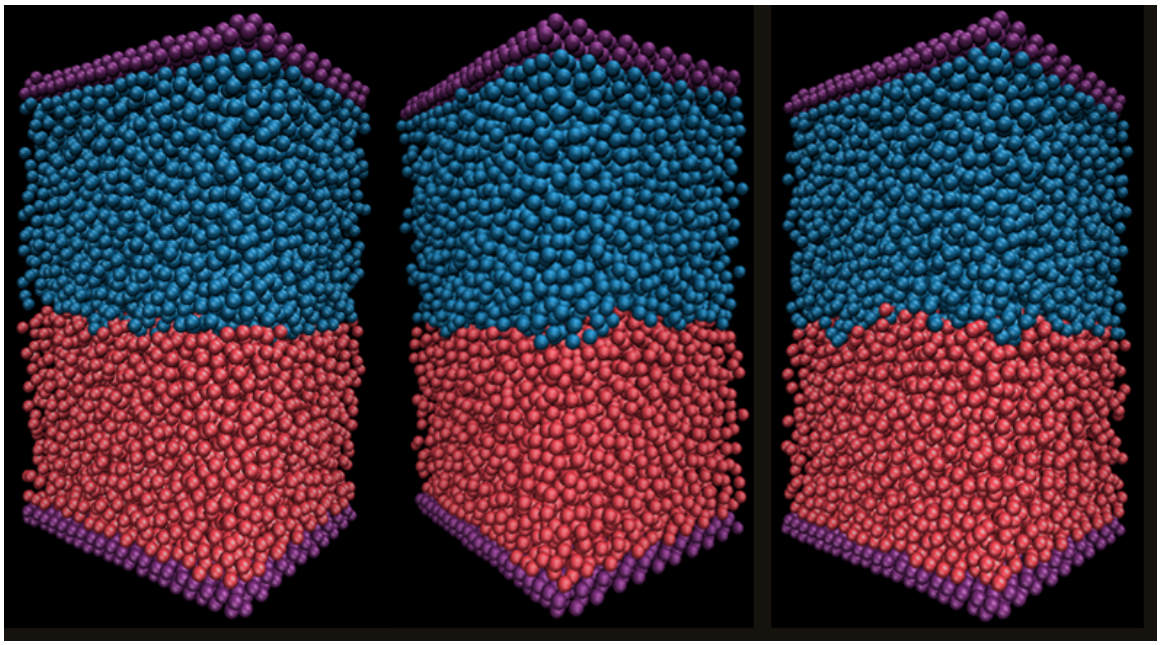

Figure 4.2. Snapshots of system with (left to right) slightly miscible, moderately miscible, and highly miscible interfaces at equilibrium.

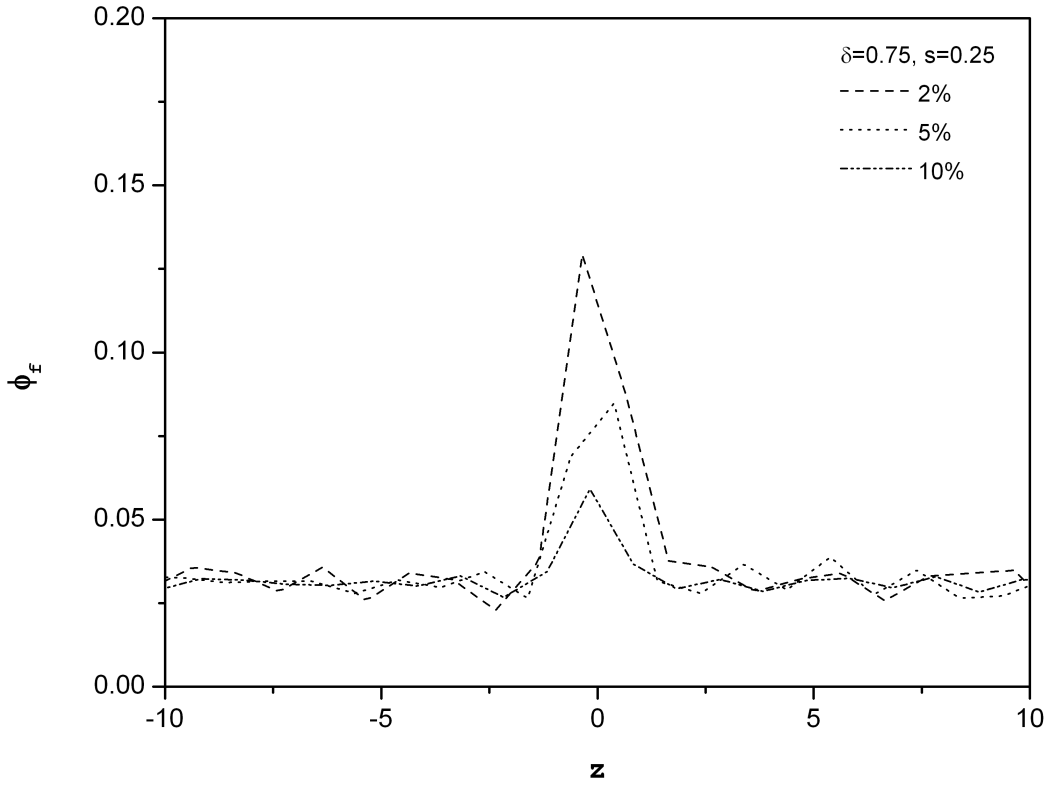

Figure 4.3. Equilibrium nanofiller distribution in a system containing small nanofillers and a slightly miscible interface.

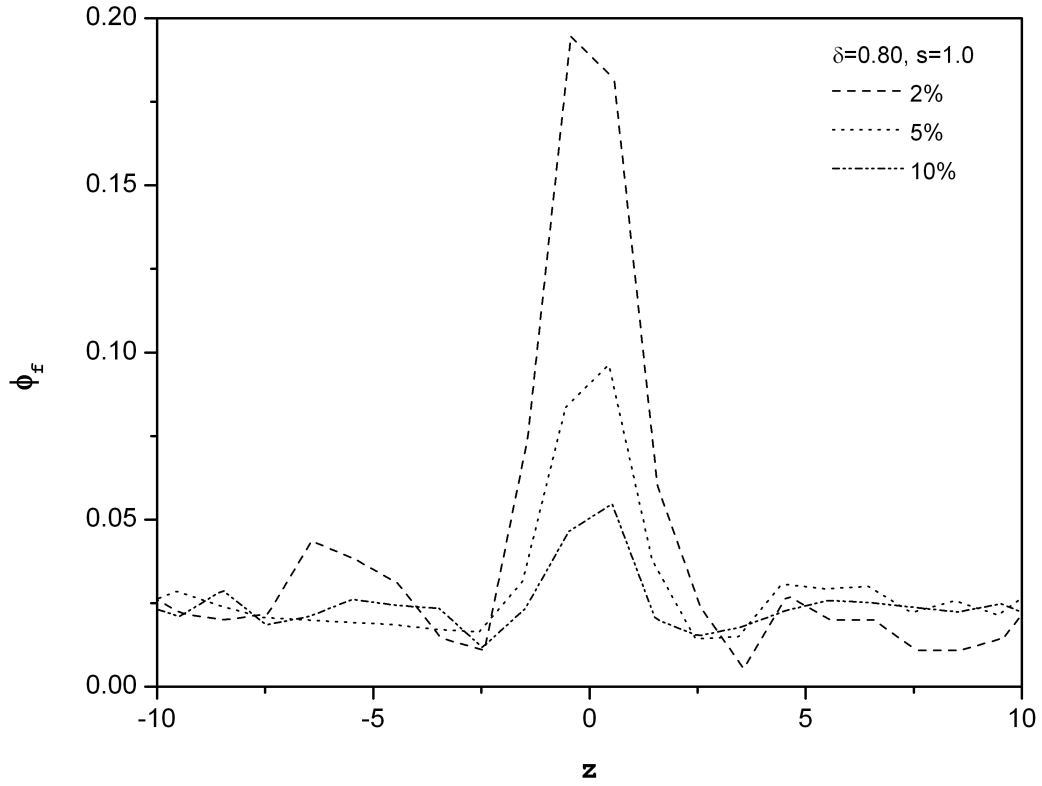

Figure 4.4. Equilibrium nanofiller distribution in a system containing large nanofillers and a moderately miscible interface.

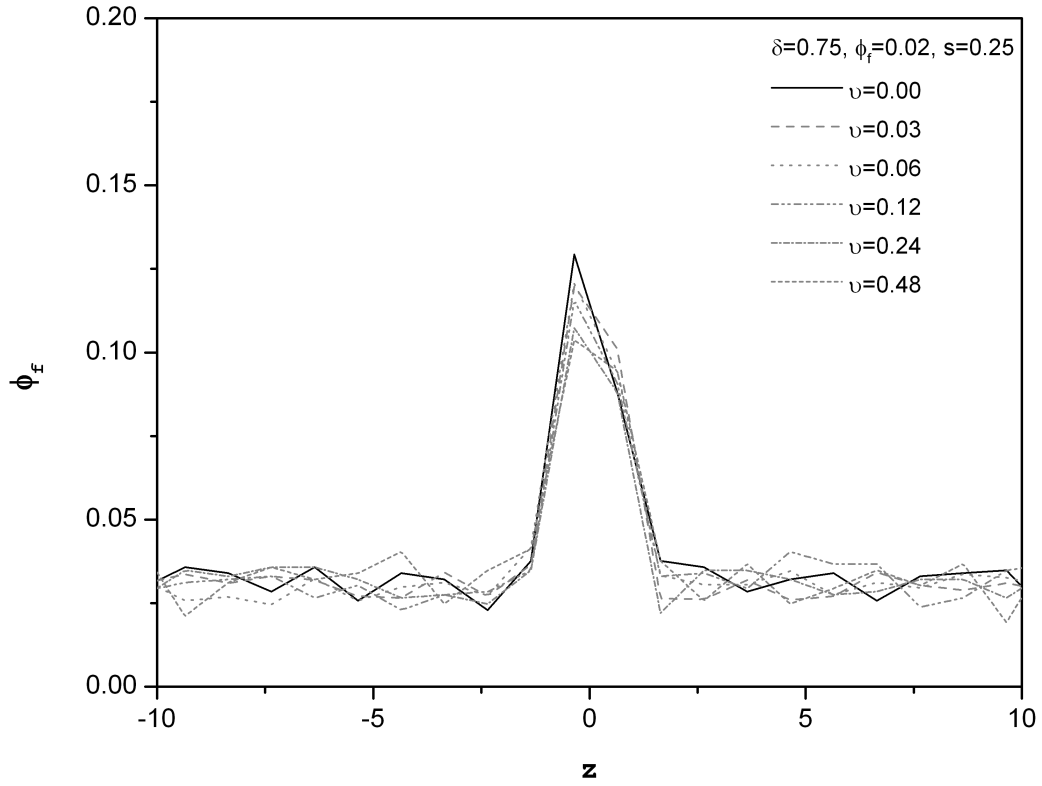

Figure 4.5. Nanofiller distribution under shear in a system containing small nanofillers at two percent concentration and a slightly miscible interface.

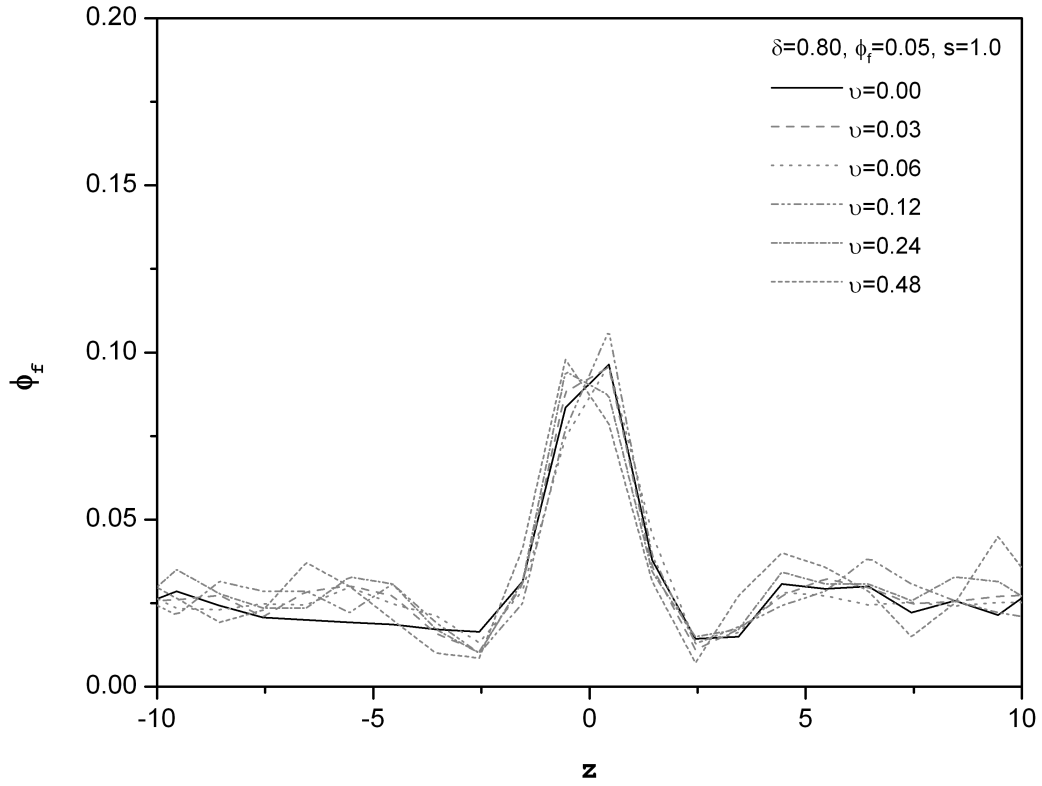

Figure 4.6. Nanofiller distribution under shear in a system containing large nanofillers at five percent concentration and a moderately miscible interface.

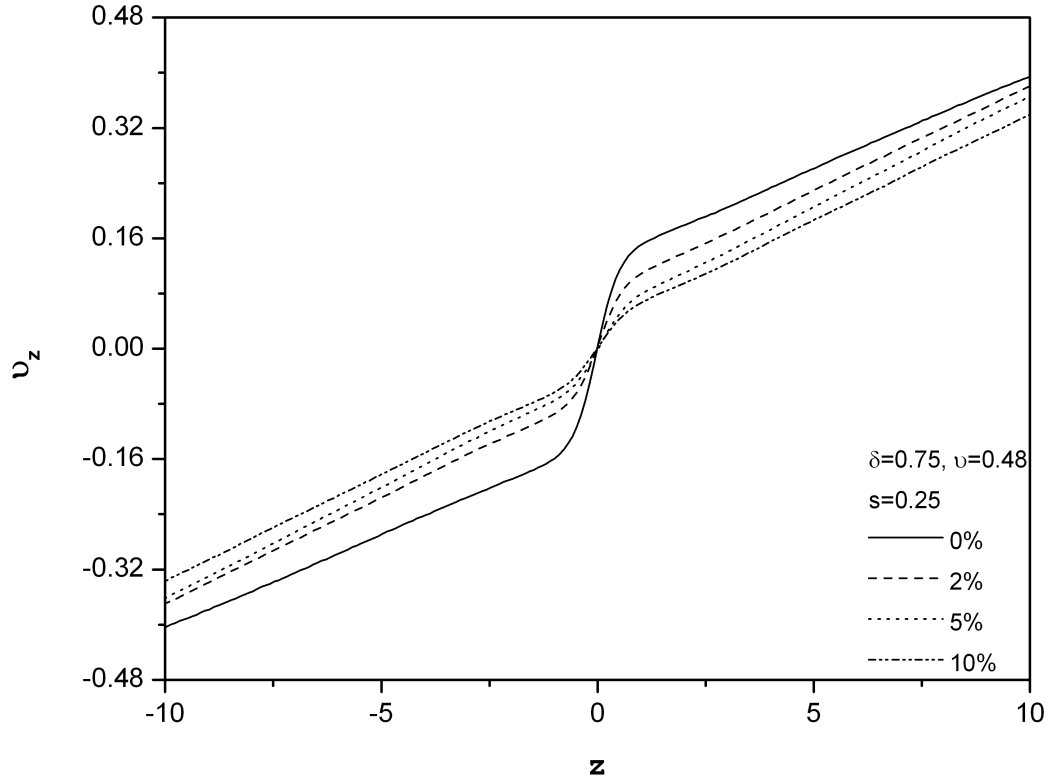

Figure 4.7. Velocity profile for a system containing small nanofillers and a slightly miscible interface, undergoing very high shear.

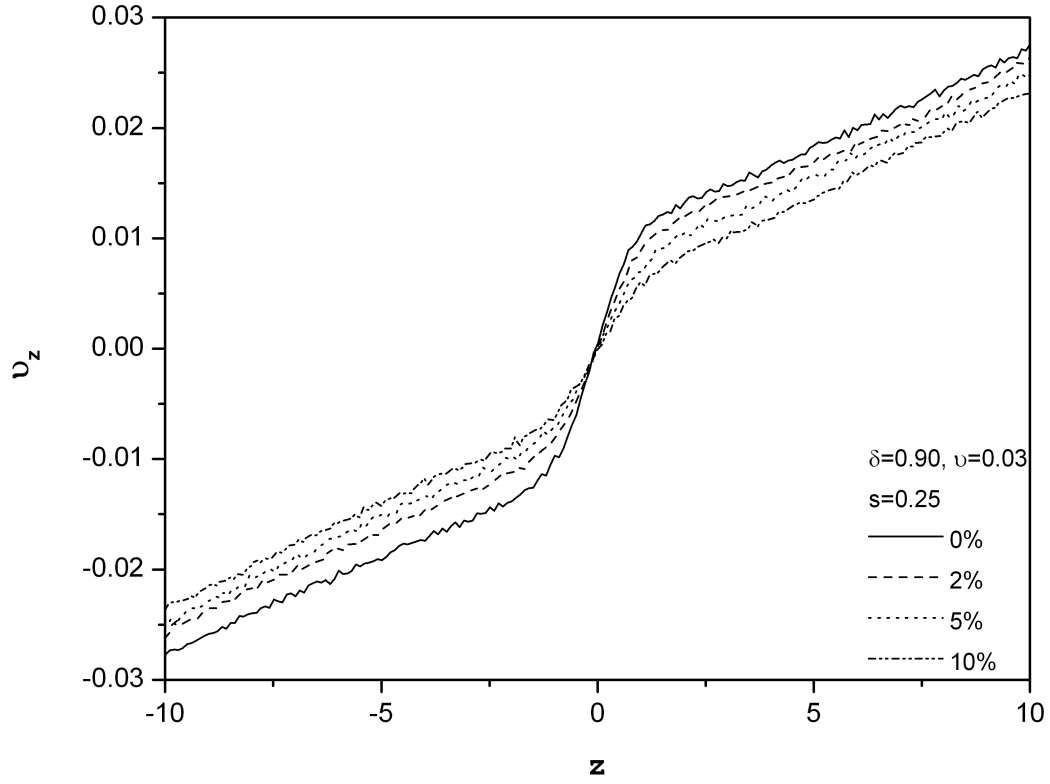

Figure 4.8. Velocity profile for a system containing small nanofillers and a moderately miscible interface, undergoing very low shear.

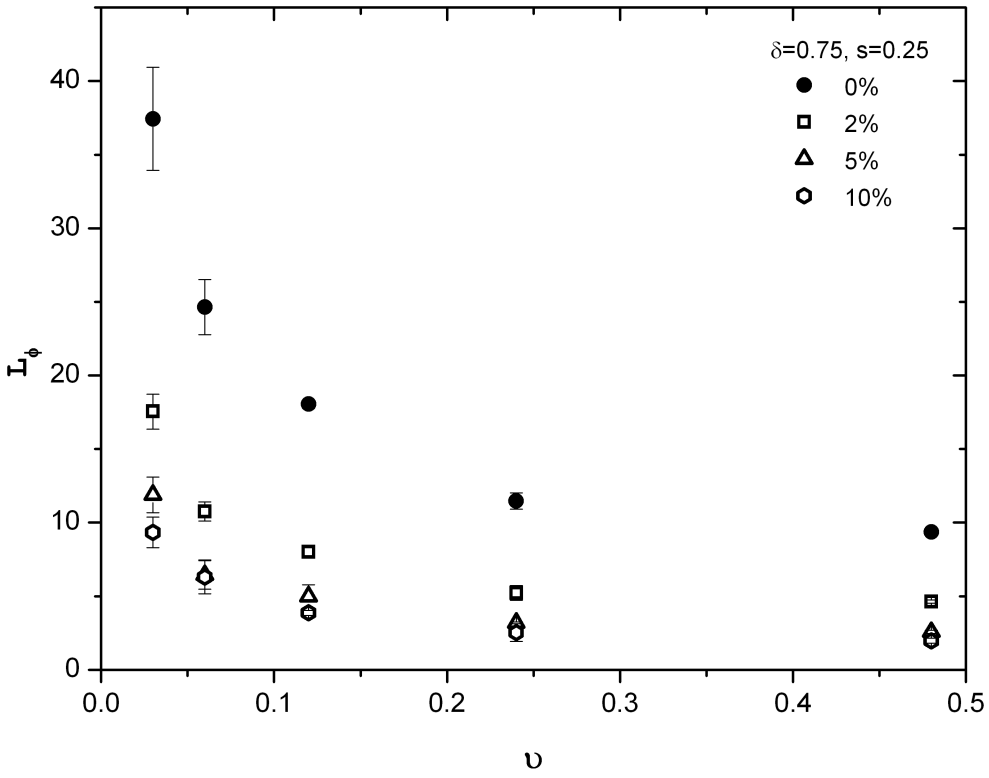

Figure 4.9. Interfacial slip lengths in systems containing small nanofillers and a slightly miscible interface.

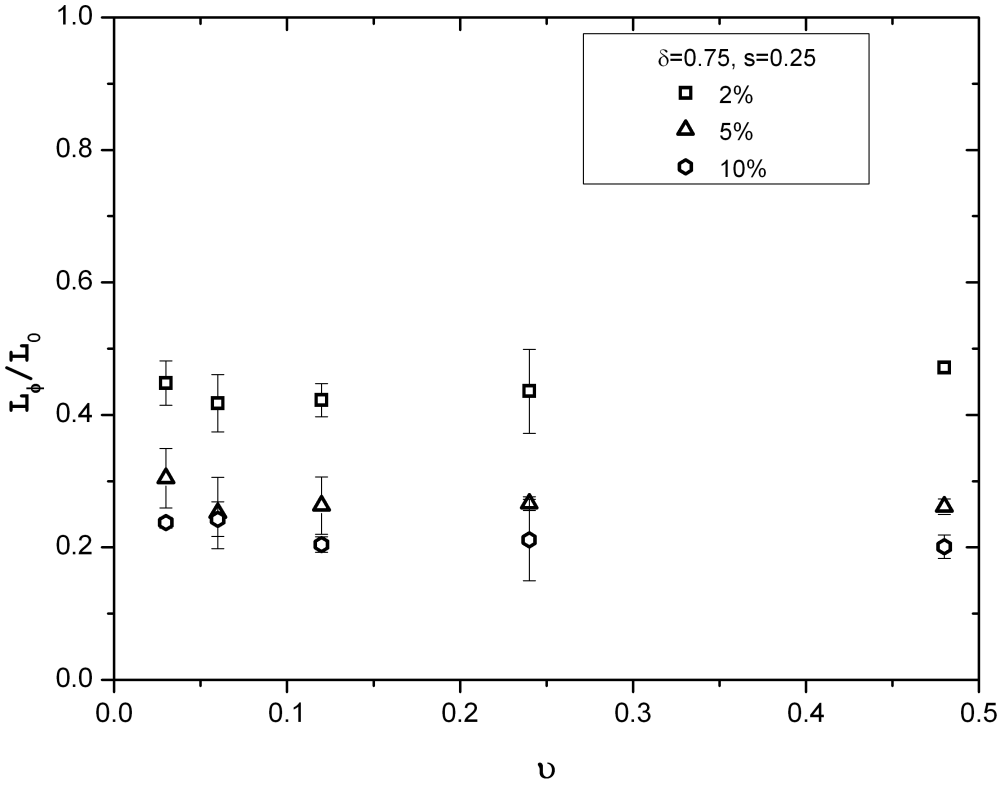

Figure 4.10. Ratio of the interfacial slip length of a system containing small nanofillers and a slightly miscible interface to that of a system lacking filler particles.

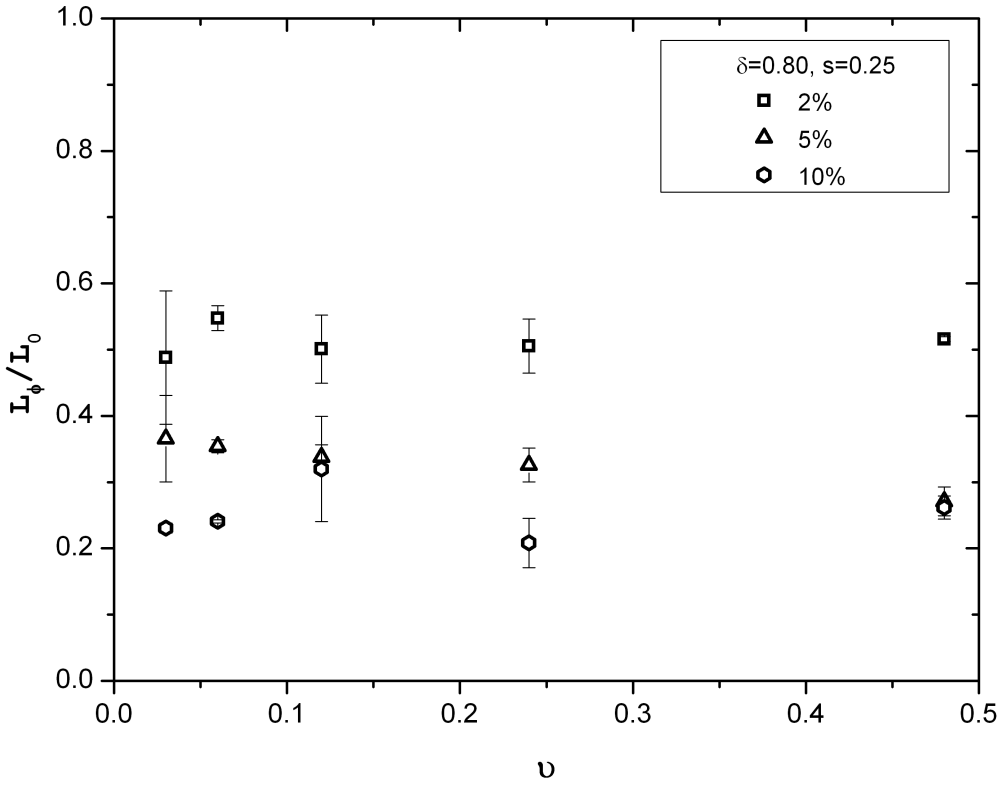

Figure 4.11. Ratio of the interfacial slip length of a system containing small nanofillers and a moderately miscible interface to that of a system lacking filler particles.

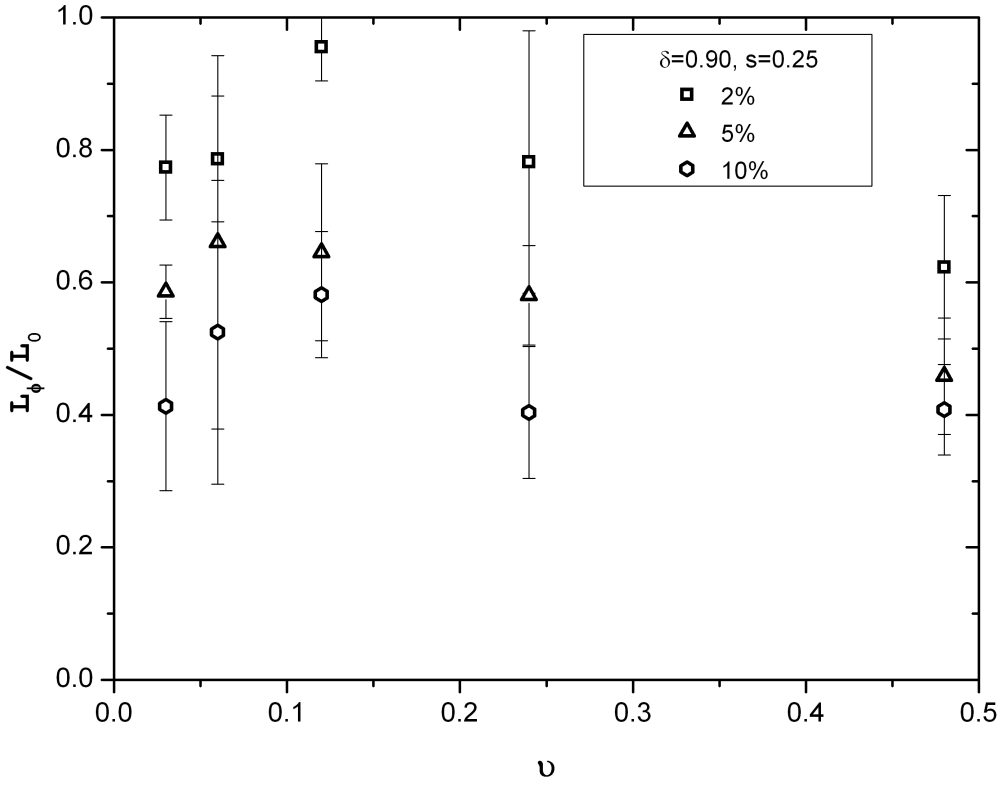

Figure 4.12. Ratio of the interfacial slip length of a system containing small nanofillers and a highly miscible interface to that of a system lacking filler particles.

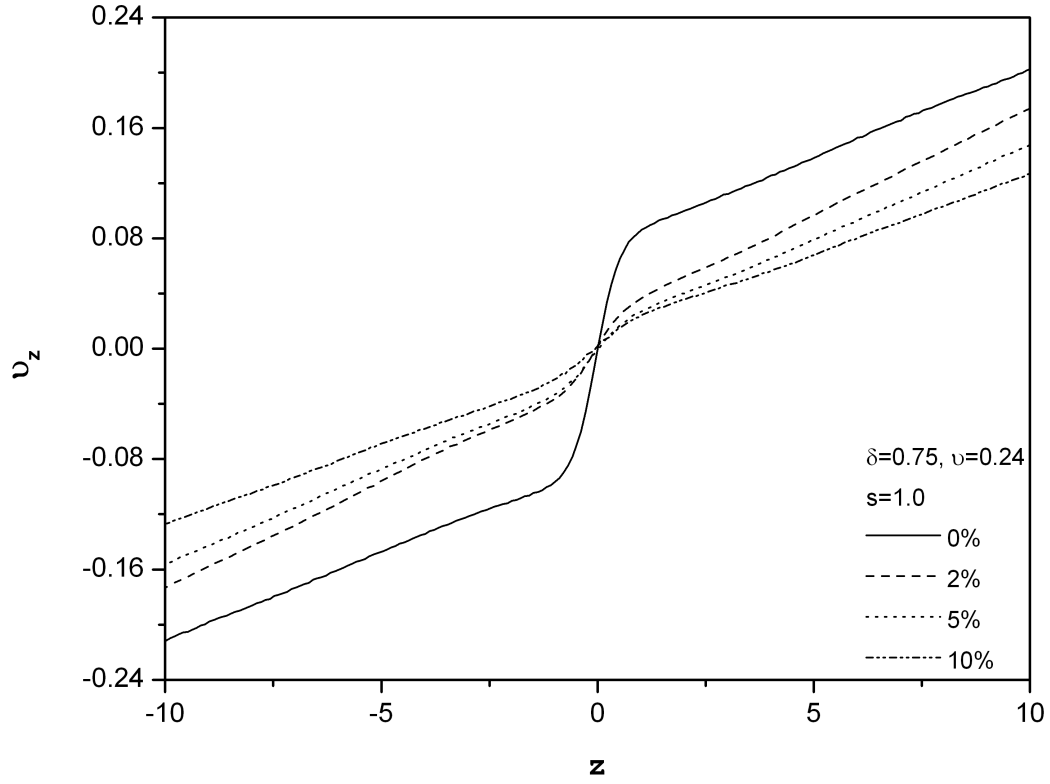

Figure 4.13. Velocity profile for a system containing large nanofillers and a slightly miscible interface, undergoing high shear.

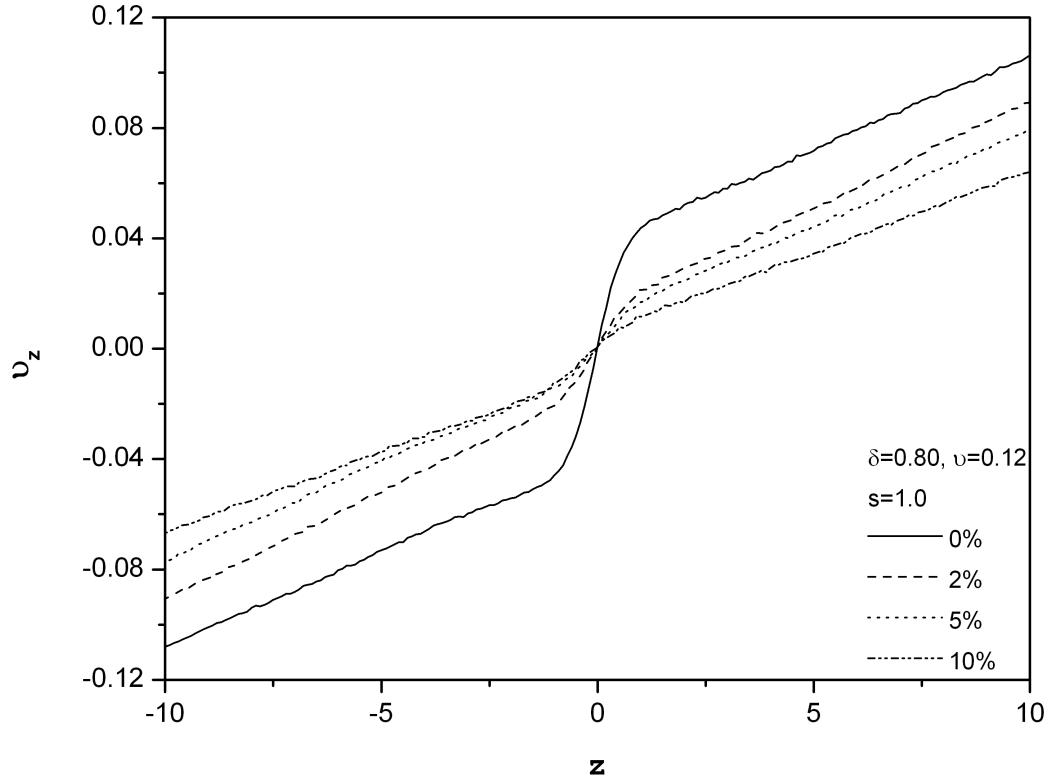

Figure 4.14. Velocity profile for a system containing large nanofillers and a moderately miscible interface, undergoing moderate shear.

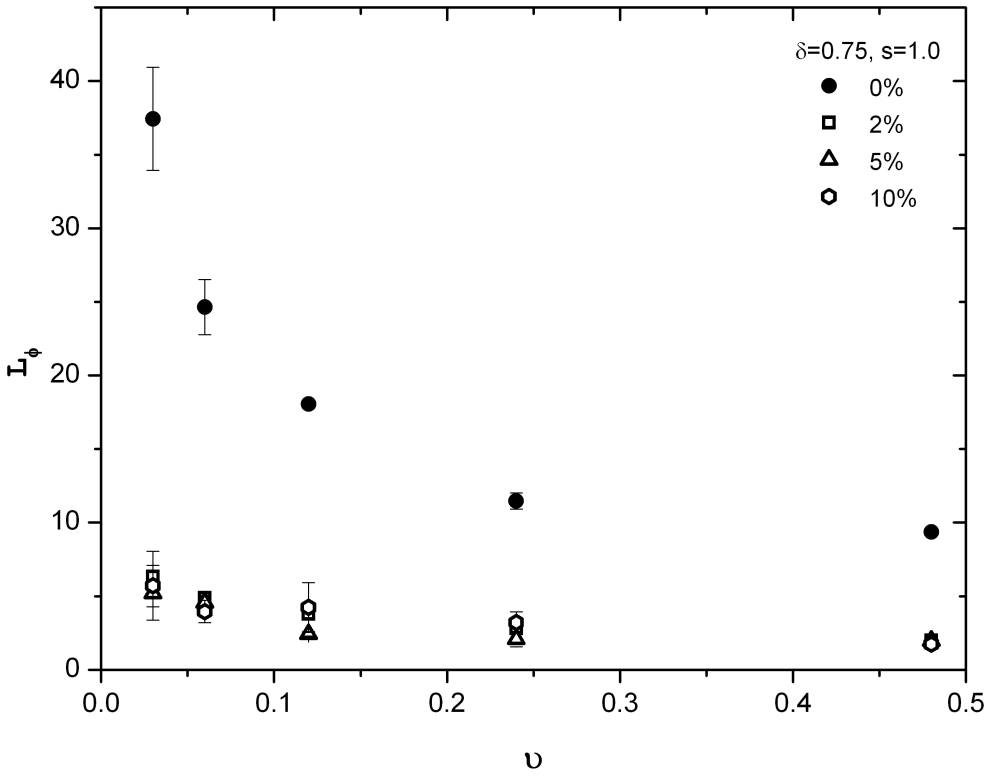

Figure 4.15. Interfacial slip lengths in systems containing large nanofillers and a slightly miscible interface.

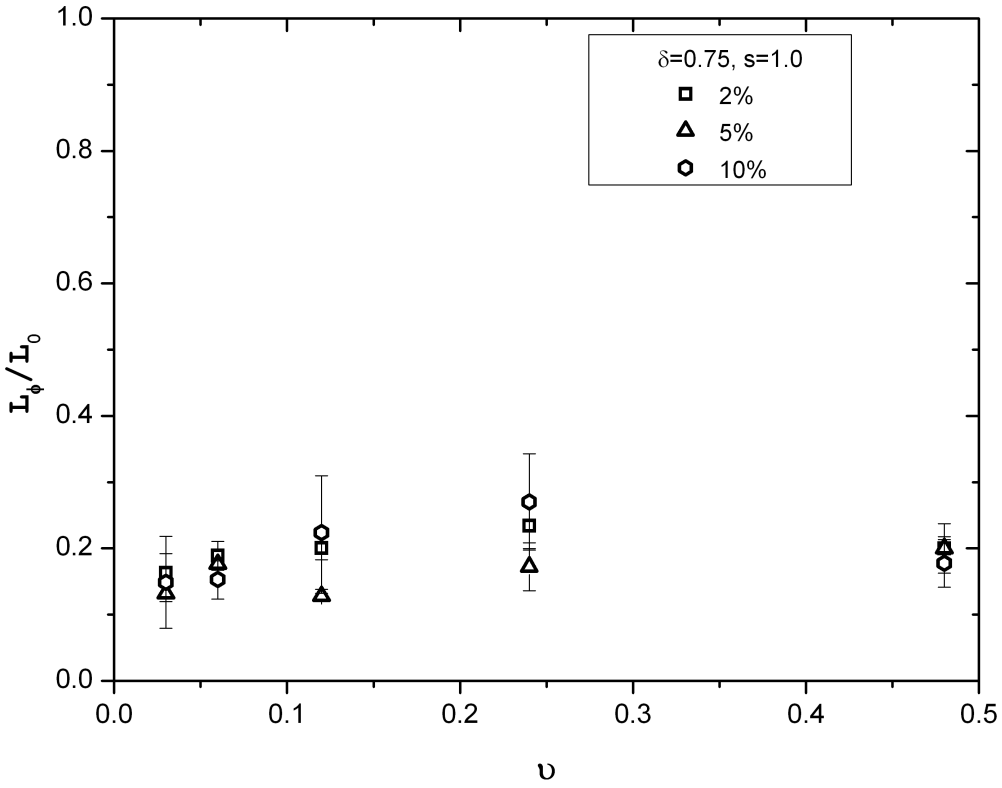

Figure 4.16. Ratio of the interfacial slip length of a system containing large nanofillers and a slightly miscible interface to that of a system lacking filler particles.

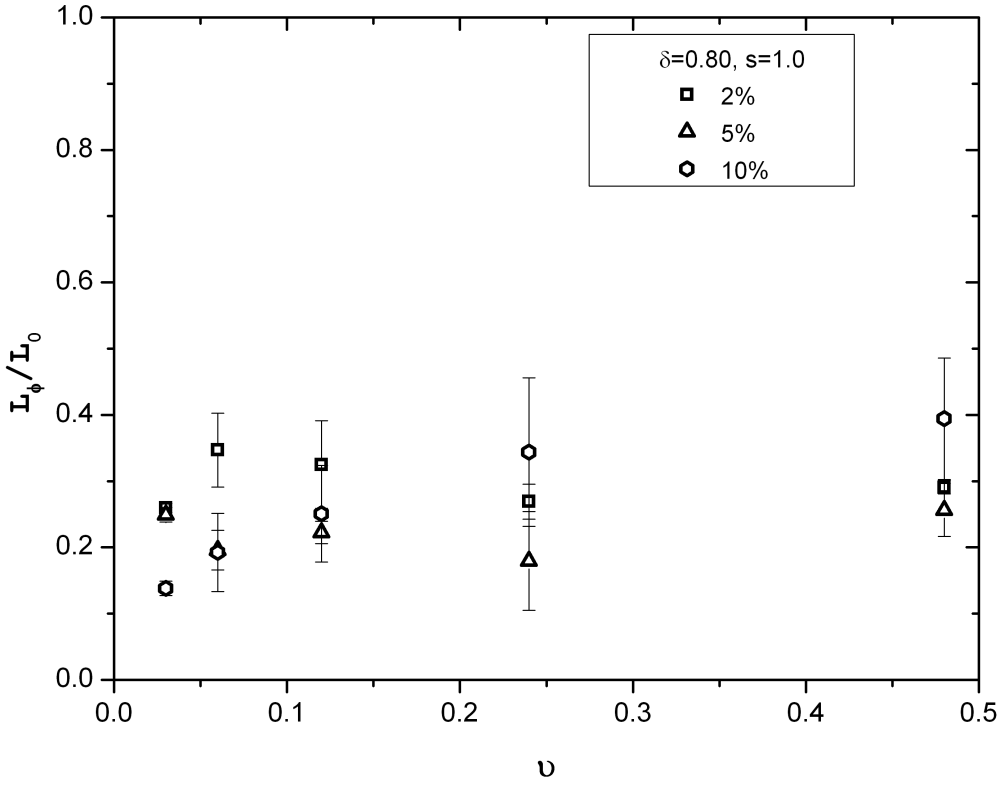

Figure 4.17. Ratio of the interfacial slip length of a system containing large nanofillers and a moderately miscible interface to that of a system lacking filler particles.

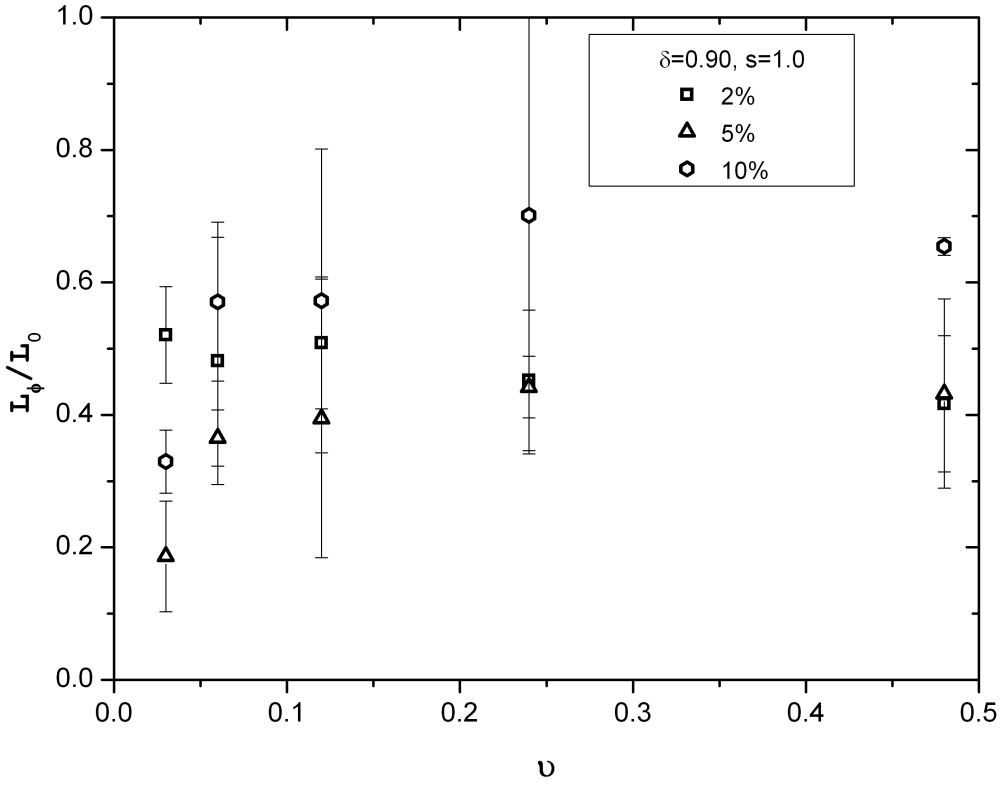

Figure 4.18. Ratio of the interfacial slip length of a system containing large nanofillers and a highly miscible interface to that of a system lacking filler particles.

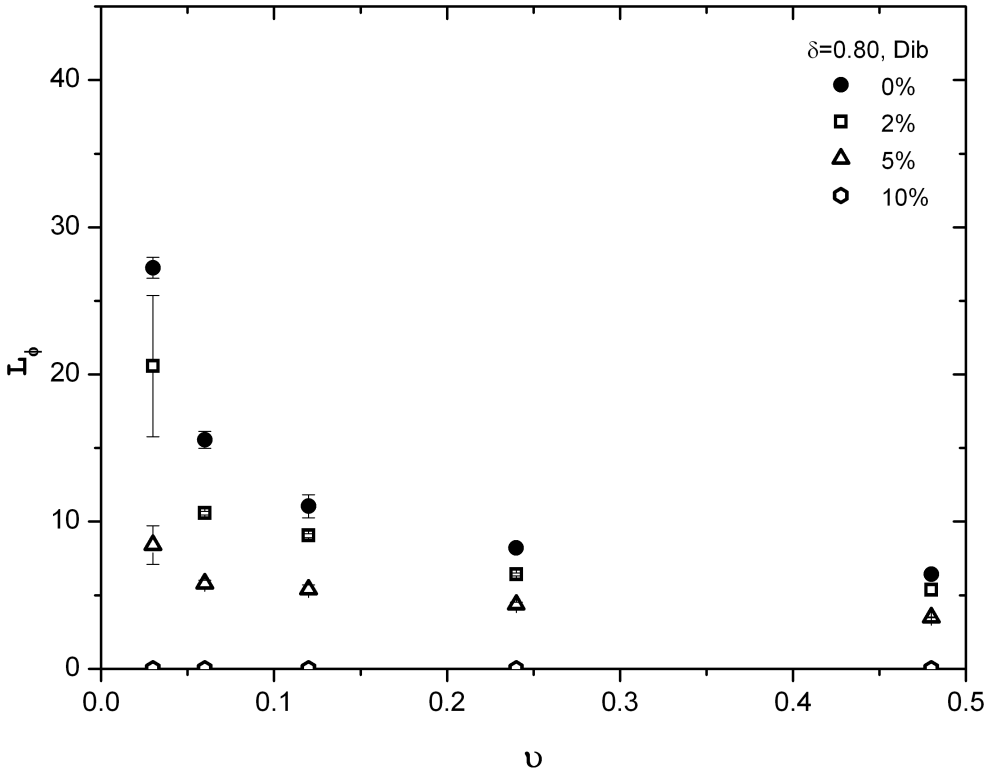

Figure 4.19. Interfacial slip lengths in systems containing diblock compatibilizers and a moderately miscible interface.

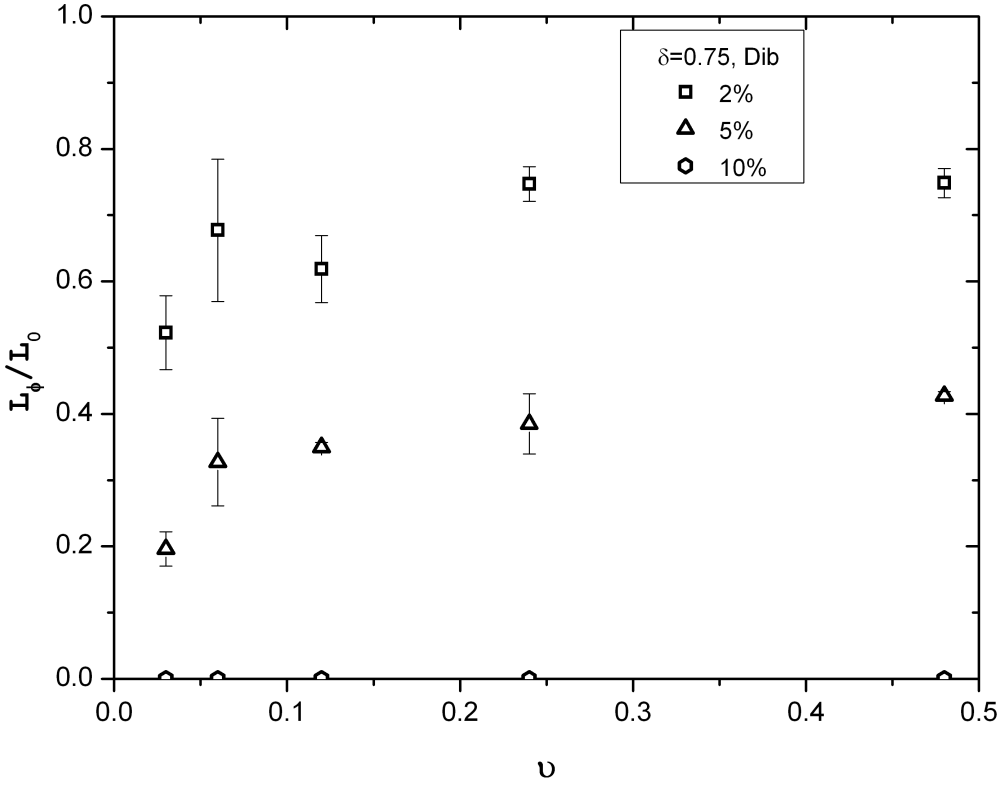

Figure 4.20. Ratio of the interfacial slip length of a system containing diblock compatibilizers and a slightly miscible interface to that of a system lacking filler particles.

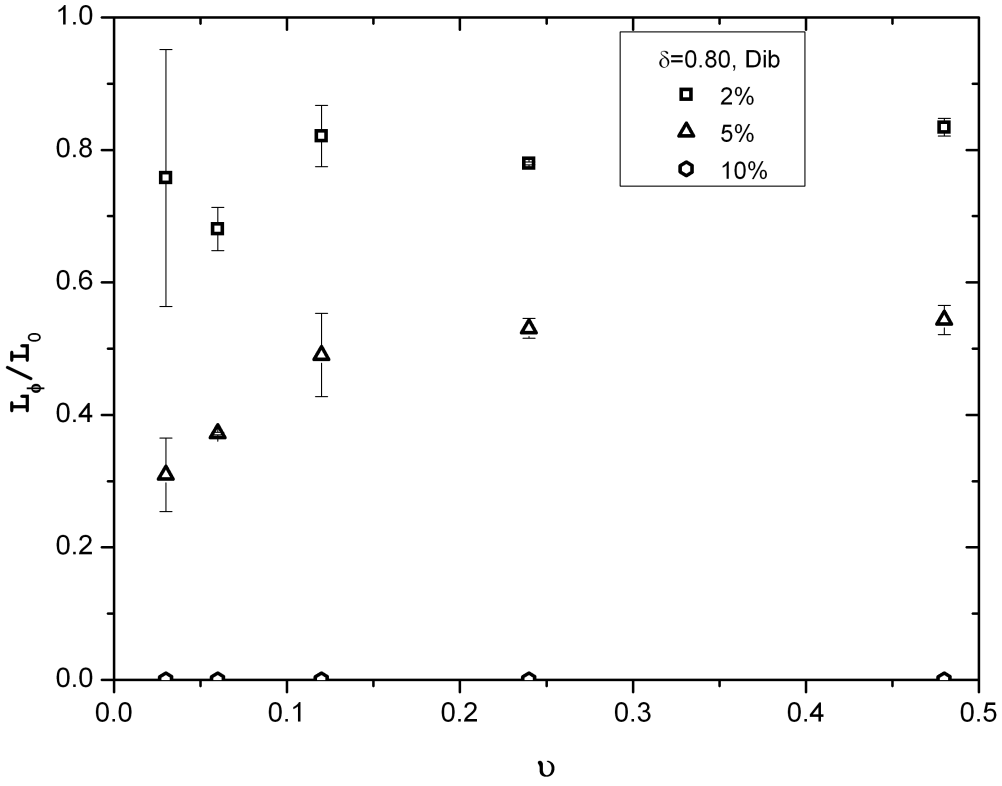

Figure 4.21. Ratio of the interfacial slip length of a system containing diblock compatibilizers and a moderately miscible interface to that of a system lacking filler particles.

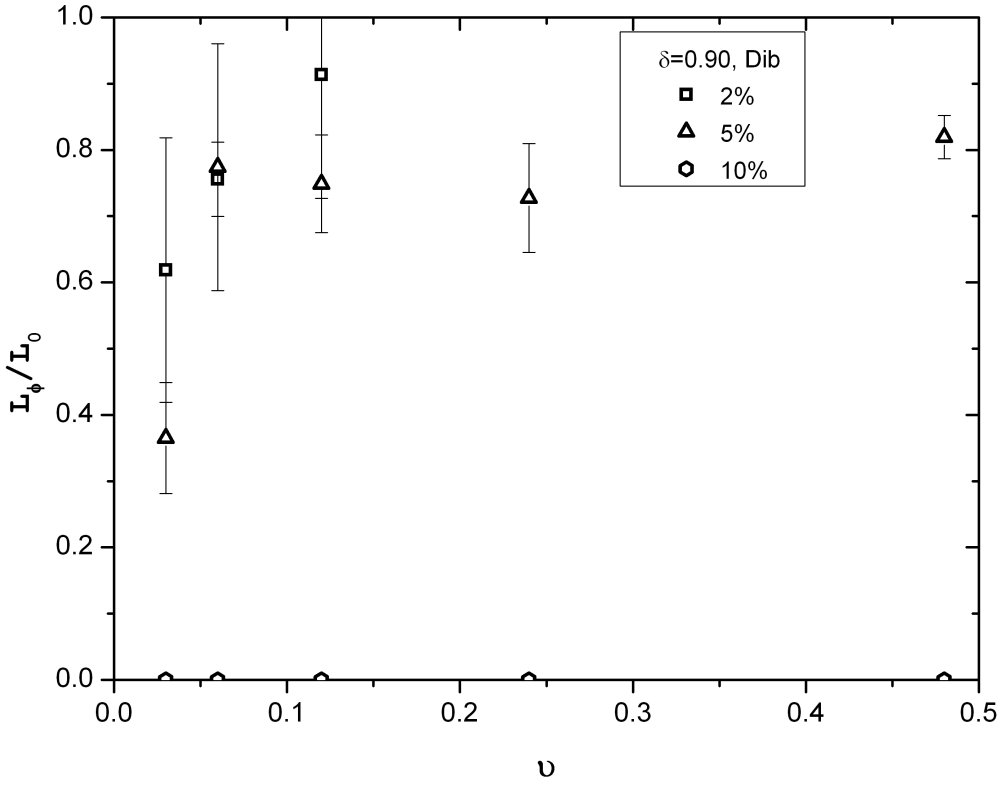

Figure 4.22. Ratio of the interfacial slip length of a system containing diblock compatibilizers and a highly miscible interface to that of a system lacking filler particles.

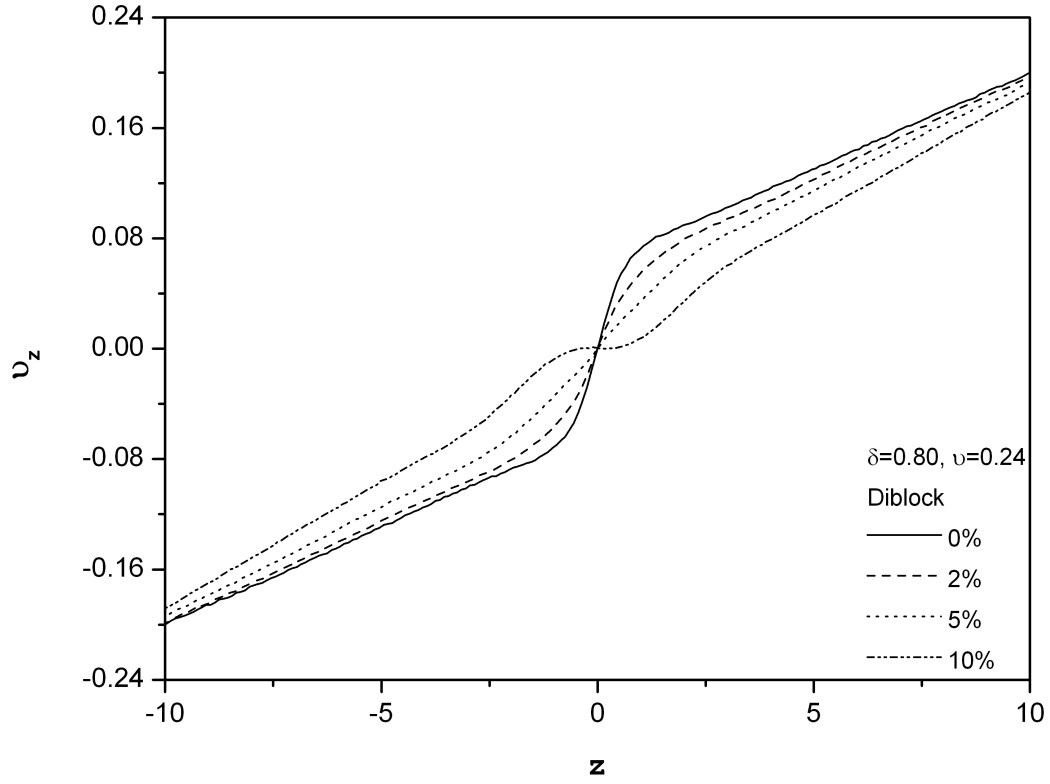

Figure 4.23. Velocity profile for a system containing diblock compatibilizers and a moderately miscible interface, undergoing high shear.

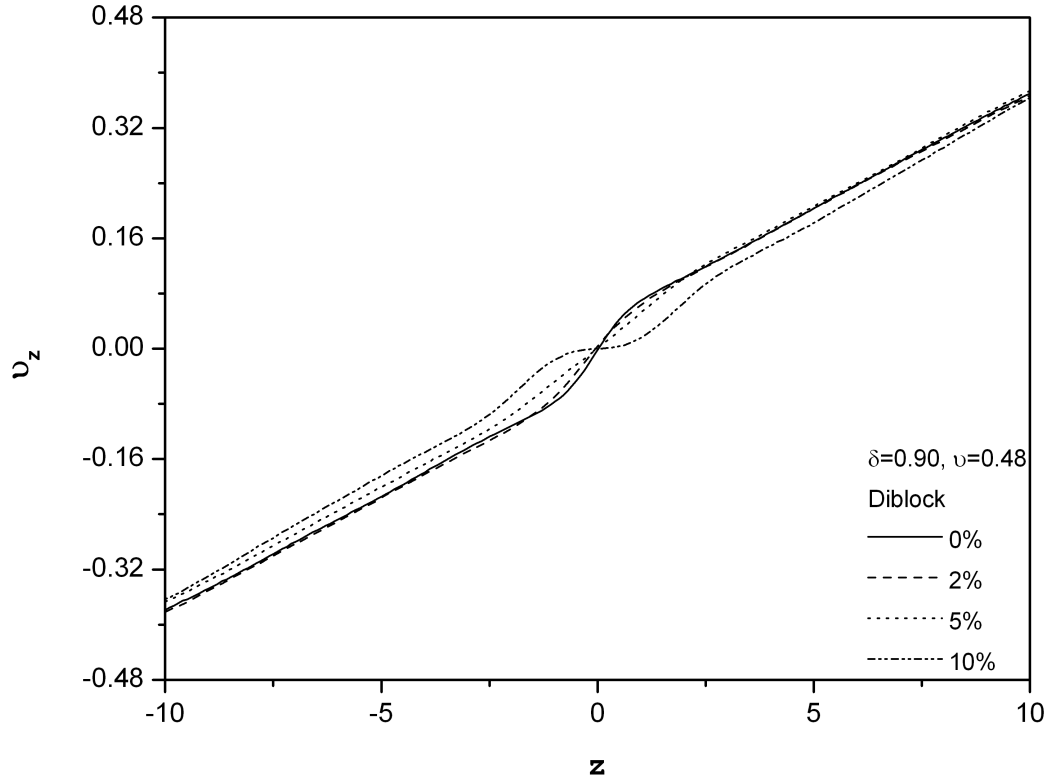

Figure 4.24. Velocity profile for a system containing diblock compatibilizers and a highly miscible interfacef, undergoing very high shear.

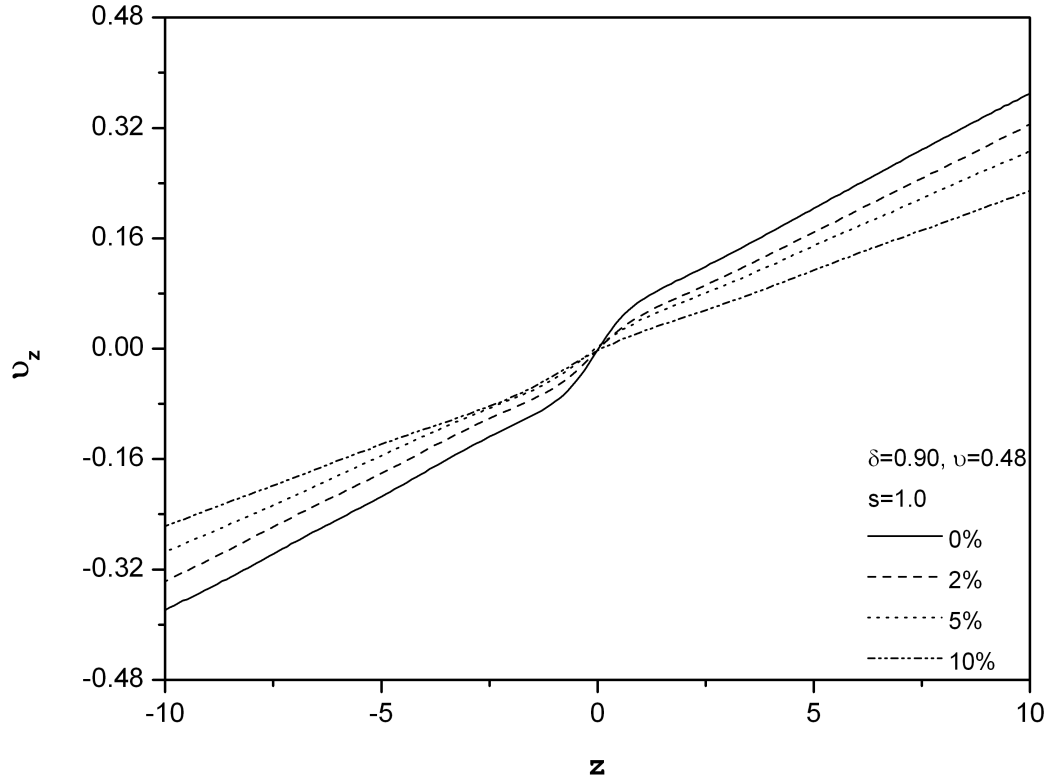

Figure 4.25. Velocity profile for a system containing large nanofillers and a highly miscible interface, undergoing very high shear.

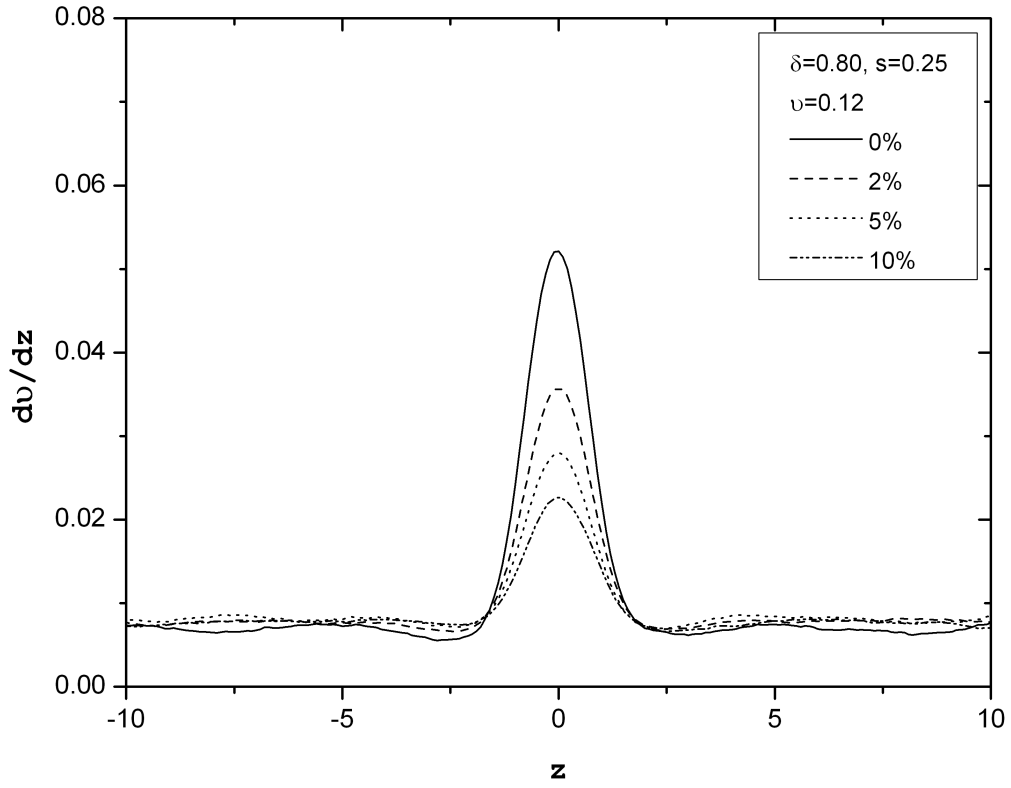

Figure 4.26. Derivative of the velocity profile for a system containing small nanofillers and a moderately miscible interface, undergoing moderate shear.

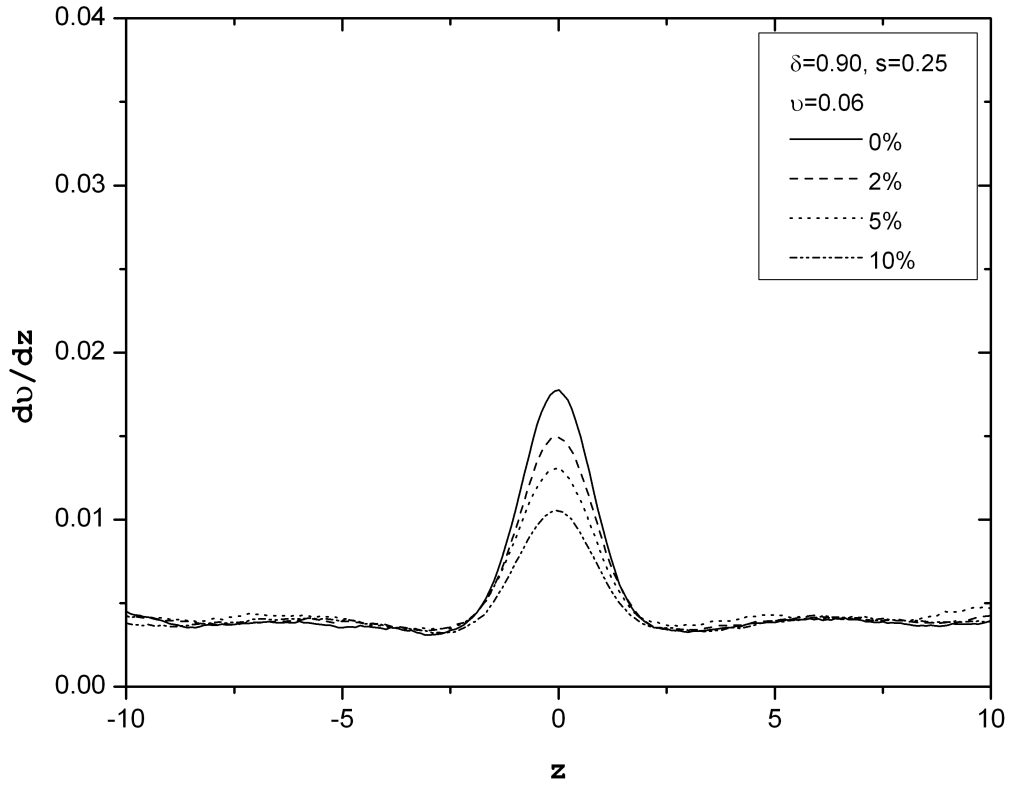

Figure 4.27. Derivative of the velocity profile for a system containing small nanofillers and a highly miscible interface, undergoing low shear.

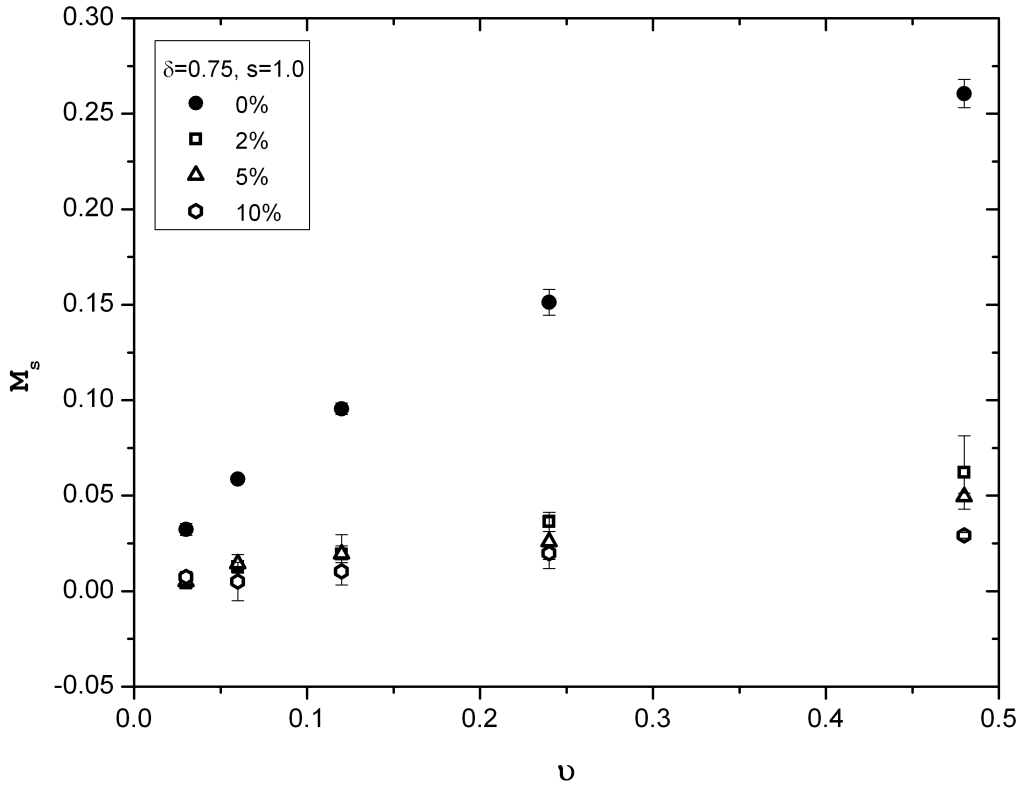

Figure 4.28. Interfacial slip magnitude in systems containing large nanofillers and a slightly miscible interface.

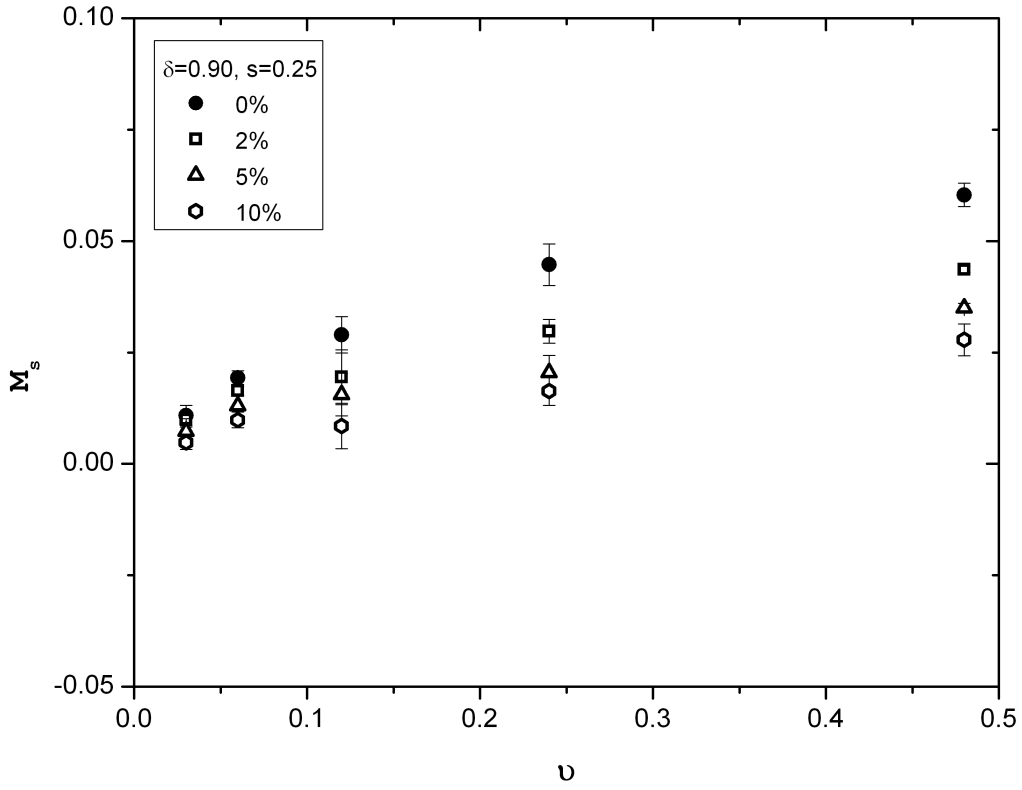

Figure 4.29. Interfacial slip magnitude in systems containing small nanofillers and a highly miscible interface.

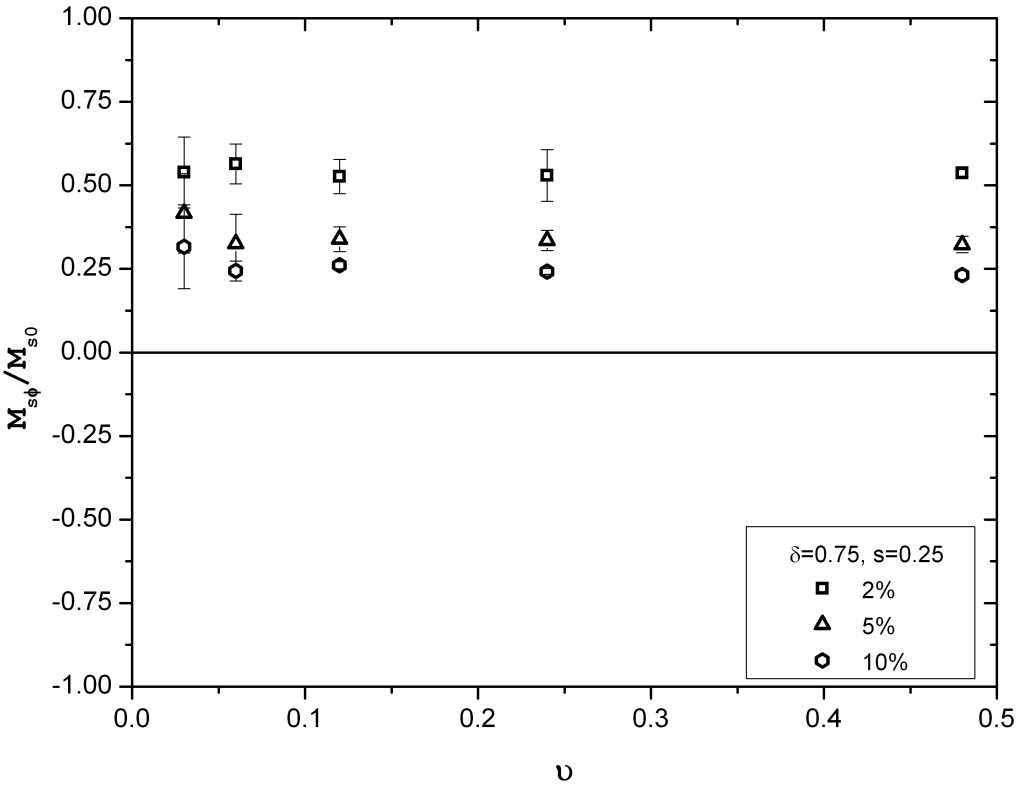

Figure 4.30. Ratio of the interfacial slip magnitude of a system containing small nanofillers and a slightly miscible interface to that of a system lacking filler particles.

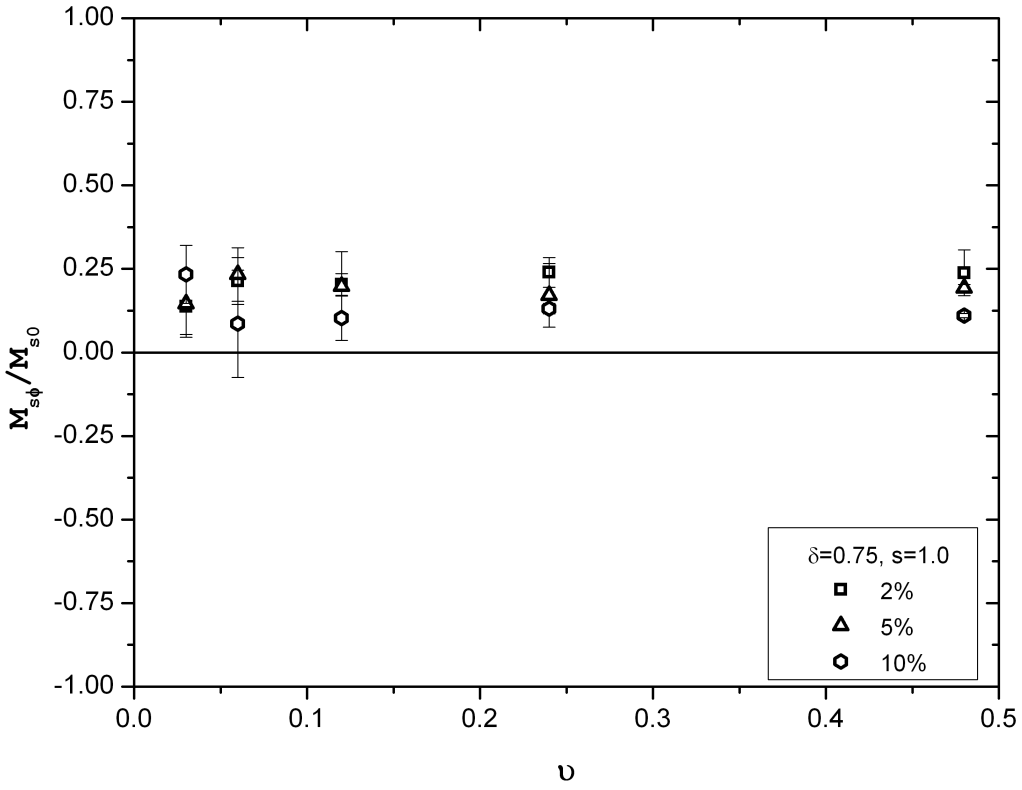

Figure 4.31. Ratio of the interfacial slip magnitude of a system containing large nanofillers and a slightly miscible interface to that of a system lacking filler particles.

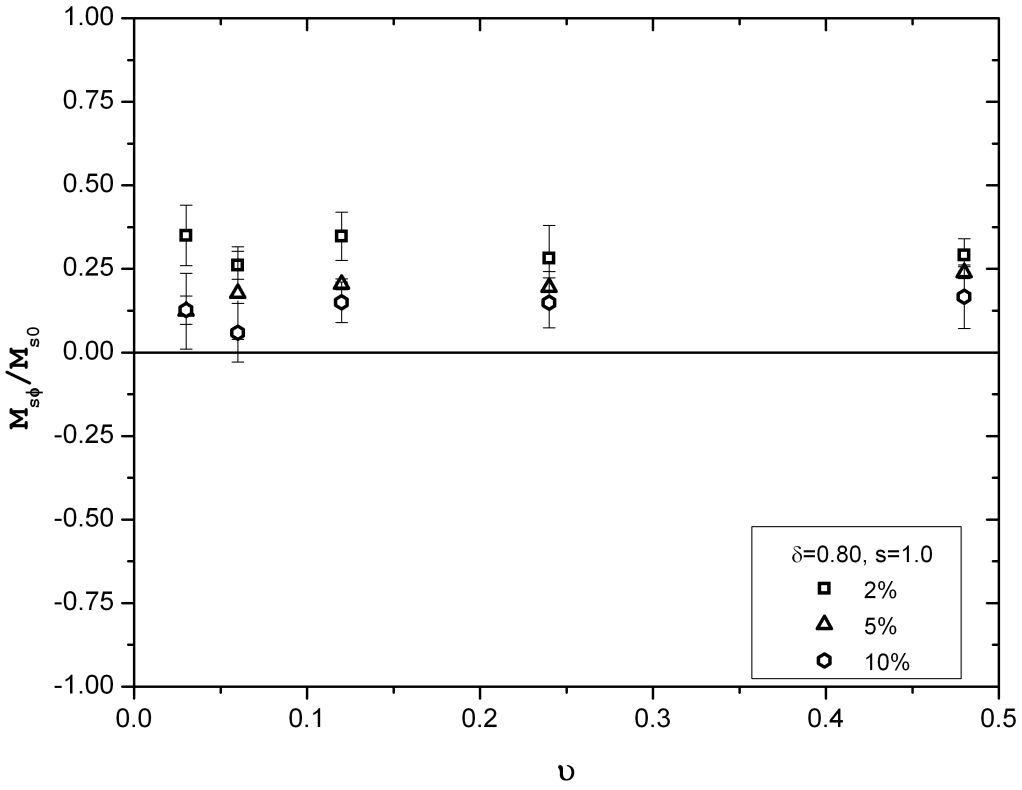

Figure 4.32. Ratio of the interfacial slip magnitude of a system containing large nanofillers and a moderately miscible interface to that of a system lacking filler particles.

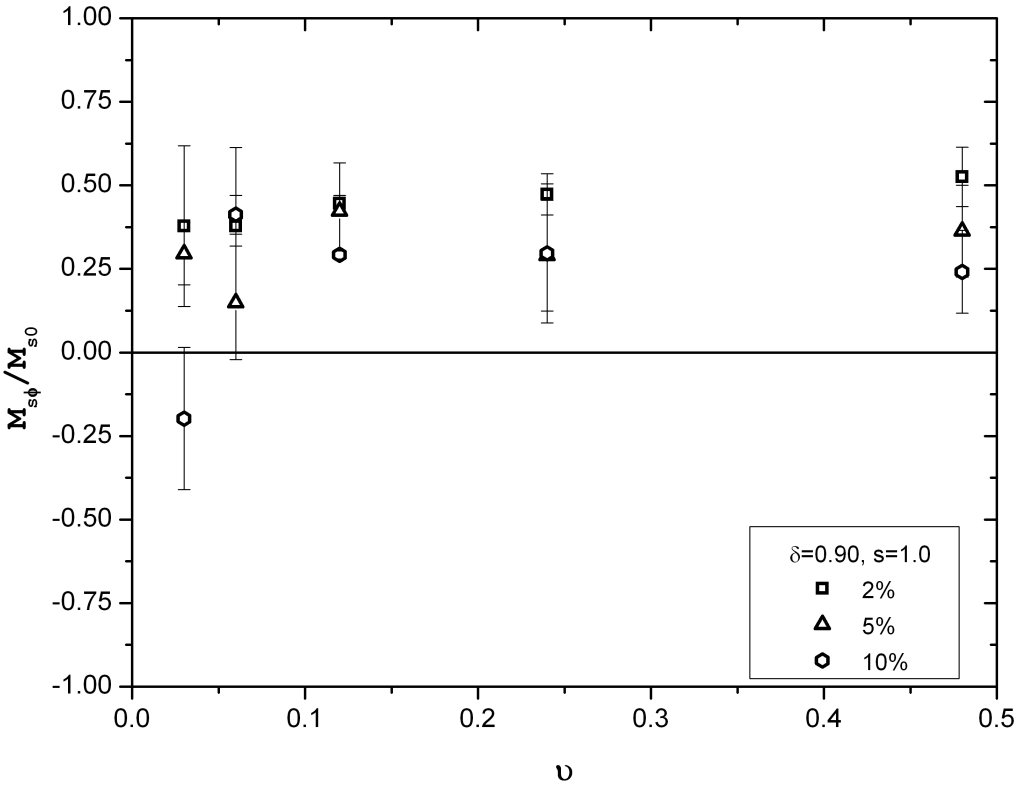

Figure 4.33. Ratio of the interfacial slip magnitude of a system containing large nanofillers and a highly miscible interface to that of a system lacking filler particles.

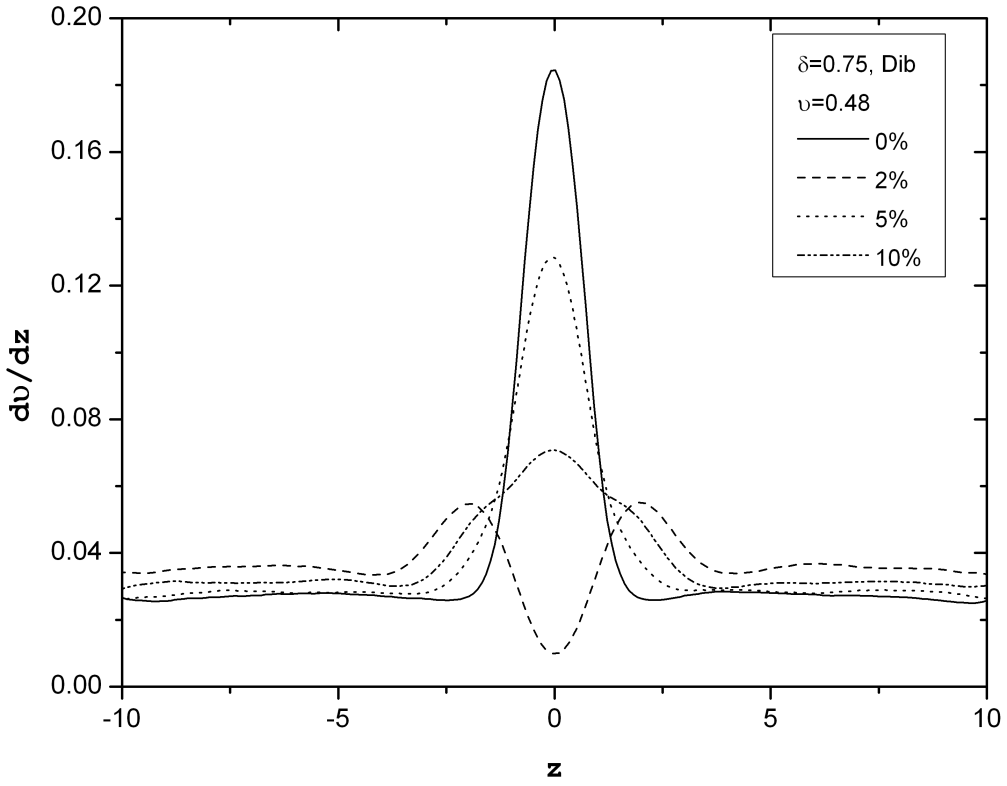

Figure 4.34. Derivative of the velocity profile for a system containing diblock compatibilizers and a slightly miscible interface, undergoing very high shear.

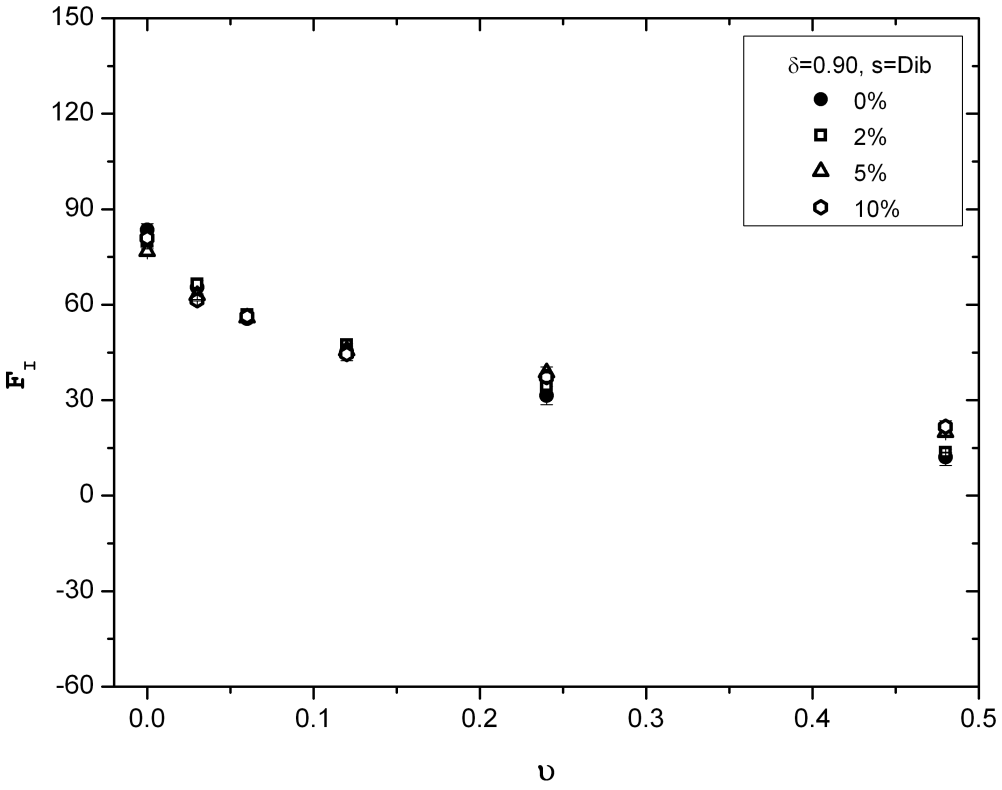

Figure 4.35. Interfacial tension in systems containing diblock compatibilizers and a highly miscible interface.

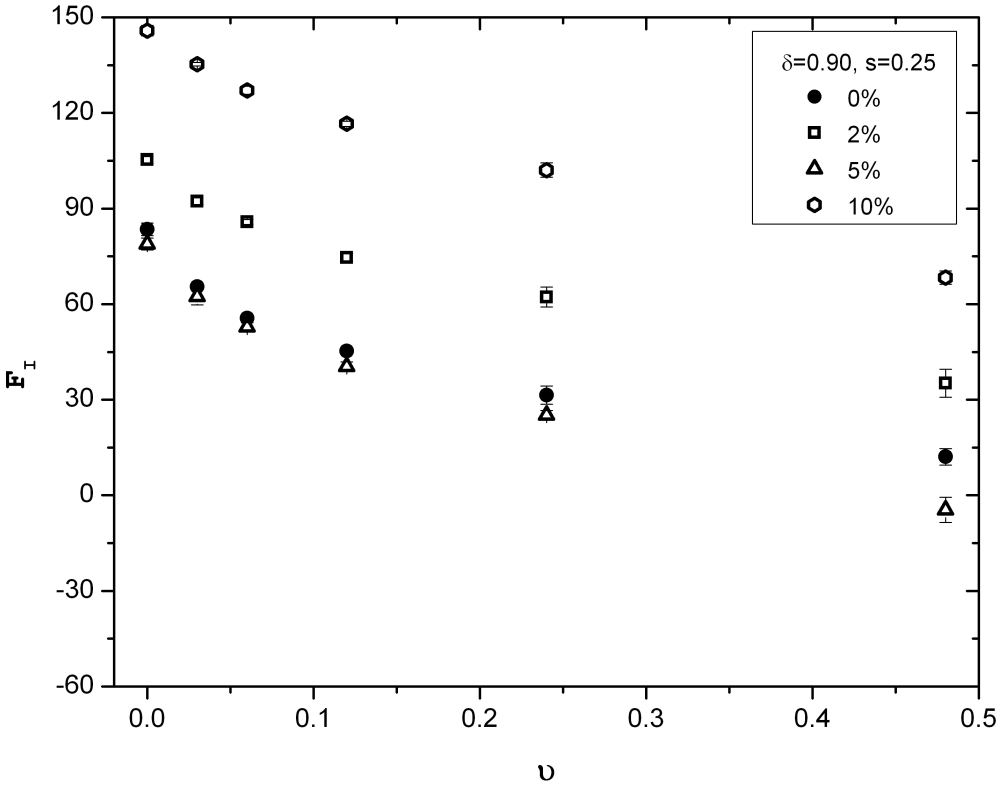

Figure 4.36. Interfacial tension in systems containing small nanofillers and a highly miscible interface.

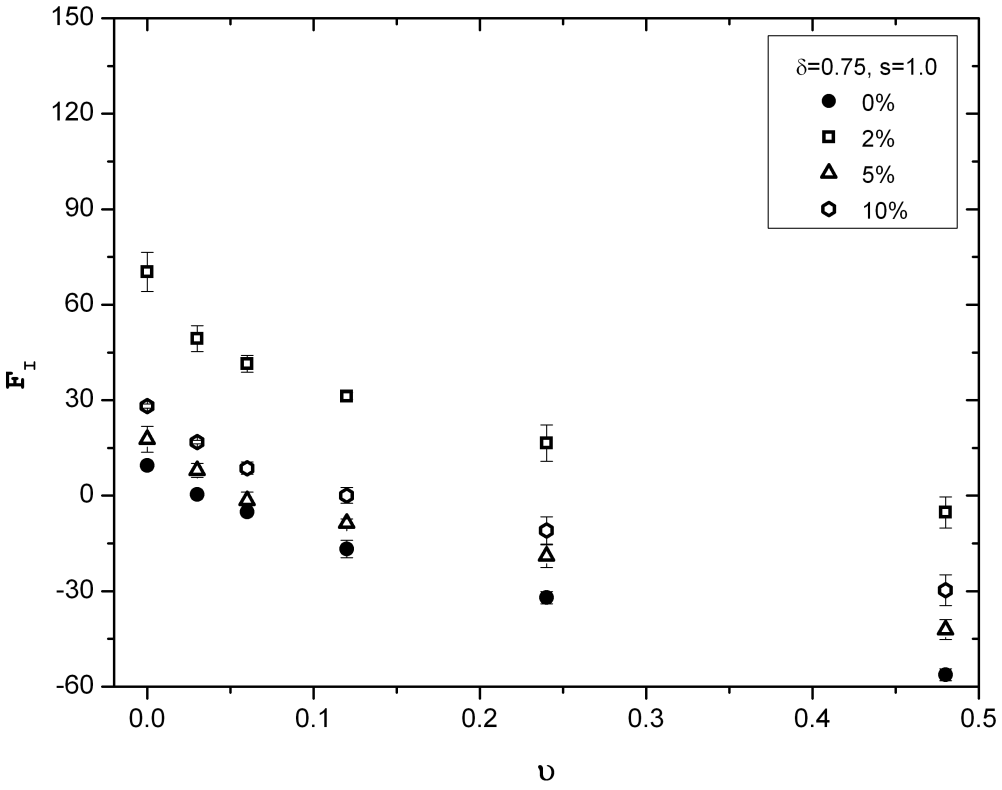

Figure 4.37. Interfacial tension in systems containing large nanofillers and a slightly miscible interface.

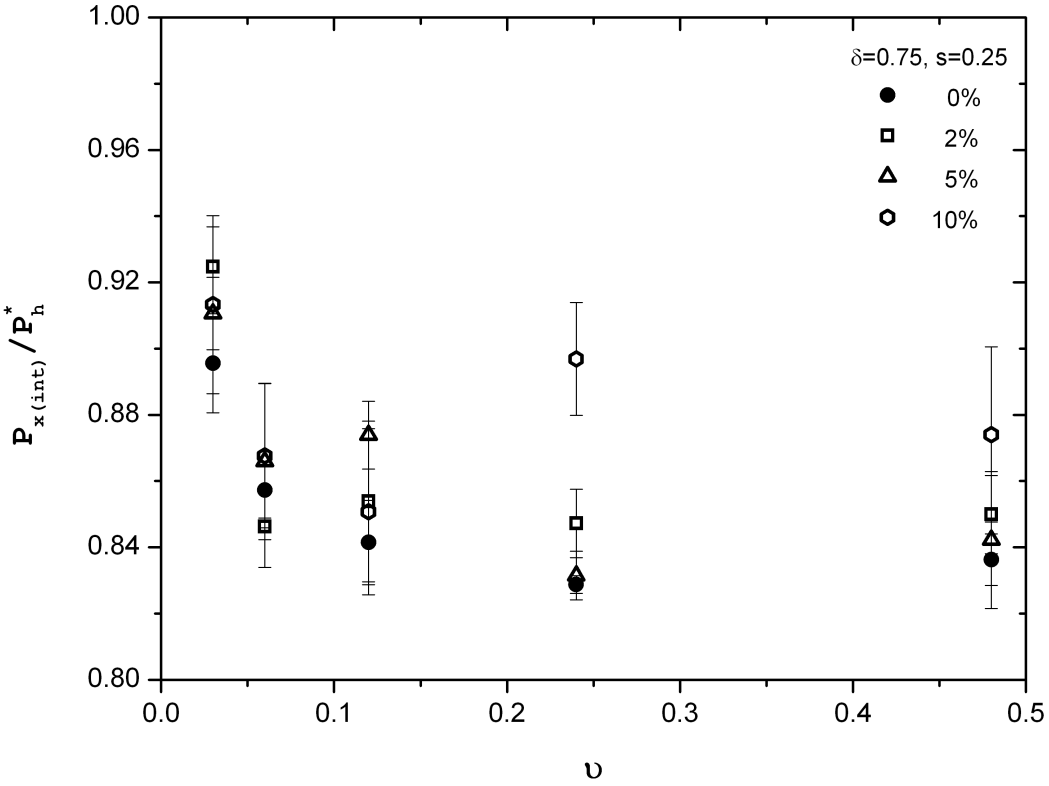

Figure 4.38. Ratio of the orientation tensor of a system containing small nanofillers and a slightly miscible interface to that of a system lacking filler particles.

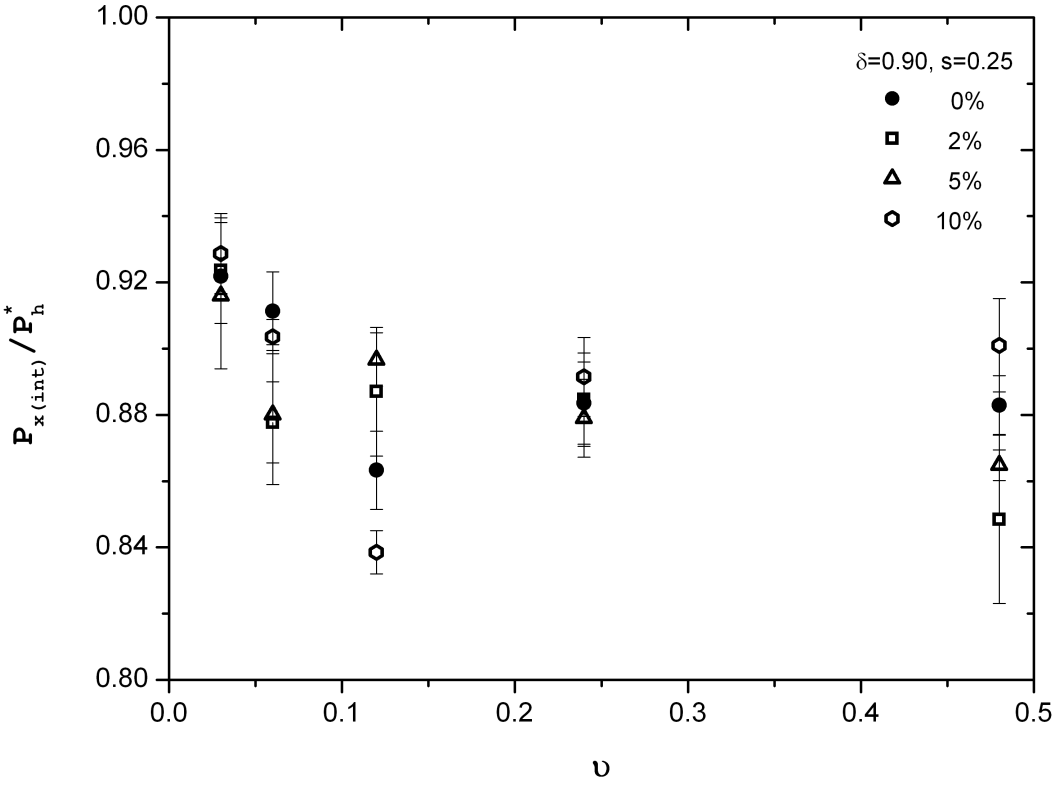

Figure 4.39. Ratio of the orientation tensor of a system containing small nanofillers and a highly miscible interface to that of a system lacking filler particles.

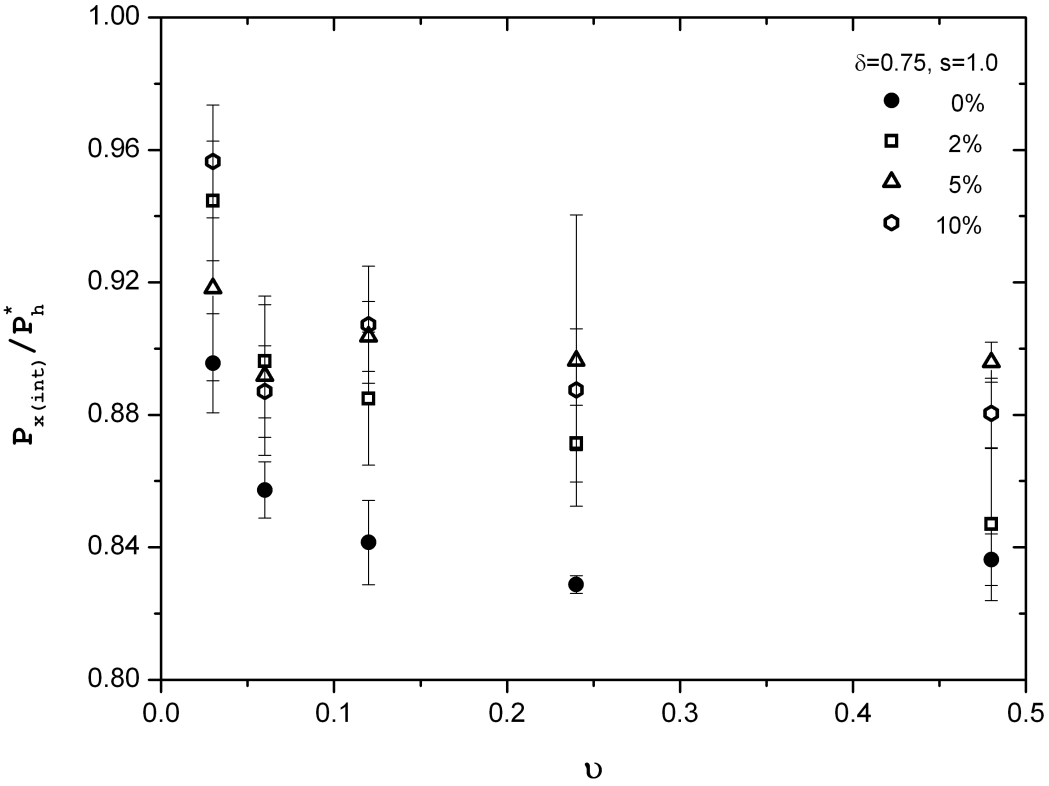

Figure 4.40. Ratio of the orientation tensor of a system containing large nanofillers and a slightly miscible interface to that of a system lacking filler particles.

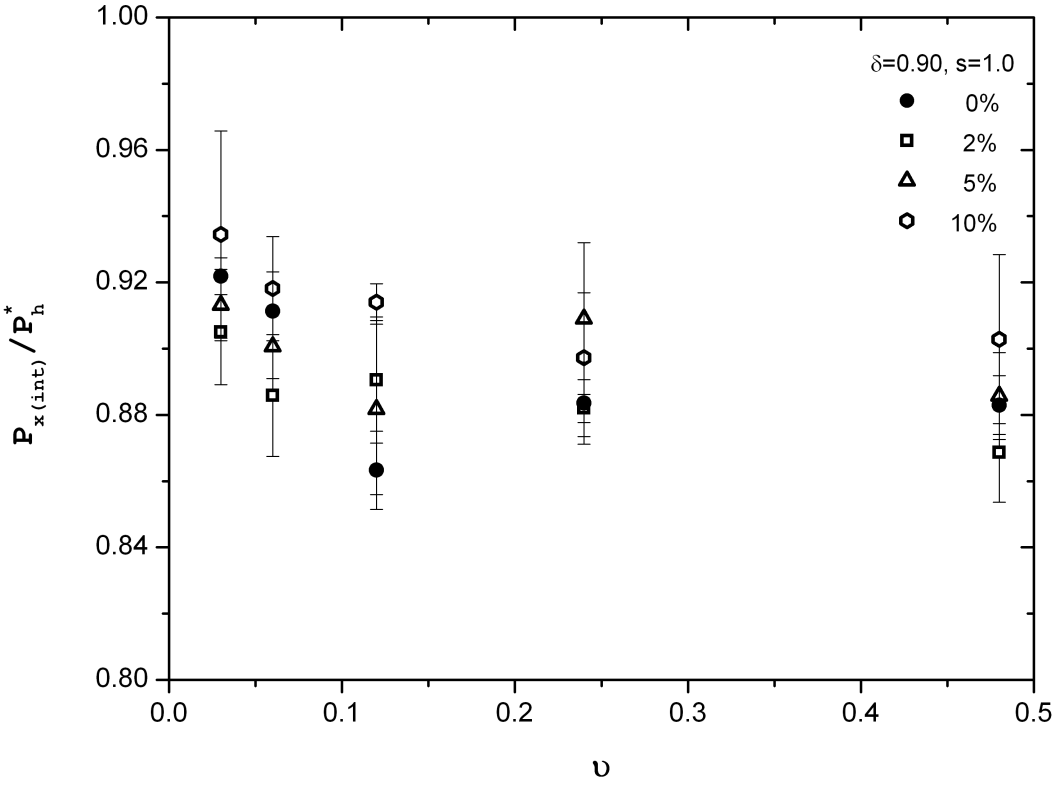

Figure 4.41. Ratio of the orientation tensor of a system containing large nanofillers and a highly miscible interface to that of a system lacking filler particles.

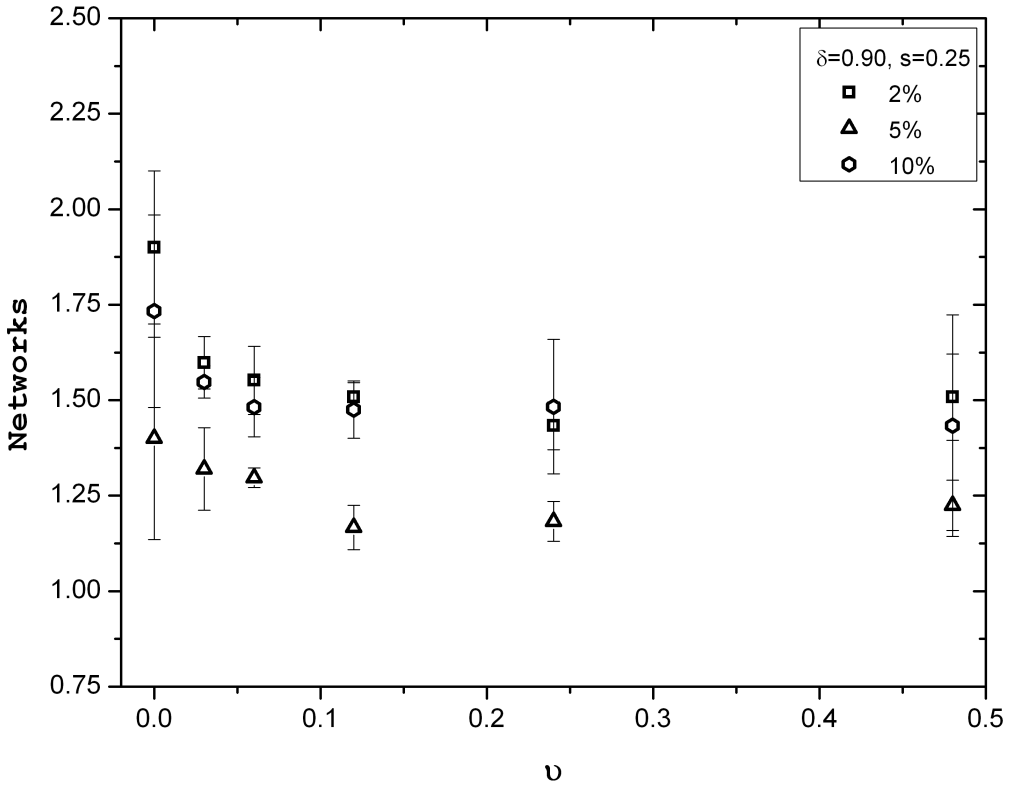

Figure 4.42. Network groups within the interfacial region of systems containing small nanofillers and a highly miscible interface.

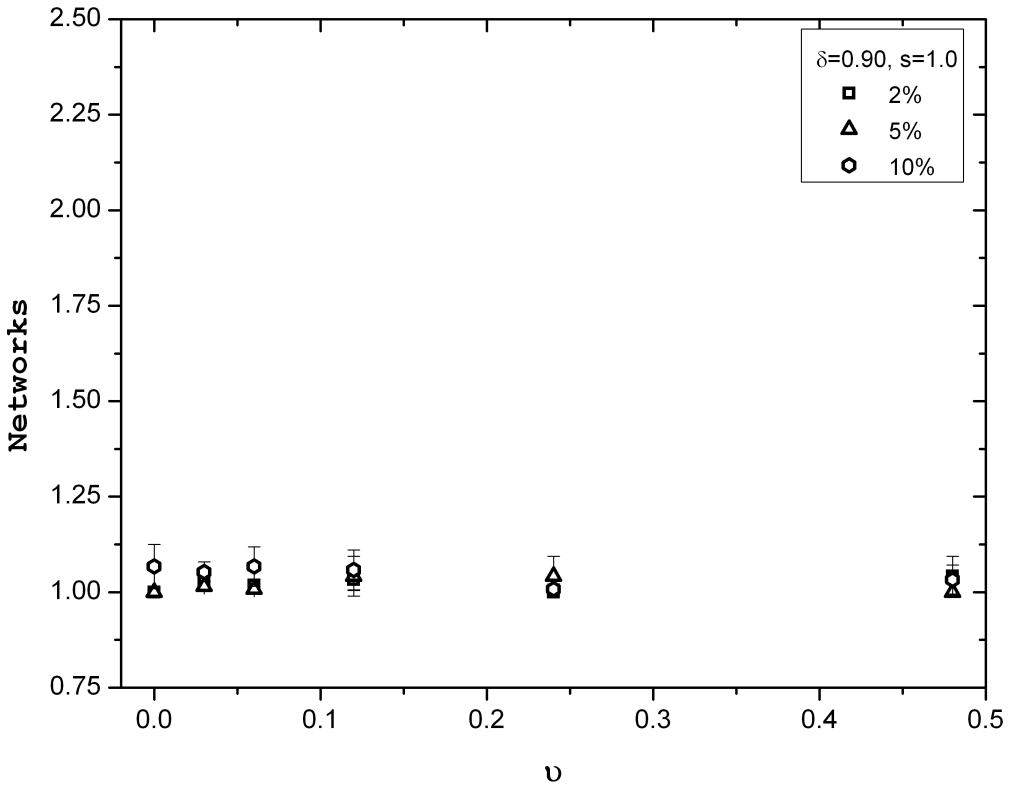

Figure 4.43. Network groups within the interfacial region of systems containing large nanofillers and a highly miscible interface.

Chapter 5 – Nanoparticles as Thermal Diffusers in Flame Retardant Polymeric Materials

5.1 Modeling Heat Transport and Lattice-Boltzmann Methods

In cases such as flame retardation and heat transfer, molecular dynamics cannot capture the mechanism as both the system sizes and mechanisms require prohibitive computational times. Therefore, other means must be considered; namely, fluid dynamics, since as a methodology it is more reflective of the bulk system as a whole than individual particle interactions. However, fluid dynamics has issues with complicated geometries, as well as boundary and interfacial reactions. To overcome these issues, Lattice-Boltzmann methods were used to model heat transport in polymer nanocomposites.

Fluid dynamics requires a different set of governing equations than those of Newtonian motion that are used to determine molecular dynamics simulations. While molecular dynamics and Monte Carlo simulations relate the actions of each particle in the system to one another, such a method is infeasible for a realistically large data set[1,2]. Using the diffusive model of heat transport, which is based on the Fourier heat conduction theory, the transport of temperature can be modeled by solving the advection-diffusion equation[3].

The advection-diffusion equation combines the transport of a physical quantity, such as heat, due to advection, or the movement of the bulk material that contains the quantity, and diffusion, the movement of the quantity itself from regions of high concentration to areas of low concentration. Without advection, the equation reduces to the heat equation, wherein heat transport is solely guided by temperature gradients. The advection-diffusion solution can be found deterministically and is accurate at the bulk scale, although not at the scale of quantum

mechanics. Solving the advection-diffusion equation requires the use of statistical mechanics and forms the Lattice-Boltzmann method, which in itself is a combination of the lattice gas automata and the Boltzmann equation, described below.

Rather than examine each particle's interaction with every other particle within the system, as would be done with molecular dynamics or Monte Carlo simulations, a probability distribution function relating position, velocity and time, *f*, wherein $f^{(N)} = f(r^{(N)},v^{(N)},t)$ is considered instead[2,4]. Boltzmann's Equation (5.1) uses the conservation of momentum to determine interparticle collisions within a system.

$$f\left(r+\frac{p}{m}dt, p+Fdt, t+dt\right)drdp - f(r,p,t)drdp = \frac{\partial f(r,p,t)}{\partial t} \quad \textbf{(5.1)}$$

Boltzmann's equation allows us to examine the system via its probability distribution function, *f*, as a function of time, where *r* is the position of the particle; *p* is the momentum; *m* is the molecular mass; and *F* is the force field acting upon the fluid. The probability function is, in turn, collision-based: $f_{1,2}$ is the probability that at time *t*, a particle exists with position and velocity, r_1 and v_1, and collides with a second particle with position, r_2, and velocity, v_2. This, in turn, is dependent on $f_{1,2,3}$ which is dependent on $f_{1,2,3,4}$ and so on and so forth interminably until the entire assembly has been described. These events are far from independent as the collision of two particles directly affects the collisions of the particles surrounding them which consequently affects the particles around them, including the first pair, and thus a simple collision reverberates throughout the system indefinitely. This infinite dependence is known as the Bogoliubov-Born-Green-Kirkwood-Yvon, or BBGKY, hierarchy[2]. For simplification of the BBGKY heirarchy,

collisions must be treated as independent processes and thus $f_{1,2}$ becomes the product of f_1 and f_2. This further simplifies $f^{(N)}$ as $f^{(1)}$ or $f(r,v,t)$ [5].

The Boltzmann equation can also be used to describe a collision term, Ω, by utilizing the evolution of the distribution function, f (5.2)[5].

$$\frac{\partial f}{\partial t} + v \cdot \nabla_r f + F \cdot \nabla_v f = \Omega \quad \textbf{(5.2)}$$

Allowing the system to relax back toward equilibrium using the BGK approximation, we can approximate the collision term (5.3), where f^{eq} is a Maxwell-Boltzmann distribution function at equilibrium and λ is the relaxation time due to collision[6].

$$\frac{\partial f}{\partial t} + v \cdot \nabla_r f + F \cdot \nabla_v f = -\frac{f - f^{eq}}{\lambda} \quad \textbf{(5.3)}$$

By eliminating external stresses that could adversely impact the system, the third term on the left zeroes out and leaves Equation 5.4.

$$\frac{\partial f}{\partial t} + v \cdot \nabla_r f = -\frac{f - f^{eq}}{\lambda} \quad \textbf{(5.4)}$$

However, as this was made for real systems, these distribution functions are continuous and do not easily allow for discretization.

5.2 Lattice-Boltzmann Discretization in Time

In order to discretize the Boltzmann Equation, the particle distribution function is fixed onto a lattice, thus creating the Lattice-Boltzmann method for solving fluid dynamics problems via computer simulation. The Lattice-Boltzmann method allows for discretization in two dimensions and can also be extended into three dimensions. The Lattice-Boltzmann method is actually a combination of the lattice gas automata and discretization of the Boltzmann equation[7,8]. Discretization of the Lattice-Boltzmann equation begins with discretization with respect to time[9]. By differentiating Equation 5.4 with respect to time, we are left with Equation 5.5.

$$\frac{df}{dt} + \frac{f}{\lambda} = \frac{f^{eq}}{\lambda} \tag{5.5}$$

Integrating by $e^{\frac{\Delta t}{\lambda}}$ over a timestep of Δt leaves us with Equation 5.6.

$$f(r + v\Delta t, v, t + \Delta t) = \frac{e^{\frac{-\Delta t}{\lambda}}}{\lambda}\int_0^{\Delta t} e^{\frac{t'}{\lambda}} f^{eq}(r + vt', v, t + t')dt' + e^{\frac{-\Delta t}{\lambda}} f(r, v, t) \tag{5.6}$$

By using a linear approximation for f^{eq} and neglecting terms of $(\Delta t)^2$ leaves Equation 5.7, while combining 5.6 and 5.7 leaves us with 5.8.

$$f^{eq}(r + vt', v, t + t') = \left(1 - \frac{t'}{\Delta t}\right) f^{eq}(r, v, t) + \frac{t'}{\Delta t} f^{eq}(r + v\Delta t, v, t + \Delta t) \tag{5.7}$$

$$f_{t+\Delta t} = \frac{e^{\frac{-\Delta t}{\lambda}}}{\lambda}\left[f_t^{eq}\left(\int_0^{\Delta t} e^{\frac{-\Delta t}{\lambda}} dt' - \int_0^{\Delta t} e^{\frac{t'}{\lambda}} \frac{t'}{\lambda} dt'\right) + f_{t+\Delta t}^{eq} \int_0^{\Delta t} e^{\frac{t'}{\lambda}} \frac{t'}{\lambda} dt'\right] + e^{\frac{-\Delta t}{\lambda}} f_t \tag{5.8}$$

A secondary version of f, $g_{t+t'}$, is representative of a different secondary timestep altogether, $g(r+vt',t+t')$. Relatively simple algebraic manipulation leaves Equation 5.9, which can then be integrated by parts to reveal 5.10.

$$f_{t+\Delta t} = \frac{e^{\frac{-\Delta t}{\lambda}}}{\lambda}\left[f_t^{eq}\int_0^{\Delta t} e^{\frac{t'}{\lambda}}dt' + \left(f_{t+\Delta t}^{eq} - f_t^{eq}\right)\int_0^{\Delta t} e^{\frac{t'}{\lambda}}\frac{t'}{\lambda}dt'\right] + e^{\frac{-\Delta t}{\lambda}}f_t \quad \textbf{(5.9)}$$

$$f_{t+\Delta t} = \frac{e^{\frac{-\Delta t}{\lambda}}}{\lambda}\left[f_t^{eq}\left(\lambda e^{\frac{\Delta t}{\lambda}} - \lambda\right) + \left(f_{t+\Delta t}^{eq} - f_t^{eq}\right)\left(\lambda e^{\frac{\Delta t}{\lambda}} - \frac{\lambda^2 e^{\frac{\Delta t}{\lambda}}}{\Delta t} + \frac{\lambda^2}{\Delta t}\right)\right] + e^{\frac{-\Delta t}{\lambda}}f_t \quad \textbf{(5.10)}$$

Further algebraic collection simplifies this equation further and leaves Equation 5.11.

$$f_{t+\Delta t} = f_t + \left(e^{\frac{\Delta t}{\lambda}} - 1\right)\left(f_t - f_t^{eq}\right) + \left[1 + \frac{\lambda}{\Delta t}\left(e^{\frac{\Delta t}{\lambda}} - 1\right)\right]\left(f_{t+\Delta t}^{eq} - f_t^{eq}\right) \quad \textbf{(5.11)}$$

A first-order Taylor expansion on $e^{\frac{\Delta t}{\lambda}}$ gives, $1+\frac{\Delta t}{\lambda}$, which after once again excluding terms including $(\Delta t)^2$, leaves us with Equation 5.12 with a dimensionless relaxation time, $\tau = \frac{\lambda}{t}$.

$$f(r + v\Delta t, v, t + \Delta t) = f(r, v, t) - \frac{f(r,v,t) - f^{eq}(r,v,t)}{\tau} \quad \textbf{(5.12)}$$

5.3 Lattice-Boltzmann Discretization in Space

Fixing the system to a lattice and then restricting velocities into distinct, discretized directions allows the discretization of the previous equation in space. Velocities are discretized

by dimension and quantity, leading to the *DxQy* system that governs motion throughout the lattice sites. A D2Q5 system, for example, would operate in two dimensions while allowing the particle to remain in place or facilitating motion in the four cardinal directions but denying diagonal movement. In such a system, diagonal motion becomes a two-step movement while a D2Q9 environment would make diagonal motion a single-step process.

Restricting the possible velocities within the system allows us to simplify $f(r,v,t)$ as $f_i(r,t)$, which is the distribution function in the i-th velocity direction. Incorporating $f_i(r,t)$ into (5.12) leaves the final Lattice-Boltzmann equation (5.13).

$$f_i(x + v_i\Delta t, t + \Delta t) = f_i(x_i, t) - \frac{f_i(x_i,t) - f_i^{eq}(x_i,t)}{\tau} \quad \textbf{(5.13)}$$

However, this leaves f_i^{eq}, the fully discretized Maxwell-Boltzmann equilibrium distribution, thus far undefined. The equilibrium distribution varies with a set of equations that must be solved by the model itself and is dependent on probabilities, w_i, attached to each velocity direction as well as the speed of sound within the lattice, c_s. In the D2Q5 system, for example, probabilities were fixed at w={1/3, 1/6, 1/6, 1/6, 1/6}, and the speed of sound through the lattice was set at 1/3.

$$f_i^{eq} = w_i\rho\left(1 + \frac{u \cdot v_i}{c_s^2}\right) \quad \textbf{(5.14)}$$

The macroscopic density, ρ, and nodal velocity, u are defined in Equations 5.15 and 5.16.

$$\rho = \sum_{i=0}^{q-1} f_i \quad \textbf{(5.15)}$$

$$u = \frac{1}{\rho}\sum_{i=0}^{q-1} f_i\, v_i \qquad \textbf{(5.16)}$$

Movement within the lattice is controlled via collisions and streaming. During collision, the distribution function values $f_i(r,t)$ are updated via the right-hand side of Equation 5.13. Streaming allows the propagation of the updated values in each velocity direction from time, t to $t+\Delta t$. The collide-and-stream process is extremely useful in fluid flow simulation and can be directly related to the lattice gas automata, the Boltzmann equation, and the Navier-Stokes equation[6,7,9,10]. Lattice-Boltzmann methods can also be used to solve advection-diffusion equations when given the correct equilibrium distribution, thus creating a powerful tool for modeling heat flow[11,12].

5.4 Parallel Computing as a Research Tool

Though unused for the examination of shear stresses upon polymer blends, parallelization allows researchers to create larger systems while simultaneously speeding up the process by dividing the system into equal sized samples based upon their location within the experimental matrix and evaluating each sample individually before sending the resulting data to the master controller. Parallelization also permits the users to optimize computational power by creating clusters of computers whose only necessary criteria is that the available nodes must run on the same operating system, though it is generally optimal should the hardware be somewhat similar in architecture[1]. However, it is possible that the hardware used may be dramatically different, as runtimes in large systems are usually limited by the processing speed of the slowest member

node within the cluster. In this way, equipment that is nearing obsolescence can be utilized, extending its lifetime as useful hardware. Utilization of the cluster structure also allows for equipment hotswapping so that should one node of the cluster become unusable or unstable for any reason, such as failed hard drives, overheating, or fan issues, that node may be replaced quickly or ignored completely without bringing the entire system down.

Despite the advantages presented by parallelization, there are distinct drawbacks to its implementation. Most importantly, the slowest component in use is the upper limit of the speed gains that may be achieved; while each processor is available to run calculations on its own segment of the data set, the system as a whole must wait until all processors have completed their assigned tasks before continuing onto the next step, lest timesteps begin to overlap[13]. Secondly, creating algorithms to be run in parallel produces a steep learning curve in syntax. Parallel processing languages, such as OpenMPI, are meant to be extensions of commonly used programming languages, such as C and FORTRAN[14,15]. Parallel programming languages are also written so as to facilitate multiprocessor access via a single line of syntax, thus preventing code being written multiple times to access different processors. In spite of these attributes, the syntax presented by these languages is markedly different from commands familiar to serial programmers. Additionally, while the code implementation is able to break up the data assign sections to the processors on its own, the programmer must take care to be able to estimate the breaks in the data so as to account for those data points that exist at the edges of those sections, allowing the programmer to know if returned data is correct and applicable. This may lead to parallel processing feeling more like an entirely new language rather than an extension of a known idiom.

5.5 The Parallel Lattice-Boltzmann Solver (Palabos)

Third-party open-source software, such as Palabos and LAMMPS, take these factors into account prior to release, meaning that the researcher need only have a passing knowledge of parallel processing to accomplish the majority of tasks. These software packages still require that the end user know how to program serially and learn how to code and understand the functions necessary to implementing the package. This sort of shortcut does result in new syntax being learned and the major drawback of this method is that new keywords are normally limited to a specific library or software extension. Beyond that, should any edits need be made to the packaged syntax as it exists, one must have a firm command of both serial and parallel programming so as to keep to data flow optimized. It is this difference that makes the distinction between these packages and other third-party packages, such as MATLAB or Mathematica, which feature drag-and-drop menus, and require little prior programming knowledge to use.

Palabos is an open-source external C++ library that allows us to approach these issues without worrying about supplying the background mathematics, allowing the focus to be on setting up the initial conditions quickly and efficiently. Palabos is the parallelizable evolution of Open-LB, another software package that was focused on moving the Boltzmann method into the realm of simulation via the Lattice-Boltzmann methodology[8]. Palabos implements Lattice-Boltzmann models via a grid of nodes, which are defined by the values of the distribution function and macroscopic density and velocity. Dynamics objects are used to define the collision and streaming behavior between nodes. These dynamics objects, as well as specific lattices, are pre-defined for several two and three-dimensional applications[16]. Utilizing the D2Q5 and D3Q7 models of motion for two and three dimension, respectively, the advection-diffusion model was used as a foundation for heat transfer simulations. Advection-diffusion was controlled via a

BGK dynamics object, whose functions are governed by the equations derived earlier within the chapter.

However, since the advection-diffusion equation actually only describes the transport of temperature, the advection-diffusion Lattice-Boltzmann models have previously only been used for modeling heat within a single phase, where there is only a single heat capacity which allows heat transport and transfer to be equivalent[11,17]. However, in systems with multiple phases – each with its own heat capacity – heat transfer between the phases must be taken into account. In order to solve this issue, a model was developed in which a preexisting prototype of advection-diffusion Lattice-Boltzmann model considered the difference in thermal properties of each phase as well as the physics of heat transfer at the interface between phases. It is this resultant model that was used to complete the simulations described in the sections below.

5.6 Proof of Concept Preliminary Model

The experiment began with a proof of concept model in which multiphase heat transport was simplified in order to verify the efficacy and accuracy of the model. After verifying a multiphase structure that utilized perfectly insulating fillers, the model could then be modified to simulate and examine heat transport through both phases, as well as the interfaces between phases.

In order to begin the initial model under the simplest interaction conditions possible, a two-dimensional prototype was created that would model heat diffusion from a heat source to a heat sink. Beginning with a cold uniform temperature throughout the matrix, a heat pulse was

generated at the inlet end of the system and the heat diffused horizontally across the matrix toward the heat sink. In order to verify that no heat was lost until it reached the heat sink, periodic boundary conditions were kept in the vertical directions. The inlet boundary was defined as a constant temperature boundary to act as a continuous heat source while an adiabatic, zero-gradient boundary formed the heat sink, impermeable to heat transfer. The heat pulse was implemented for a fixed amount of time, at which point the inlet was reset to cold, allowing the existing heat from the pulse to dissipate throughout the system. Tests on this system revealed that the model was accurate and allowed for clear heat diffusion from source to sink.

5.7 The Insulating Filler Model

Having verified the proof of concept configuration, the next step would be extending the model to better simulate a composite material. In this system, randomly distributed, non-conducting, insulated particles within the lattice were designated as filler material. Since these particles do not allow for heat propagation, they were implemented in the material via the bounce-back dynamic; the bulk material retained the advection-diffusion dynamic.

Bounce-back dynamics work by reflecting, rather than transferring, the density, f_i, acting upon a bounce-back particle. In essence, a particle governed by bounce-back dynamics creates an obstacle to fluid flow: one that must be redirected around, rather than passed over. However, bounce-back dynamics have not been extensively utilized in advection-diffusion Lattice-Boltzmann examples prior to this study; therefore, the model's numerical accuracy had to be

proven. By examining the percolation transition and threshold within the model, the model could be confirmed to mirror known systems.

The percolation threshold is the concentration at which the bounce-back fillers would prevent heat diffusion from inlet to outlet. This value, 59.27% of conducting material, has been discussed thoroughly in experimental settings and would have to be matched in order for the system to be deemed accurate[18]. With respect to this determination, the percolation algorithm examines clusters of connected particle to determine overall lattice connectivity. Each conducting particle was labeled as its own cluster, while every non-conducting filler particle was ignored. Should a conducting particle have a nearest neighbor of another conducting particle, both were now clustered, with a cluster value of that of the lowest valued node. This process was repeated until no further changes could be made in cluster labeling. Once completed, cluster values along the inlet boundary were compared to those along the outlet boundary; should one cluster exist on both boundaries, it indicated that a percolated cluster existed within the system.

The model was then tested near and at the percolation threshold, producing the cluster maps seen in Figure 5.1. Each color within the cluster maps (on the left) indicates a different cluster, while black indicates non-conducting filler. It should be noted that the cluster maps only take into account material within the bulk as there is no material, conducting or otherwise, available at either boundary. The figures on the right are the thermal maps that correspond to each cluster map. At thirty-eight percent filler concentration, the system is dominated by one large cluster, allowing heat to diffuse unfettered through the system. A one percent increase results in the growth of smaller clusters within the bulk, though none large enough to impede heat flow. The outlet boundary also begins the shift from pink (warm) to blue (cold), though in this case it is grey, indicating a mild temperature increase that is shifting downward. The forty

percent filler concentration marks the lower limit of the experimental percolation threshold and the smaller clusters, while not yet impenetrable, clearly have begun to overtake the outlet boundary. The thermal map's outlet boundary, meanwhile, is now a periwinkle color indicating that the sink is still yet colder than it was in the previous examples. Finally, at forty-one percent filler concentration, large clusters have formed within the system, preventing the pervasiveness of heat flow as indicated by the dark shade of blue in the corresponding thermal map. Meanwhile, the cluster maps seem to indicate some level of striation within the system, signifying long and persistent boundaries of filler material within the bulk.

Numerical analysis was also done on the ratio of the number of clusters present and the number of conductive particles within the system against given filler concentration. Figure 5.2 demonstrates a dramatic increase in the number of clusters near the percolation threshold ($\phi_f \sim$ 0.40). While this cluster shift should be starker, much like a Heaviside step function, this smearing of the transition point may be due to finite-size scaling. Both the cluster maps and thermal maps indicate that the percolation threshold resides at just over forty percent filler concentration, which is in agreement with the experimental value of 40.73% for a square lattice with site connectivity, denoting that bounce-back dynamics can be used to model insulating filler dynamics within a advection-diffusion Lattice-Boltzmann simulation.

Figure 5.3 shows that higher concentrations of non-conducting filler particles delay heat propagation within the bulk material. Although these filler concentrations are well below the percolation threshold, the fillers are enough to impede heat diffusion. In a ten percent filler configuration, heat reached the middle of the bulk quickly, as indicated by the light pink spots near the center of the bulk. While these filler concentrations were not enough to prevent heat

flow, the bounce-back dynamics governing the fillers further reduced the reach of the heat pulse as concentration increased, further verifying the accuracy of the bounce-back dynamics.

5.8 The Enhanced Heat-Resistant Filler Model

While the insulating filler model served well as proof of concept for the use of bounce-back dynamics as governing criteria for filler behavior, realistic fillers cannot repel or reflect all heat back into the system. In order to create a more realistic model of thermal transport and transfer, the fillers would have to be able to absorb a portion of the heat while reflecting the remaining portion back into the system. Additionally, heat should diffuse more easily through bulk-bulk and filler-filler node interactions than bulk-filler interactions due to the connected structures these two phases create within the system. Bulk-filler interactions require heat transfer across an interface and thus, the governing criteria that defines that dynamic must be written.

This essentially creates three phases within the system and consequently, six different interactions to be considered. It is important to define the interactions at play since each phase has heat capacity and thermal diffusivity properties that are specific to that phase. Assuming that like-type interactions (bulk-bulk, filler-filler, interface-interface) are governed by the same dynamics in line with the previous model while taking into account the differences in specific heat and thermal diffusivity, this still leaves the bulk-filler, filler-interface, and bulk-interface interactions without governing dynamics. One can also remove the bulk-filler interaction since the introduction of an interfacial phase negates direct interaction between the bulk and filler phases. Finally, with the exception of the bounce-back mechanic, heat absorption and transfer

must be the same for the bulk-interface and filler-interface interactions. Simply speaking, this narrows the six interactions to just two: like-type interactions and phase-interface interactions.

A thermal boundary resistance defines heat transfer at an interface; therefore, the thermal diffusivities of each phase must be treated by defining different relaxation times, τ, for each[19]. Previous studies have already shown that thermal diffusivity is proportional to the relaxation time within advection-diffusion Lattice-Boltzmann models. Within these models, heat diffusion is implemented through the propagation of the distribution. However, at the interface, the collide-and-stream process must be modified to account for the differences in heat capacity and thermal diffusivity.

Since these interactions are generally the same with the exception of the values for respective thermal properties, modifications will be discussed in generic terms. In order to determine these modifications, two generic phases ***A*** and ***B***, each with its own respective heat capacity, C_A and C_B, are defined. A heat transfer coefficient, H_{AB}, is used to describe the heat flow resistance between both phases and must always have a value between zero and one, inclusive, and be commutative such that H_{AB} is always equivalent to H_{BA}. Consider the streaming of a distribution function value, f_i, from position x_A with temperature T_A in phase ***A*** to position x_B with temperature T_B in phase ***B***. Since phase ***B*** maintains thermal properties distinctive from those in phase ***A***, only a portion of f_I is transferred into ***B***, with the remainder reflected into ***A***. This combination of normal Lattice-Boltzmann mechanics and bounce-back schema is dependent on H_{AB} and the local temperature gradient, ΔT, shown below.

$$\Delta T = \frac{T_1 - T_2}{T_1 + T_2} \qquad \textbf{(5.17)}$$

Basic thermodynamics specifies that heat traverses only from areas of higher temperature to areas with lower temperature; hence, for ΔT less than or equal to zero, f_i, is completely reflected back into A. For ΔT greater than zero, however, ***B*** absorbs $H_{AB}\Delta T$ of f_i and reflects (1-$H_{AB}\Delta T$) of f_i into ***A***. However, this accounts only for temperature rather than heat and thus must be multiplied by a ratio of the heat capacities. Incorporating these adjustments into the model leaves the following equation for a zero or negative temperature gradient since no change is expected and all heat is subject to bounce-back.

$$f_j' = f_j' + f_i - \frac{f_i - f_i^{eq}}{\tau}, \tag{5.18}$$

Meanwhile, a positive temperature gradient leaves the equations that follow, wherein $g_i = f_i(x + v_i\Delta T)$; $f_i = f_i(x, t)$; $f_i^{eq} = f_i^{eq}(x, t)$; and j is the direction index opposite to i, or the direction in which bounce-back will occur.

$$g_i' = g_i' + H_{AB}\Delta T \frac{C_A}{C_B}\left(f_i - \frac{f_i - f_i^{eq}}{\tau}\right) \tag{5.19}$$

$$f_j' = f_j' + (1 - H_{AB}\Delta T)\left(f_i - \frac{f_i - f_i^{eq}}{\tau}\right) \tag{5.20}$$

The use of the prime marker (g', f') is used to denote that these values were stored in a secondary matrix of values that was initialized to zero prior to each iteration of the procedure. This is necessary because the values of each distribution function, g and f, may be updated by one of two ways: the addition of multiple values due to absorption and bounce-back occurring around the node, or the two updates necessary when transferring heat between phases. To this

end, once the iteration had been completed, the temporary values stored on the secondary matrix were then copied into the primary matrix and the simulation continued.

5.9 Extension into Three Dimensions

Once the model had been extended to account for heat absorption within the filler as well as the bulk nodes, the next challenge lay in extending the model into three dimensions, thus creating a model that could account for depth as well as width and height. The bulk of the extension into the third dimension is rather simple as Palabos can quite easily be manipulated into accounting for the D3Q7 environ and also has incorporated three-dimensional counterparts for nearly every offered two-dimensional dynamics schema. In this new model, boundaries were periodic in the y and z directions, while the x-direction boundaries remained the same as before, only extended to account for the face of the simulation box.

However, while the previous models were limited to point and square fillers, a shift into the third dimension allows for a wider variety of filler morphologies, with variable complexity, that could be examined. Applying this new level of complexity, tube-like fillers were made, of particular interest given the high thermal conductivity and popularity of carbon nanotubes. Initialization of the tubular fillers began much the same way the point fillers began – random positions were selected within the lattice that became the fillers' seed points.

While the D3Q7 schema does give a new flexibility in terms of dimension, it does not come without limits; heat may only move laterally up or down, left or right, forward or back, or stay in place, as there is no diagonal movement built into the schema. To overcome this

limitation, diagonal rod fillers were created in a staircase pattern, wherein a collection of point fillers were not allowed to disassociate from one another; moreover, once a direction had been chosen, each point filler could be placed only in that direction, forming a step or staircase pattern. This continued until the filler collection had reached a predetermined length, l. However, when a direction has been chosen, the length was first examined to ensure that there was no overlap with another filler; otherwise, a new direction was chosen. The length check also ensured that filler creation remained within the bounds of the bulk, especially in the x-direction, where no periodic boundary conditions exist.

An orientation probability, P, was created that was used to determine whether a tube filler would be oriented parallel to the x-axis. Orientation was achieved via a random number generator; only if a number less than or equal to P was generated, the filler rod would be oriented parallel to the x-axis. The orientation probability parameter allowed for an inspection of whether tube alignment could affect heat transport within the bulk and filler materials.

5.10 Validation and Results of the Three-Dimensional Model

Validation of the three-dimensional model lay in studying the effect of filler concentration on heat transport in the bulk and filler materials. Though tubular fillers could and had already been created, the initial verification tests were run on simple point fillers with greater thermal diffusivity and heat capacity than the bulk material. The expectation of the heat-resistant filler is that, with the fillers absorbing heat from the surrounding bulk material, heat will dissipate out of the system more quickly. As more filler is added, particularly once the

percolation threshold has been reached, heat within the filler phase should dissipate more quickly due to the incorporation of connected structures.

Having applied a heat pulse that was allowed to run for one thousand steps, the average temperature in the bulk and filler phases were plotted over time. The boundary face between inlet and bulk was used as a constant heat source for the duration of the pulse, rather than allow the entire inlet to act as a heat source as was done in the two-dimensional model. The inlet, no longer used as a heat source, was switched to heat sink, allowing heat to exit the system. Figures 5.4 and 5.5 show that the system worked as expected, absorbing heat until the pulse had concluded and then dissipating it slowly as the system relaxed toward equilibrium. Systems incorporating point fillers did, in fact, reduce the average temperature within the bulk and filler nodes. Additionally, an increase in filler concentration produced lower temperature curves within the bulk as well as the filler.

Having verified that the model was functional for point fillers and having established a baseline of model reaction, the model was set to determine the heat dissipation under a series of the thermal and morphological properties. Thermal diffusivity for the filler materials, for instance, was set by default to be slightly higher than that of the bulk, specifically to allow for heat absorption. Diffusivity was also tested at much higher levels for comparative purposes. Figures 5.6 and 5.7 show that for a filler concentration well under the percolation threshold, the temperature curves for the bulk and filler materials are indistinguishable. Increased filler concentration, as before, returned a lower thermal curve, while the systems with a much higher diffusivity are generally lower than that of the slightly higher diffusivity system. However, it is a stretch to call this difference significant; thus, it is fair to say that filler concentration and internal connectivity play a more dominant role in reducing node temperature than diffusivity does.

Finally, the newly constructed tube fillers were tested against the point particles. Tube alignment was also taken into account to determine whether the alignment in the direction of heat flow was a significant factor in heat transference. Assuming a tube filler length of seven and a filler concentration of forty percent, random tubes were given an alignment value of P=0 while the aligned tubes were designated at 0.5. Figure 5.8 indicates that tube fillers resulted in higher bulk temperatures than the systems incorporating point fillers. Furthermore, systems containing aligned fillers performed much worse at removing heat from the bulk than their random counterparts. Meanwhile, Figure 5.9 indicates that for filler node temperature, random tube fillers and the point particles are nearly indistinguishable while the aligned fillers dissipated heat much more slowly. This suggests that heat dissipation is more a factor of surface area normal to the direction of heat flow rather than to the incorporated filler morphology.

5.11 Summary and Conclusions

A versatile model for simulating heat transport in multiphase systems was created by modifying a Lattice-Boltzmann model used in single-phase systems. The multiphase model developed can account for differences in thermal diffusivity and heat capacity for various materials as well as the heat transfer at the interface between bulk and filler nodes. As such, it produces an efficient method with which to study the dynamics of heat flow in composite materials. Simulations of materials with various thermal diffusivities, morphologies, heat capacities, and thermal boundary resistances in contact with a heat pulse have been reported and

are considered reasonable and justifiable, thus giving notice to the robustness of the developed model.

The model was used to show that a higher concentration of fillers could be used to dissipate more quickly as well as keep bulk temperatures lower. Results also indicate that point fillers are more effective than tube fillers at heat dissipation. It was also demonstrated that heat dissipation via tubular fillers is highly dependent on orientation normal to the direction of heat flow. Given the robustness of the developed model, there are still more environments which would benefit from simulation, and a few of these are discussed in the next chapter.

5.12 References

1 Pappetti, F. & Succi, S. *An Introduction to Parallel Computational Fluid Dynamics*. (Nova Science Pub Incorporated, 1996).

2 Succi, S. *The Lattice-Boltzmann equation for fluid dynamics and beyond*. (Clarendon Press ; Oxford University Press, 2001).

3 Narasimhan, T. N. Fourier's heat conduction equation: History, influence, and connections (Reprinted from Reviews of Geophysics vol 37, pg 151-172, 1999). *P Indian as-Earth* **108**, 117-148 (1999).

4 Sukop, M. C. & Thorne, D. T. *Lattice-Boltzmann modeling : an introduction for geoscientists and engineers*. (Springer, 2006).

5 Nourgaliev, R., Dinh, T.-N., Theofanous, T. & Joseph, D. The Lattice-Boltzmann equation method: theoretical interpretation, numerics and implications. *International Journal of Multiphase Flow* **29**, 117-169 (2003).

6 He, X. Y., Shan, X. W. & Doolen, G. D. Discrete Boltzmann equation model for nonideal gases. *Phys Rev E* **57**, R13-R16, doi:Doi 10.1103/Physreve.57.R13 (1998).

7 Chen, S. & Doolen, G. D. Lattice-Boltzmann method for fluid flows. *Annu Rev Fluid Mech* **30**, 329-364, doi:Doi 10.1146/Annurev.Fluid.30.1.329 (1998).

8 Mcnamara, G. R. & Zanetti, G. Use of the Boltzmann-Equation to Simulate Lattice-Gas Automata. *Phys Rev Lett* **61**, 2332-2335, doi:Doi 10.1103/Physrevlett.61.2332 (1988).

9 He, X. Y. & Luo, L. S. Theory of the Lattice-Boltzmann method: From the Boltzmann equation to the Lattice-Boltzmann equation. *Phys Rev E* **56**, 6811-6817, doi:Doi 10.1103/Physreve.56.6811 (1997).

10 Qian, Y., d'Humieres, D. & Lallemand, P. Lattice BGK models for Navier-Stokes equation. *EPL (Europhysics Letters)* **17**, 479 (1992).

11 Chopard, B., Falcone, J. L. & Latt, J. The Lattice-Boltzmann advection-diffusion model revisited. *Eur Phys J-Spec Top* **171**, 245-249, doi:Doi 10.1140/Epjst/E2009-01035-5 (2009).

12 Guo, Z.-L., Shi, B.-C. & Wang, N.-C. Fully Lagrangian and Lattice-Boltzmann methods for the advection-diffusion equation. *Journal of scientific computing* **14**, 291-300 (1999).

13 Grama, A. *Introduction to Parallel Computing*. (ADDISON WESLEY Publishing Company Incorporated, 2003).

14 Barrett, B., Squyres, J. M., Lumsdaine, A., Graham, R. L. & Bosilca, G. Analysis of the component architecture overhead in open MPI. *Lect Notes Comput Sc* **3666**, 175-182 (2005).

15 M. Squyres, J. & Lumsdaine, A. in *Component Models and Systems for Grid Applications* (eds Vladimir Getov & Thilo Kielmann) Ch. 11, 167-185 (Springer US, 2005).

16 Palabos - Parallel Lattice Boltmann Solver (2009).

17 Stiebler, M., T, J., #246, lke & Krafczyk, M. Advection-diffusion Lattice-Boltzmann scheme for hierarchical grids. *Comput. Math. Appl.* **55**, 1576-1584, doi:10.1016/j.camwa.2007.08.024 (2008).

18 Stauffer, D. & Aharony, A. *Introduction to percolation theory*. 2nd edn, (Taylor & Francis, 1992).

19 Guo, Z. L., Shi, B. C. & Zheng, C. G. A coupled lattice BGK model for the Boussinesq equations. *Int J Numer Meth Fl* **39**, 325-342, doi:Doi 10.1002/Fld.337 (2002).

5.13 Figures

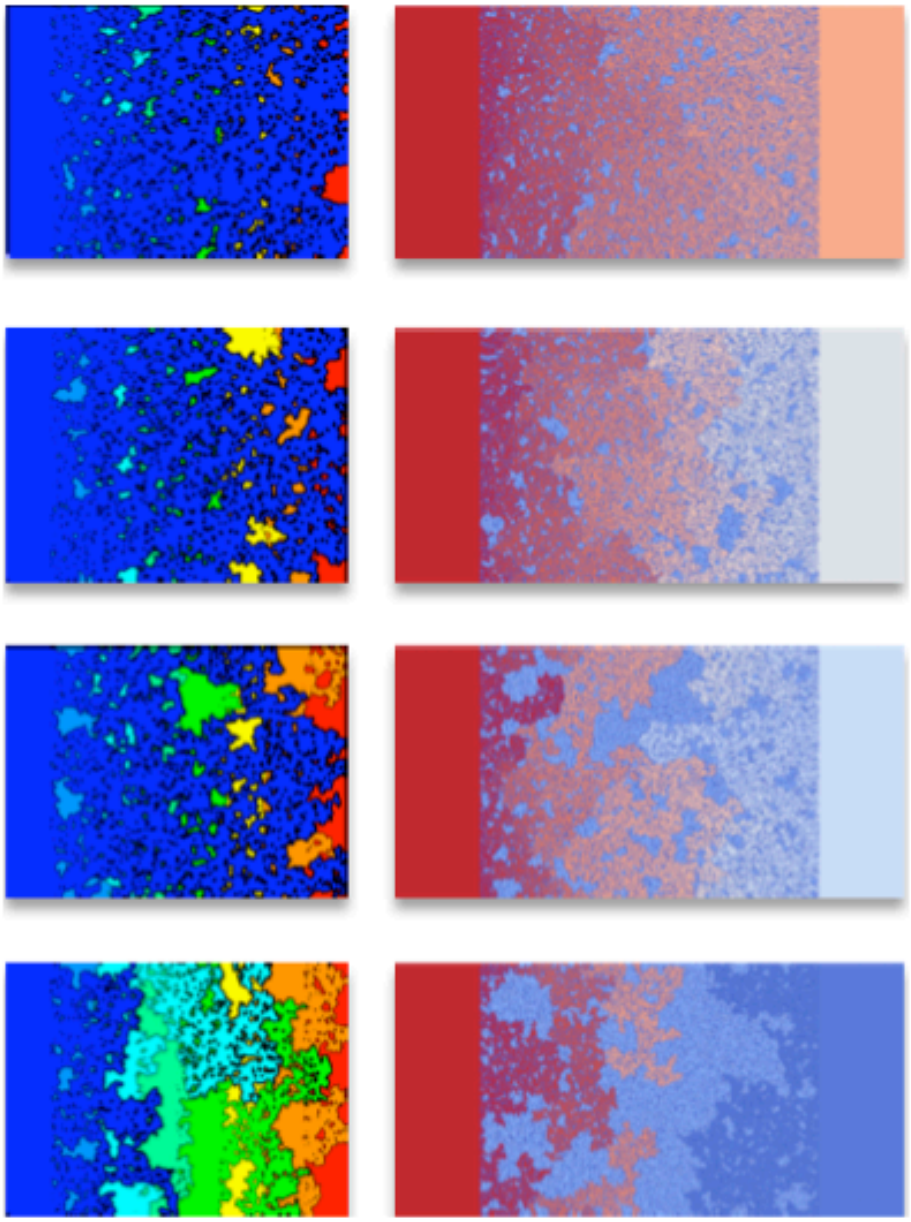

Figure 5.1. Cluster formation maps produced by the percolation algorithm (left) and corresponding thermal maps produced by the advection-diffusion Lattice-Boltzmann method. Rows are 38, 39, 40, and 41 percent filler concentration, respectively.

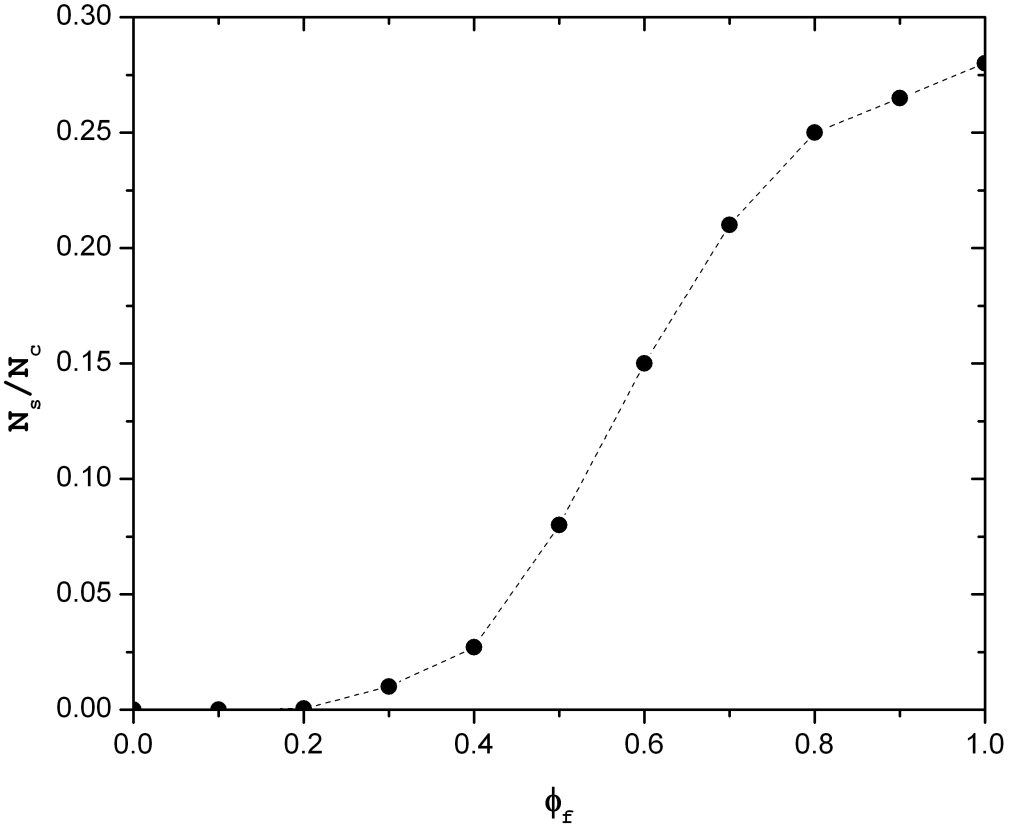

Figure 2. Ratio of number of clusters to number of conductive particles by non-conductive filler concentration

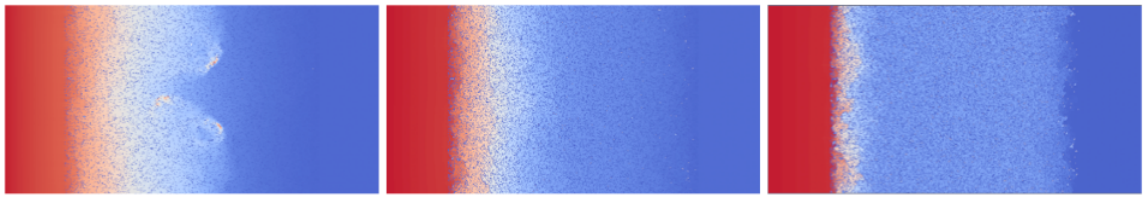

Figure 5.3. Heat propagation in systems containing (from left to right): 10%, 20%, and 30% non-conductive point fillers.

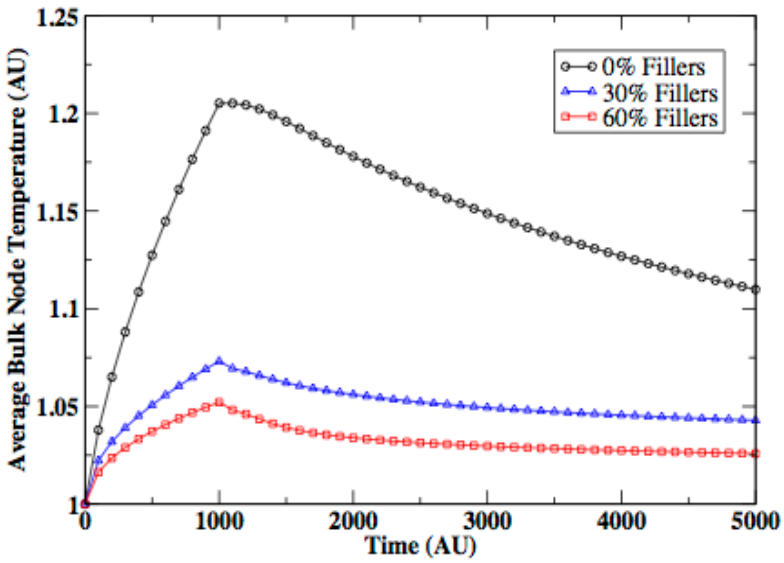

Figure 5.4. The effects of increased point filler concentration on average bulk node temperature within the system.

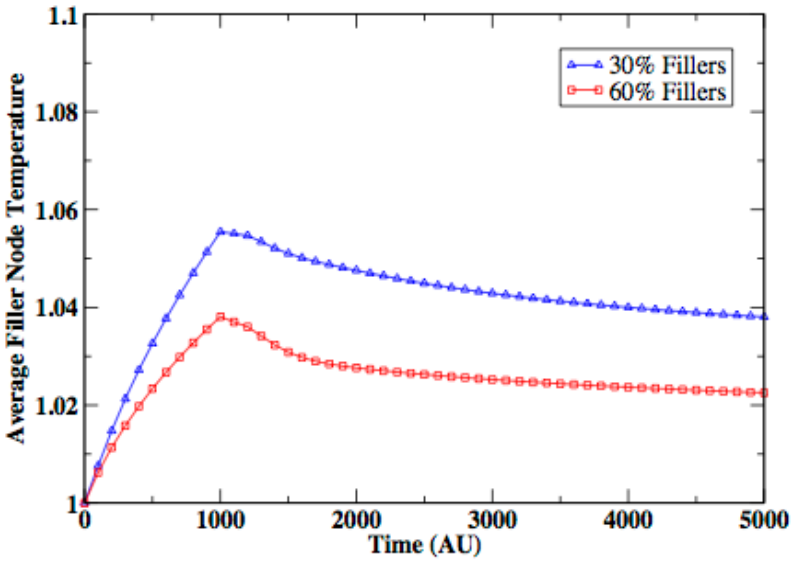

Figure 5.5. The effects of increased point filler concentration on average filler node temperature within the system.

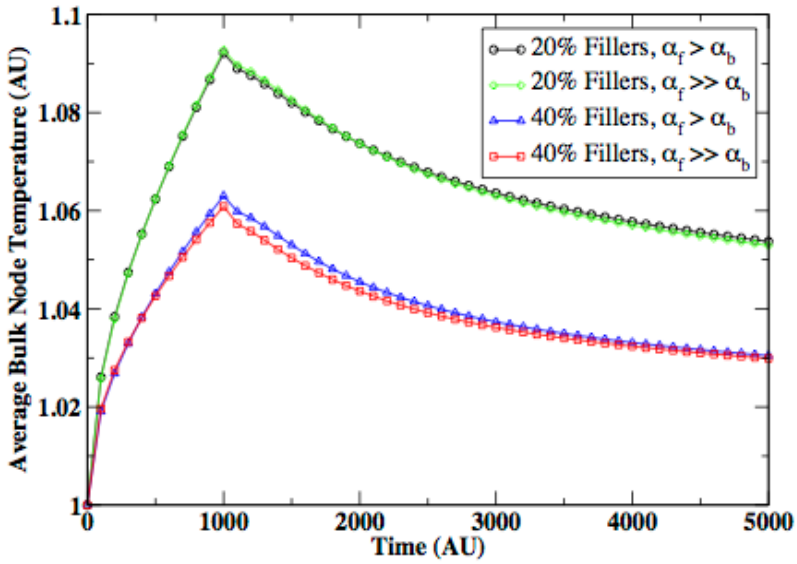

Figure 5.6. The effects of filler thermal diffusivity on average bulk node temperature within the system.

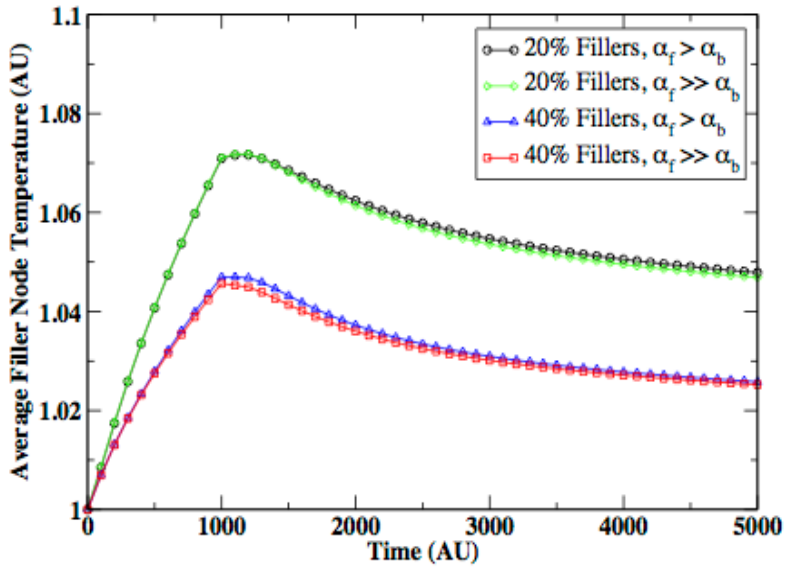

Figure 5.7. The effects of filler thermal diffusivity on average filler node temperature within the system.

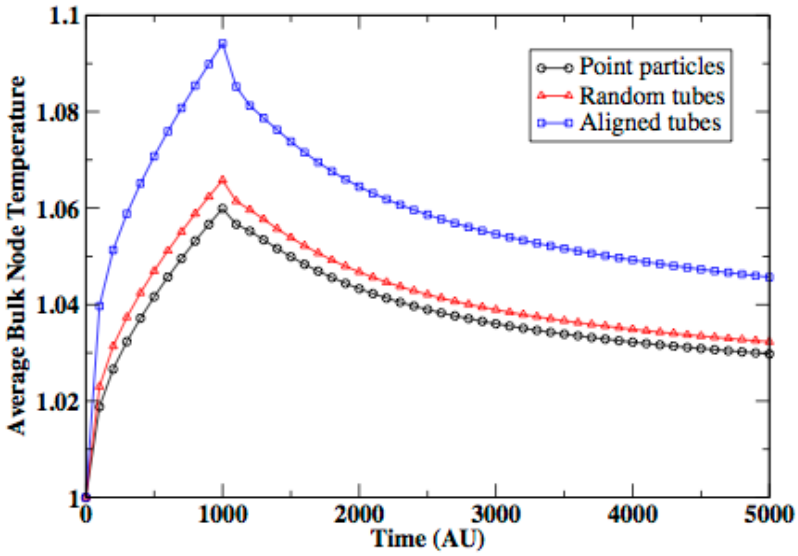

Figure 5.8. The effects of filler morphology and orientation on average bulk node temperature within the system.

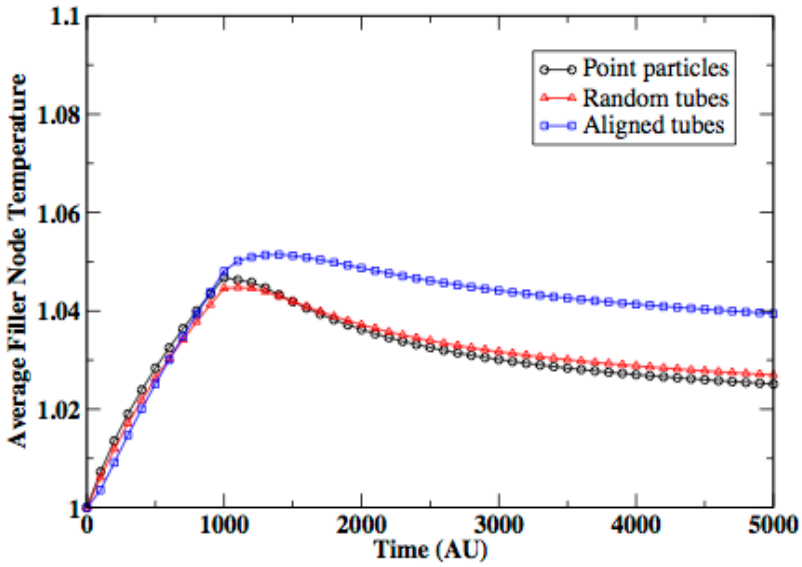

Figure 5.9. The effects of filler morphology and orientation on average filler node temperature within the system.

Chapter 6 – Summaries, Conclusions, and Future Work

6.1 Summary and Conclusions – Nanoparticles as Compatibilizers in Polymer Blends

Throughout the course of Chapter Four, it was shown that nanofiller particles could, in fact, be used as compatibilizers in order to strengthen polymer blends. Even just a two percent concentration of small nanofiller inclusion could dampen slip significantly, something that could not be achieved with the same concentration of diblock inclusion. Furthermore, in cases where there is a limited amount of polymeric phase mixing at the interface, slip reduction tended to be consistent and predictable regardless of shear velocity. This is in direct contrast to diblock inclusion, wherein slip reduction is velocity dependent, due to the relationship between shear velocity and chain alignment and orientation.

As nanofiller concentration increased, slip reduction also increased. This held true for increased filler size as well. In fact, systems incorporating large fillers were found to perform better than their smaller filler counterparts in all cases. As such, a ten percent inclusion of small nanofillers was shown to reduce slip at about the same rate as a two percent addition of large nanofillers. However, as miscibility increased, there was evidence that the polymer chains within the interfacial region were being crowded out by the nanofillers, and it is unknown how the system would react to even higher concentrations of filler additives. Moreover, it was discovered that the extrapolation method commonly used for determining slip length was inadequate for systems in which slip was understated, leading to the use of the differentiated velocity profile curve in order to determine slip magnitude.

An examination in the structures by which strength enhancement occurs showed an assumption of *in situ* diblock constructs to be false. The limitations necessary for these structures to be mechanically relevant were shown to be too constricting as there were only a few chains by which to create these structures and a lack of compulsory intermolecular forces allowed the chains to attach and detach temporarily as necessary. A further exploration of the internal structures showed that smaller networks were responsible for blend strength enhancement. These networks tended to be dominated by one larger network within the interfacial region while the inferior networks tended to consist of only a couple of nanofillers and a chain or two. After determining the method by which nanofiller addition assisted in strength enhancement, this study set out to resolve whether nanofillers could also be used to curb polymer ignition and combustion.

6.2 Future Work – Mixed Nanofiller Systems

While the work done thus far has been significant and comprehensive in understanding the role of nanofillers and their utility as compatibilizers within blends, it is far from complete. As with any field of research, resulting answers only lead to more questions. What follows are ideas for how to extend the research described thus far into future projects of varying length and difficulty.

Up to this point, this line of simulations has been concerned only with systems in which the nanofillers were uniform spheres, representative of carbon black. However, the system is not limited to uniform spheres as it would also be possible to utilize platelets and fillers in order to

examine how filler morphology affects strength enhancement. Meanwhile, it is entirely possible to create systems wherein nanofillers of varying scales and morphologies exist.

Varying the size scale of filler particles would allow researchers to examine whether the addition of both small and large fillers would further enhance the reduction of interfacial slip. Since the large filler systems seemed to experience crowding at the interface upon reaching a relatively low volume percentage threshold, could the added mobility of the smaller fillers aid in bridging the interfacial gap without sacrificing the utility presented by the large fillers? If these systems prove to be more efficient, at what point does the ratio of large-to-small fillers become counterproductive? And finally, at which point does cost-effectiveness outweigh utility?

These are all questions that must be answered in order to create a more comprehensive understanding of how nanofillers enhance the strength of polymer composites. While the research presented in the majority of this thesis is important in understanding their role on reducing planar shear, it is merely a small part of the field as a whole. The system, as created, is robust enough to answer all of these with relatively minor modifications. This is to say nothing about examining the role of nanofillers upon thin film stresses and processes, which can also be handled by the program.

6.3 Future Work – Phase-Preferential Nanofiller Manipulation Within Polymer Blends

Consider though, the focus of this research was based on allowing the nanofillers to remain attractively neutral to either polymer phase. However, there may be much to be gained from allowing phase preference to these particles. Of particular interest is whether phase-

preferential fillers still segregate to the interface in order to relieve any specific energy demands therein or if they remain in-phase, showing little to no effect on interfacial slip. While this project is also something that can be examined relatively quickly and economically, it may be worthwhile to determine whether adding phase-preferential fillers can result in more organized *in situ* microstructures or if these microstructures are only apparent within systems with neutral nanofillers.

In keeping with the theme of phase-preferential nanofillers while incorporating the diblock ideal, a further evolution of this project could examine the efficacy of Janus particles within the system. The Janus particle is a filler particle with a surface engineered with two hemispheres, with each hemisphere preferential to a different phase. The creation of such a nanofiller particle would be ideal for increasing miscibility along the interface since it would be attractive to both phases, yet small enough to retain mobility within the region. If placed directly at the interface, the particle would likely remain fixed at the interface, rotating only to orient the hemispheres to their best possible positions in accordance with the surrounding phases. It may be preferential, however, to study their behavior within the bulk. Since these particles are dual-phase like a diblock chain, would these Janus particles aggregate within the bulk or move toward the interface? Would any strength enhancements presented be comparable to those offered by diblocks, or would they combine the benefits of both spherical nanoparticles and diblocks?

Since the program has already been created and has been used to make planar interfaces, most of the legwork for the proposed work has already been done. The work that has been proposed has more to do with creating and mixing filler morphologies – platelets, tubes, spheres, and Janus particles. As with any project, the more work put into preparation means that there is less to do and worry about once experimentation begins. However, as robust as the system is, it

is limited by processor availability and speed as well as available memory. It is for this reason that it is probably best that these problems be examined using the advantages presented by parallel computing.

6.4 Summary and Conclusions – The Effectiveness of Nanofillers as Flame Retardant Nodes Within Polymer Blends

Using a modified version of the advection-diffusion lattice Boltzmann method, a simulation model was created that is able to examine heat transfer within a multiphase system. This model considers the bulk, the filler, and the interface between as phases and also accounts for differences in thermal diffusivity and heat capacity in order to accurately calculate heat transfer between the phases. The model progresses from two dimensions to three, and also considers the possibility of insulating fillers as well as absorbing fillers. Filler absorption was partially controlled by the bounce-back method, in which part of the heat acting upon a filler node was reflected back into the bulk, while the remaining heat was absorbed into the filler. Additionally, tube-like fillers were created, in order to mimic nanostructures known for thermal robustness, such as carbon nanotubes. Finally, the research revealed that while point fillers and randomly oriented tube fillers perform similarly, fillers aligned in the direction of heat flow are much less effective at limiting heat transfer. This is perhaps due to the minimal amount of surface area normal to the direction of heat flow.

6.5 Future Work – Predicting Better Thermally Resistant Materials via the Lattice-Boltzmann Methodology

The model can now be modified and used to study heat flow through a material with multiple bulk phases and/or several filler morphologies. Small modifications to the filler phase will also allow for the exploration of flame retardant fillers within a combustible bulk, thus allowing for modeling of flame retardant materials. Such a project would require the user to define the ignition and combustion threshold temperatures, but is otherwise relatively straightforward. By accurately modeling polymer ignition and combustion, tests of flame retardancy within polymer composites could be simulated in their entirety. As the current model only simulates heat transport, there is still a gap that must be filled in order to simulate flame resistance; however, such simulations would be helpful in guiding flame retardant research.

The model could also be modified to examine yet even more complex filler morphologies, such as those to mimic carbon nanotubes or graphene, with distinct thermal properties. Such studies would be beneficial in further understanding the role filler morphology plays in heat transport. It also opens up the exploration of how these methods can be combined to develop more efficient thermal transport devices. However, this model was ultimately an overall proof-of-concept; therefore, future expansions must do better to conform to experimental situations, such as ignition temperatures, gaseous ignition, and development of the protective char layer.

6.6 Closing Statements

While much was accomplished under the scope of this dissertation, the work presented herein can be logically extended into many other fields of research within materials science. This chapter has covered but a few examples, and there is still much data to be mined from the systems at hand. While it may be helpful to take advantage of the advancements offered by parallel programming and third-party software suites, based on the examples given, there are still plenty of experiments worth conducting given the structural methods used within this thesis.

Collected References

Chapter 1

1 Drexler, K. E., Peterson, C. & Pergamit, G. *Unbounding the future: the nanotechnology revolution*. (Morrow, 1991).

2 Nielsen, L. E. & Landel, R. F. *Mechanical Properties of Polymers and Composites*. (M. Dekker, 1994).

3 Dufresne, A. Processing of Polymer Nanocomposites Reinforced with Polysaccharide Nanocrystals. *Molecules* 15, 4111-4128 (2010).

4 Reynaud, E., Jouen, T., Gauthier, C., Vigier, G. & Varlet, J. Nanofillers in polymeric matrix: a study on silica reinforced PA6. *Polymer* 42, 8759-8768 (2001).

5 Kim, K. J. & White, J. L. Rheological investigations of suspensions of talc, calcium carbonate, and their mixtures in a polystyrene melt. *Polym Eng Sci* 39, 2189-2198, doi:Doi 10.1002/Pen.11608 (1999).

6 Flores, A., Cagiao, M. E., Ezquerra, T. A. & Calleja, F. J. B. Influence of filler structure on microhardness of carbon black-polymer composites. *J Appl Polym Sci* 79, 90-95, doi:Doi 10.1002/1097-4628(20010103)79:1<90::Aid-App110>3.0.Co;2-F (2001).

7 Yin, D., Horiuchi, S. & Masuoka, T. Lateral assembly of metal nanoparticles directed by nanodomain control in block copolymer thin films. *Chem Mater* 17, 463-469, doi:Doi 10.1021/Cm048695g (2005).

8 Yin, D. H., Horiuchi, S., Morita, M. & Takahara, A. Tunable metallization by assembly of metal nanoparticles in polymer thin films by photo- or electron beam lithography. *Langmuir* 21, 9352-9358, doi:Doi 10.1021/La0511485 (2005).

9 Gersappe, D. Molecular mechanisms of failure in polymer nanocomposites. *Phys Rev Lett* 89, doi:Artn 058301 Doi 10.1103/Physrevlett.89.058301 (2002).

10 Lobe, V. M. & White, J. L. Experimental-Study of the Influence of Carbon-Black on the Rheological Properties of a Polystyrene Melt. *Polym Eng Sci* 19, 617-624, doi:Doi 10.1002/Pen.760190905 (1979).

11 Minagawa, N. & White, J. L. Influence of Titanium-Dioxide on Rheological and Extrusion Properties of Polymer Melts. *J Appl Polym Sci* 20, 501-523, doi:Doi 10.1002/App.1976.070200222 (1976).

12 Yurekli, K. *et al.* Structure and dynamics of carbon black-filled elastomers. *Journal of Polymer Science Part B: Polymer Physics* 39, 256-275, doi:10.1002/1099-0488(20010115)39:2<256::aid-polb80>3.0.co;2-z (2001).

13 Balberg, I. A comprehensive picture of the electrical phenomena in carbon black–polymer composites. *Carbon* 40, 139-143 (2002).

14 Kim, K., Utracki, L. A. & Kamal, M. R. Numerical simulation of polymer nanocomposites using self-consistent mean-field model. *J Chem Phys* 121, 10766-10777, doi:Doi 10.1063/1.1794636 (2004).

15 Vaia, R. A. & Maguire, J. F. Polymer nanocomposites with prescribed morphology: Going beyond nanoparticle-filled polymers. *Chem Mater* 19, 2736-2751, doi:Doi 10.1021/Cm062693+ (2007).

16 Zhang, W. *et al.* The use of functionalized nanoparticles as non-specific compatibilizers for polymer blends. *Polym Advan Technol* 22, 65-71, doi:Doi 10.1002/Pat.1875 (2011).

17 Bubenhofer, S. B. *et al.* Large-Scale Synthesis of PbS-TiO2 Heterojunction Nanoparticles in a Single Step for Solar Cell Application. *J Phys Chem C* 116, 16264-16270, doi:Doi 10.1021/Jp3036814 (2012).

18 Buzea, C., Pacheco, II & Robbie, K. Nanomaterials and nanoparticles: sources and toxicity. *Biointerphases* 2, MR17-71 (2007).

19 Kumar, V. R. & Prasad, V. S. Synthesis, Characterization and Photocatalytic Activities of Ba2ybzro5.5 Nanoparticles under Solar Irradiation. *Nano* 6, 279-286, doi:Doi 10.1142/S1793292011002585 (2011).

20 Tsekouras, G. *et al.* Charge Transport in Dye-Sensitized Solar Cells Based on Flame-made TiO2 Nanoparticles. *Ieee J Sel Top Quant* 16, 1641-1648, doi:Doi 10.1109/Jstqe.2010.2049734 (2010).

21 Xiao, Q., Zhang, J., Xiao, C., Si, Z. C. & Tan, X. O. Solar photocatalytic degradation of methylene blue in carbon-doped TiO2 nanoparticles suspension. *Sol Energy* 82, 706-713, doi:Doi 10.1016/J.Solener.2008.02.006 (2008).

22 Calandra, P., Calogero, G., Sinopoli, A. & Gucciardi, P. G. Metal Nanoparticles and Carbon-Based Nanostructures as Advanced Materials for Cathode Application in Dye-Sensitized Solar Cells. *Int J Photoenergy*, doi:Artn 109495 Doi 10.1155/2010/109495 (2010).

23 Chen, X. H. *et al.* Ionic liquid-functionalized carbon nanoparticles-modified cathode for efficiency enhancement in polymer solar cells. *Appl Phys Lett* 95, doi:Artn 133305 Doi 10.1063/1.3237161 (2009).

24 Gong, F., Li, Z. Q., Wang, H. & Wang, Z. S. Enhanced electrocatalytic performance of graphene via incorporation of SiO2 nanoparticles for dye-sensitized solar cells. *J Mater Chem* 22, 17321-17327, doi:Doi 10.1039/C2jm33483f (2012).

25 Jia, R. R. *et al.* Synthesis of highly nitrogen-doped hollow carbon nanoparticles and their excellent electrocatalytic properties in dye-sensitized solar cells. *J Mater Chem* 20, 10829-10834, doi:Doi 10.1039/C0jm01799j (2010).

26 Kim, H. I., Moon, G. H., Monllor-Satoca, D., Park, Y. & Choi, W. Solar Photoconversion Using Graphene/TiO2 Composites: Nanographene Shell on TiO2 Core versus TiO2 Nanoparticles on Graphene Sheet. *J Phys Chem C* 116, 1535-1543, doi:Doi 10.1021/Jp209035e (2012).

27 Narayanan, R., Deepa, M. & Srivastava, A. K. Nanoscale connectivity in a TiO2/CdSe quantum dots/functionalized graphene oxide nanosheets/Au nanoparticles composite for enhanced photoelectrochemical solar cell performance. *Phys Chem Chem Phys* 14, 767-778, doi:Doi 10.1039/C1cp22548k (2012).

28 Sun, S. R., Gao, L. A., Liu, Y. Q. & Sun, J. Assembly of CdSe nanoparticles on graphene for low-temperature fabrication of quantum dot sensitized solar cell. *Appl Phys Lett* 98, doi:Artn 093112 Doi 10.1063/1.3558732 (2011).

29 Yen, M. Y. *et al.* Platinum nanoparticles/graphene composite catalyst as a novel composite counter electrode for high performance dye-sensitized solar cells. *J Mater Chem* 21, 12880-12888, doi:Doi 10.1039/C1jm11850a (2011).

30 Ghosh, P., Han, G., De, M., Kim, C. K. & Rotello, V. M. Gold nanoparticles in delivery applications. *Advanced drug delivery reviews* 60, 1307-1315, doi:10.1016/j.addr.2008.03.016 (2008).

31 Han, G., Ghosh, P. & Rotello, V. M. Multi-functional gold nanoparticles for drug delivery. *Advances in experimental medicine and biology* 620, 48-56 (2007).

32 Han, G., Ghosh, P. & Rotello, V. M. Functionalized gold nanoparticles for drug delivery. *Nanomedicine (Lond)* 2, 113-123, doi:10.2217/17435889.2.1.113 (2007).

33 Kim, C. K., Ghosh, P. & Rotello, V. M. Multimodal drug delivery using gold nanoparticles. *Nanoscale* 1, 61-67, doi:10.1039/b9nr00112c (2009).

34 Morimoto, Y. [Pulmonary toxicity of manufactured nanomaterials]. *Nihon eiseigaku zasshi. Japanese journal of hygiene* 67, 396-400 (2012).

35 Alder, B. J. & Wainwright, T. E. Studies in Molecular Dynamics .1. General Method. *J Chem Phys* 31, 459-466, doi:Doi 10.1063/1.1730376 (1959).

36 Hoover, W. G. Nonequilibrium Molecular Dynamics. *Annual Review of Physical Chemistry* 34, 103-127, doi:doi:10.1146/annurev.pc.34.100183.000535 (1983).

37 Buxton, G. A. & Balazs, A. C. Simulating the morphology and mechanical properties of filled diblock copolymers. *Phys Rev E* 67, -, doi:Artn 031802 Doi 10.1103/Physreve.67.031802 (2003).

38 Buxton, G. A., Lee, J. Y. & Balazs, A. C. Computer simulation of morphologies and optical properties of filled diblock copolymers. *Macromolecules* 36, 9631-9637, doi:Doi 10.1021/Ma034322+ (2003).

39 Lyatskaya, Y., Gersappe, D., Gross, N. A. & Balazs, A. C. Designing compatibilizers to reduce interfacial tension in polymer blends. *J Phys Chem-Us* 100, 1449-1458, doi:Doi 10.1021/Jp952422e (1996).

40 Li, S. Y., Niklasson, G. A. & Granqvist, C. G. Nanothermochromics: Calculations for VO2 nanoparticles in dielectric hosts show much improved luminous transmittance and solar energy transmittance modulation. *J Appl Phys* 108, doi:Artn 063525 Doi 10.1063/1.3487980 (2010).

41 Qin, Z. *et al.* Influences of low temperature thermal treatment on ZnO nanowire arrays and nanoparticles based flexible dye-sensitized solar cells. *Colloid Surface A* 402, 127-131, doi:Doi 10.1016/J.Colsurfa.2012.03.037 (2012).

42 Won, J. *et al.* Photothermal fixation of laser-trapped polymer microparticles on polymer substrates. *Appl Phys Lett* 75, 1506-1508, doi:Doi 10.1063/1.124737 (1999).

43 Buxton, G. A., Verberg, R., Jasnow, D. & Balazs, A. C. Newtonian fluid meets an elastic solid: Coupling lattice Boltzmann and lattice-spring models. *Phys Rev E* 71, -, doi:Artn 056707 Doi 10.1103/Physreve.71.056707 (2005).

44 Zeng, Q. H., Yu, A. B. & Lu, G. Q. Multiscale modeling and simulation of polymer nanocomposites. *Prog Polym Sci* 33, 191-269, doi:Doi 10.1016/J.Progpolymsci.2007.09.002 (2008).

Chapter 2

1 Nicholson, P. T. & Shaw, I. *Ancient Egyptian materials and technology*. (Cambridge University Press, 2000).

2 Hosler, D., Burkett, S. L. & Tarkanian, M. J. Prehistoric polymers: Rubber processing in ancient Mesoamerica. *Science* **284**, 1988-1991, doi:Doi 10.1126/Science.284.5422.1988 (1999).

3 Osswald, T. A. & Menges, G. *Materials science of polymers for engineers*. 2nd edn, (Hanser Publishers ; Cincinnati : Hanser Gardner Publications, 2003).

4 Flinn, R. A. & Trojan, P. K. *Engineering materials and their applications*. 2nd edn, (Houghton Mifflin, 1981).

5 Drexler, K. E., Peterson, C. & Pergamit, G. *Unbounding the future: the nanotechnology revolution*. (Morrow, 1991).

6 Abbasian, K., Rostami, A. & Pourkhorshidi, S. Design of Hybrid Solar Cell Based on Dye-Sensitized TiO2 Nanoparticles with Conjugated Polymer. *Acta Phys Pol A* **121**, 10-12 (2012).

7 Ghosh, P., Han, G., De, M., Kim, C. K. & Rotello, V. M. Gold nanoparticles in delivery applications. *Advanced drug delivery reviews* **60**, 1307-1315, doi:10.1016/j.addr.2008.03.016 (2008).

8 Bichler, O. *et al.* Functional Model of a Nanoparticle Organic Memory Transistor for Use as a Spiking Synapse. *Ieee T Electron Dev* **57**, 3115-3122, doi:Doi 10.1109/Ted.2010.2065951 (2010).

9 Goveas, J. L. & Fredrickson, G. H. Apparent slip at a polymer-polymer interface. *Eur Phys J B* **2**, 79-92 (1998).

10 Barsky, S. & Robbins, M. O. Molecular dynamics study of slip at the interface between immiscible polymers. *Phys Rev E* **6302**, -, doi:Artn 021801 (2001).

11 Narayanan, B., Pryamitsyn, V. A. & Ganesan, V. Interfacial phenomena in polymer blends: A self-consistent brownian dynamics study. *Macromolecules* **37**, 10180-10194, doi:Doi 10.1021/Ma048986a (2004).

12 Larson, R. G. *The structure and rheology of complex fluids*. (Oxford University Press, 1999).

13 Barsky, S. & Robbins, M. O. Bulk and interfacial shear thinning of immiscible polymers. *Phys Rev E* **65**, -, doi:Artn 021808 Doi 10.1103/Physreve.65.021808 (2002).

14 Utracki, L. A. Compatibilization of polymer blends. *The Canadian Journal of Chemical Engineering* **80**, 1008-1016 (2002).

15 Deanin, R. D. & Manion, M. A. Compatibilization of polymer blends. *PLASTICS ENGINEERING-NEW YORK*- **52**, 1-22 (1999).

16 Macosko, C. W. *et al.* Compatibilizers for melt blending: Premade block copolymers. *Macromolecules* **29**, 5590-5598 (1996).

17 Semenov, A. Microphase separation in diblock-copolymer melts: ordering of micelles. *Macromolecules* **22**, 2849-2851 (1989).

18 Bütün, V., Billingham, N. & Armes, S. Unusual aggregation behavior of a novel tertiary amine methacrylate-based diblock copolymer: formation of micelles and reverse micelles in aqueous solution. *J Am Chem Soc* **120**, 11818-11819 (1998).

19 Laun, H. M. *et al.* Rheological and Small-Angle Neutron-Scattering Investigation of Shear-Induced Particle Structures of Concentrated Polymer Dispersions Submitted to Plane Poiseuille and Couette-Flow. *J Rheol* **36**, 743-&, doi:Doi 10.1122/1.550314 (1992).

20 Sundararaj, U. & Macosko, C. W. Drop Breakup and Coalescence in Polymer Blends - the Effects of Concentration and Compatibilization. *Macromolecules* **28**, 2647-2657, doi:Doi 10.1021/Ma00112a009 (1995).

21 Tsai, S. C., Botts, D. & Plouff, J. Effects of Particle Properties on the Rheology of Concentrated Noncolloidal Suspensions. *J Rheol* **36**, 1291-1305, doi:Doi 10.1122/1.550260 (1992).

22 Tsagaropoulos, G. & Eisenberg, A. Direct Observation of 2 Glass Transitions in Silica-Filled Polymers - Implications for the Morphology of Random Ionomers. *Macromolecules* **28**, 396-398, doi:Doi 10.1021/Ma00105a059 (1995).

23 Schultz, A. J., Hall, C. K. & Genzer, J. Computer simulation of block copolymer/nanoparticle composites. *Macromolecules* **38**, 3007-3016, doi:Doi 10.1021/Ma0496910 (2005).

24 Koning, C., van Duin, M., Pagnoulle, C. & Jerome, R. Strategies for compatibilization of polymer blends. *Prog Polym Sci* **23**, 707-757, doi:Doi 10.1016/S0079-6700(97)00054-3 (1998).

25 Gubbels, F. *et al.* Design of Electrical Conductive Composites - Key Role of the Morphology on the Electrical-Properties of Carbon-Black Filled Polymer Blends. *Macromolecules* **28**, 1559-1566, doi:Doi 10.1021/Ma00109a030 (1995).

26 Beatty, C. L. Evidence of Interaction of Fillers with Matrix Polymers Via Transition Maps. *Polym Composite* **5**, 319-326, doi:Doi 10.1002/Pc.750050412 (1984).

27 Zhang, J. B., Cole, P. J., Nagpal, U., Macosko, C. W. & Lodge, T. P. Direct correlation between adhesion promotion and coupling reaction at immiscible polymer-polymer interfaces. *J Adhesion* **82**, 887-902, doi:Doi 10.1080/00218460600875847 (2006).

28 Si, M. *et al.* Compatibilizing bulk polymer blends by using organoclays. *Macromolecules* **39**, 4793-4801 (2006).

29 Hu, X. *et al.* Dynamics of Polymers in Organosilicate Nanocomposites. *Macromolecules* **36**, 823-829, doi:10.1021/ma020937f (2003).

30 Tang, H., Chen, X. F. & Luo, Y. X. Electrical and dynamic mechanical behavior of carbon black filled polymer composites. *Eur Polym J* **32**, 963-966, doi:Doi 10.1016/0014-3057(96)00026-2 (1996).

31 Thompson, C. M., Besuden, T. W. & Beumel, L. L. Resistivity of Rubber as a Function of Mold Pressure. *Rubber Chem Technol* **61**, 828-841, doi:Doi 10.5254/1.3536221 (1988).

32 Willey, S. J. & Macosko, C. W. Steady Shear Rheological Behavior of Pvc Plastisols. *J Rheol* **22**, 525-545, doi:Doi 10.1122/1.549487 (1978).

33 Alexandre, M. & Dubois, P. Polymer-layered silicate nanocomposites: preparation, properties and uses of a new class of materials. *Materials Science and Engineering: R: Reports* **28**, 1-63, doi:http://dx.doi.org/10.1016/S0927-796X(00)00012-7 (2000).

34 Chung, H., Ohno, K., Fukuda, T. & Composto, R. J. Self-regulated structures in nanocomposites by directed nanoparticle assembly. *Nano Lett* **5**, 1878-1882, doi:Doi 10.1021/Nl051079e (2005).

35 Buxton, G. A. & Balazs, A. C. Lattice spring model of filled polymers and nanocomposites. *J Chem Phys* **117**, 7649-7658, doi:Doi 10.1063/1.1509447 (2002).

36 Lipatov, Y. S. Polymer blends and interpenetrating polymer networks at the interface with solids. *Prog Polym Sci* **27**, 1721-1801 (2002).

37 Nesterov, A., Lipatov, Y. S. & Ignatova, T. Effect of an interface with solid on the component distribution in separated phases of binary polymer mixtures. *Eur Polym J* **37**, 281-285 (2001).

38 Lipatov, Y. S., Nesterov, A. E., Ignatova, T. D. & Nesterov, D. A. Effect of polymer-filler surface interactions on the phase separation in polymer blends. *Polymer* **43**, 875-880, doi:Doi 10.1016/S0032-3861(01)00632-2 (2002).

39 Nesterov, A. E. & Lipatov, Y. S. Compatibilizing effect of a filler in binary polymer mixtures. *Polymer* **40**, 1347-1349, doi:Doi 10.1016/S0032-3861(98)00277-8 (1999).

40 Lo, T. S., Mihajlovic, M., Shnidman, Y., Li, W. T. & Gersappe, D. Interfacial slip in sheared polymer blends. *Phys Rev E* **72**, -, doi:Artn 040801 Doi 10.1103/Physreve.72.040801 (2005).

41 Jaber, E., Luo, H. B., Li, W. T. & Gersappe, D. Network formation in polymer nanocomposites under shear. *Soft Matter* **7**, 3852-3860, doi:Doi 10.1039/C0sm00990c (2011).

42 Salaniwal, S., Kant, R., Colby, R. H. & Kumar, S. K. Computer simulations of local concentration variations in miscible polymer blends. *Macromolecules* **35**, 9211-9218, doi:Doi 10.1021/Ma020624k (2002).

43 Salaniwal, S., Kumar, S. K. & Douglas, J. F. Amorphous solidification in polymer-platelet nanocomposites. *Phys Rev Lett* **89**, doi:Artn 258301 Doi 10.1103/Physrevlett.89.258301 (2002).

44 Manias, E. *et al.* Intercalation kinetics of long polymers in 2 nm confinements. *Macromolecules* **33**, 7955-7966, doi:Doi 10.1021/Ma0009552 (2000).

45 Lyon, R. E. & Quintiere, J. G. Criteria for piloted ignition of combustible solids. *Combustion and Flame* **151**, 551-559, doi:http://dx.doi.org/10.1016/j.combustflame.2007.07.020 (2007).

46 Walters, R. N., Hackett, S. M. & Lyon, R. E. Heats of combustion of high temperature polymers. *Fire and materials* **24**, 245-252 (2000).

47 Mouritz, A. P. & Gibson, A. G. *Fire Properties of Polymer Composite Materials*. (Springer London, Limited, 2006).

48 Macskásy, H. & Palyi, G. *Plastics: Their Behaviour in Fires*. (Elsevier Science, 1991).

49 Hirschler, M. M. Fire hazard and toxic potency of the smoke from burning materials. *Journal of fire sciences* **5**, 289-307 (1987).

50 Nelson Gordon, L. in *Fire and Polymers II* Vol. 599 *ACS Symposium Series* Ch. 1, 1-26 (American Chemical Society, 1995).

51 Laoutid, F., Bonnaud, L., Alexandre, M., Lopez-Cuesta, J. M. & Dubois, P. New prospects in flame retardant polymer materials: From fundamentals to nanocomposites. *Materials Science and Engineering: R: Reports* **63**, 100-125, doi:http://dx.doi.org/10.1016/j.mser.2008.09.002 (2009).

52 Fereres, S., Lautenberger, C., Fernandez-Pello, A. C., Urban, D. L. & Ruff, G. A. Understanding ambient pressure effects on piloted ignition through numerical modeling. *Combustion and Flame* **159**, 3544-3553, doi:http://dx.doi.org/10.1016/j.combustflame.2012.08.006 (2012).

53 Blum, A. & Ames, B. N. Flame-Retardant Additives as Possible Cancer Hazards. *Science* **195**, 17-23, doi:Doi 10.1126/Science.831254 (1977).

54 Darnerud, P. O. Toxic effects of brominated flame retardants in man and in wildlife. *Environment International* **29**, 841-853, doi:http://dx.doi.org/10.1016/S0160-4120(03)00107-7 (2003).

55 Dhawan, A. & Sharma, V. Toxicity assessment of nanomaterials: methods and challenges. *Analytical and bioanalytical chemistry* **398**, 589-605, doi:10.1007/s00216-010-3996-x (2010).

56 Sharifi, S. *et al.* Toxicity of nanomaterials. *Chem Soc Rev* **41**, 2323-2343, doi:10.1039/c1cs15188f (2012).

57 Schrand, A. M., Dai, L., Schlager, J. J. & Hussain, S. M. Toxicity testing of nanomaterials. *Advances in experimental medicine and biology* **745**, 58-75, doi:10.1007/978-1-4614-3055-1_5 (2012).

58 Dhawan, A., Pandey, A. & Sharma, V. Toxicity assessment of engineered nanomaterials: resolving the challenges. *Journal of biomedical nanotechnology* **7**, 6-7 (2011).

59 Beyer, G. Nanocomposites — a new class of flame retardants. *Plastics, Additives and Compounding* **11**, 16-21, doi:http://dx.doi.org/10.1016/S1464-391X(09)70048-0 (2009).

60 Beyer, G. Nanocomposites: a new class of flame retardants for polymers. *Plastics, Additives and Compounding* **4**, 22-28, doi:http://dx.doi.org/10.1016/S1464-391X(02)80151-9 (2002).

61 Beyer, G. Flame retardant properties of EVA-nanocomposites and improvements by combination of nanofillers with aluminium trihydrate. *Fire and Materials* **25**, 193-197, doi:10.1002/fam.776 (2001).

62 Beyer, G. Short communication: Carbon nanotubes as flame retardants for polymers. *Fire and Materials* **26**, 291-293, doi:10.1002/fam.805 (2002).

63 Lewin, M. Reflections on migration of clay and structural changes in nanocomposites. *Polym Advan Technol* **17**, 758-763 (2006).

64 Zanetti, M., Kashiwagi, T., Falqui, L. & Camino, G. Cone calorimeter combustion and gasification studies of polymer layered silicate nanocomposites. *Chem Mater* **14**, 881-887 (2002).

65 Berber, S., Kwon, Y. K. & Tomanek, D. Unusually high thermal conductivity of carbon nanotubes. *Phys Rev Lett* **84**, 4613-4616, doi:Doi 10.1103/Physrevlett.84.4613 (2000).

66 Balandin, A. A. *et al.* Superior thermal conductivity of single-layer graphene. *Nano Lett* **8**, 902-907, doi:Doi 10.1021/Nl0731872 (2008).

67 Balandin, A. A., Shamsa, M., Liu, W. L., Casiraghi, C. & Ferrari, A. C. Thermal conductivity of ultrathin tetrahedral amorphous carbon films. *Appl Phys Lett* **93**, doi:Artn 043115 Doi 10.1063/1.2957041 (2008).

68 Shamsa, M. *et al.* Thermal conductivity of nitrogenated ultrananocrystalline diamond films on silicon. *J Appl Phys* **103**, doi:Artn 083538 Doi 10.1063/1.2907865 (2008).

69 Kashiwagi, T. *et al.* Relation between the viscoelastic and flammability properties of polymer nanocomposites. *Polymer* **49**, 4358-4368, doi:http://dx.doi.org/10.1016/j.polymer.2008.07.054 (2008).

70 Kashiwagi, T. *et al.* Flammability properties of polymer nanocomposites with single-walled carbon nanotubes: effects of nanotube dispersion and concentration. *Polymer* **46**, 471-481, doi:http://dx.doi.org/10.1016/j.polymer.2004.10.087 (2005).

71 Pack, S. *et al.* Segregation of Carbon Nanotubes/Organoclays Rendering Polymer Blends Self-Extinguishing. *Macromolecules* **42**, 6698-6709, doi:10.1021/ma900966k (2009).

Chapter 3

1 Haile, J. M. *Molecular Dynamics Simulation: Elementary Methods*. (Wiley, 1997).

2 Allen, P. & D. J. Tildesley, M. P. A. *Computer Simulation of Liquids*. (Clarendon Press, 1989).

3 Roe, R. J. & Chemistry, A. C. S. D. o. P. *Computer Simulation of Polymers*. (Prentice Hall, 1991).

4 Wilkins, M. L. *Computer Simulation of Dynamic Phenomena*. (Springer, 1999).

5 Mattson, T. G., Chemistry, A. C. S. D. o. C. i. & Meeting, A. C. S. *Parallel computing in computational chemistry*. (American Chemical Society, 1995).

6 Hoover, W. G. Nonequilibrium Molecular Dynamics. *Annual Review of Physical Chemistry* **34**, 103-127, doi:doi:10.1146/annurev.pc.34.100183.000535 (1983).

7 Huang, C., Li, C., Choi, P. Y. K., Nandakumar, K. & Kostiuk, L. W. Effect of cut-off distance used in molecular dynamics simulations on fluid properties. *Mol Simulat* **36**, 856-864, doi:10.1080/08927022.2010.489556 (2010).

8 Rapaport, D. C. *The Art of Molecular Dynamics Simulation*. (Cambridge University Press, 2004).

9 Verlet, L. Computer "Experiments" on Classical Fluids. I. Thermodynamical Properties of Lennard-Jones Molecules. *Physical Review* **159**, 98-103 (1967).

10 Gear, C. W. *Numerical initial value problems in ordinary differential equations*. (Prentice-Hall, 1971).

11 Nosé, S. A molecular dynamics method for simulations in the canonical ensemble. *Mol Phys* **52**, 255-268, doi:10.1080/00268978400101201 (1984).

12 Kremer, K. & Grest, G. S. Dynamics of Entangled Linear Polymer Melts - a Molecular-Dynamics Simulation. *J Chem Phys* **92**, 5057-5086 (1990).

13 Grest, G. S. & Kremer, K. Molecular dynamics simulation for polymers in the presence of a heat bath. *Phys Rev A* **33**, 3628-3631 (1986).

14 Larson, R. G. *The structure and rheology of complex fluids*. (Oxford University Press, 1999).

15 Grest, G. S., Lacasse, M. D., Kremer, K. & Gupta, A. M. Efficient continuum model for simulating polymer blends and copolymers. *J Chem Phys* **105**, 10583-10594 (1996).

16 Barsky, S. & Robbins, M. O. Bulk and interfacial shear thinning of immiscible polymers. *Phys Rev E* **65**, -, doi:Artn 021808 Doi 10.1103/Physreve.65.021808 (2002).

17 Barsky, S. & Robbins, M. O. Molecular dynamics study of slip at the interface between immiscible polymers. *Phys Rev E* **6302**, -, doi:Artn 021801 (2001).

18 Riess, G. Micellization of block copolymers. *Prog Polym Sci* **28**, 1107-1170, doi:http://dx.doi.org/10.1016/S0079-6700(03)00015-7 (2003).

19 Rodríguez-Hernández, J. & Lecommandoux, S. Reversible Inside−Out Micellization of pH-responsive and Water-Soluble Vesicles Based on Polypeptide Diblock Copolymers. *J Am Chem Soc* **127**, 2026-2027, doi:10.1021/ja043920g (2005).

20 Gohy, J.-F. in *Block Copolymers II* Vol. 190 *Advances in Polymer Science* (ed Volker Abetz) Ch. 48, 65-136 (Springer Berlin Heidelberg, 2005).

21 Brochard, F. & Degennes, P. G. Shear-Dependent Slippage at a Polymer Solid Interface. *Langmuir* **8**, 3033-3037, doi:Doi 10.1021/La00048a030 (1992).

22 Adhikari, N. P. & Goveas, J. L. Effects of slip on the viscosity of polymer melts. *J Polym Sci Pol Phys* **42**, 1888-1904, doi:Doi 10.1002/Polb.20066 (2004).

23 Li, W. *Modeling the Static and Dynamic Properties of Polymers at Interfaces*. (State University of New York at Stony Brook, 2001).

24 Jaber, E. *Rheology and dynamics in polymeric nano-composites*. (Stony Brook University, 2005).

25 Jaber, E., Luo, H. B., Li, W. T. & Gersappe, D. Network formation in polymer nanocomposites under shear. *Soft Matter* **7**, 3852-3860, doi:Doi 10.1039/C0sm00990c (2011).

26 Goveas, J. L. & Fredrickson, G. H. Apparent slip at a polymer-polymer interface. *Eur Phys J B* **2**, 79-92 (1998).

27 Macosko, C. W. *et al.* Compatibilizers for melt blending: Premade block copolymers. *Macromolecules* **29**, 5590-5598 (1996).

28 Winey, K. I., Patel, S. S., Larson, R. G. & Watanabe, H. Interdependence of Shear Deformations and Block Copolymer Morphology. *Macromolecules* **26**, 2542-2549 (1993).

29 Lee, E. C., Solomon, M. J. & Muller, S. J. Molecular orientation and deformation of polymer solutions under shear: A flow light scattering study. *Macromolecules* **30**, 7313-7321, doi:Doi 10.1021/Ma9706945 (1997).

30 Wilson, M. R. Molecular dynamics simulations of flexible liquid crystal molecules using a Gay-Berne/Lennard-Jones model. *J Chem Phys* **107**, 8654-8663 (1997).

Chapter 4

1 Larson, R. G. *The structure and rheology of complex fluids*. (Oxford University Press, 1999).

2 Leonov, A. I. A linear model of the stick-slip phenomena in polymer flow in rheometers. *Rheol Acta* **23**, 591-600, doi:10.1007/bf01438799 (1984).

3 Tanner, R. I. Partial Wall Slip in Polymer Flow. *Industrial & Engineering Chemistry Research* **33**, 2434-2436, doi:10.1021/ie00034a027 (1994).

4 Jaber, E. *Rheology and dynamics in polymeric nano-composites*. (Stony Brook University, 2005).

5 Grest, G. S., Lacasse, M. D., Kremer, K. & Gupta, A. M. Efficient continuum model for simulating polymer blends and copolymers. *J Chem Phys* **105**, 10583-10594 (1996).

6 Barsky, S. & Robbins, M. O. Bulk and interfacial shear thinning of immiscible polymers. *Phys Rev E* **65**, -, doi:Artn 021808Doi 10.1103/Physreve.65.021808 (2002).

7 Barsky, S. & Robbins, M. O. Molecular dynamics study of slip at the interface between immiscible polymers. *Phys Rev E* **6302**, -, doi:Artn 021801 (2001).

8 Humphrey, W., Dalke, A. & Schulten, K. VMD: Visual molecular dynamics. *J Mol Graph Model* **14**, 33-38, doi:Doi 10.1016/0263-7855(96)00018-5 (1996).

9 Adhikari, N. P. & Goveas, J. L. Effects of slip on the viscosity of polymer melts. *J Polym Sci Pol Phys* **42**, 1888-1904, doi:Doi 10.1002/Polb.20066 (2004).

10 Brochard, F. & Degennes, P. G. Shear-Dependent Slippage at a Polymer Solid Interface. *Langmuir* **8**, 3033-3037, doi:Doi 10.1021/La00048a030 (1992).

11 Jaber, E., Luo, H. B., Li, W. T. & Gersappe, D. Network formation in polymer nanocomposites under shear. *Soft Matter* **7**, 3852-3860, doi:Doi 10.1039/C0sm00990c (2011).

12 Gohy, J.-F. in *Block Copolymers II* Vol. 190 *Advances in Polymer Science* (ed Volker Abetz) Ch. 48, 65-136 (Springer Berlin Heidelberg, 2005).

13 Gnichwitz, J. F. *et al.* Efficient Synthetic Access to Cationic Dendrons and Their Application for ZnO Nanoparticles Surface Functionalization: New Building Blocks for Dye-Sensitized Solar Cells. *J Am Chem Soc* **132**, 17910-17920, doi:Doi 10.1021/Ja106076h (2010).

14 Riess, G. Micellization of block copolymers. *Prog Polym Sci* **28**, 1107-1170, doi:http://dx.doi.org/10.1016/S0079-6700(03)00015-7 (2003).

15 *A Textbook of Fluid Mechanics*. (Laxmi Publications Pvt Limited, 2005).

16 Beatty, C. L. Evidence of interaction of fillers with matrix polymers via transition maps. *Polym Composite* **5**, 319-326, doi:10.1002/pc.750050412 (1984).

17 Ilnytskyi, J. M. & Wilson, M. R. Molecular models in computer simulation of liquid crystals. *J Mol Liq* **92**, 21-28 (2001).

Chapter 5

1 Pappetti, F. & Succi, S. *An Introduction to Parallel Computational Fluid Dynamics*. (Nova Science Pub Incorporated, 1996).

2 Succi, S. *The Lattice-Boltzmann equation for fluid dynamics and beyond*. (Clarendon Press ; Oxford University Press, 2001).

3 Narasimhan, T. N. Fourier's heat conduction equation: History, influence, and connections (Reprinted from Reviews of Geophysics vol 37, pg 151-172, 1999). *P Indian as-Earth* **108**, 117-148 (1999).

4 Sukop, M. C. & Thorne, D. T. *Lattice-Boltzmann modeling : an introduction for geoscientists and engineers*. (Springer, 2006).

5 Nourgaliev, R., Dinh, T.-N., Theofanous, T. & Joseph, D. The Lattice-Boltzmann equation method: theoretical interpretation, numerics and implications. *International Journal of Multiphase Flow* **29**, 117-169 (2003).

6 He, X. Y., Shan, X. W. & Doolen, G. D. Discrete Boltzmann equation model for nonideal gases. *Phys Rev E* **57**, R13-R16, doi:Doi 10.1103/Physreve.57.R13 (1998).

7 Chen, S. & Doolen, G. D. Lattice-Boltzmann method for fluid flows. *Annu Rev Fluid Mech* **30**, 329-364, doi:Doi 10.1146/Annurev.Fluid.30.1.329 (1998).

8 Mcnamara, G. R. & Zanetti, G. Use of the Boltzmann-Equation to Simulate Lattice-Gas Automata. *Phys Rev Lett* **61**, 2332-2335, doi:Doi 10.1103/Physrevlett.61.2332 (1988).

9 He, X. Y. & Luo, L. S. Theory of the Lattice-Boltzmann method: From the Boltzmann equation to the Lattice-Boltzmann equation. *Phys Rev E* **56**, 6811-6817, doi:Doi 10.1103/Physreve.56.6811 (1997).

10 Qian, Y., d'Humieres, D. & Lallemand, P. Lattice BGK models for Navier-Stokes equation. *EPL (Europhysics Letters)* **17**, 479 (1992).

11 Chopard, B., Falcone, J. L. & Latt, J. The Lattice-Boltzmann advection-diffusion model revisited. *Eur Phys J-Spec Top* **171**, 245-249, doi:Doi 10.1140/Epjst/E2009-01035-5 (2009).

12 Guo, Z.-L., Shi, B.-C. & Wang, N.-C. Fully Lagrangian and Lattice-Boltzmann methods for the advection-diffusion equation. *Journal of scientific computing* **14**, 291-300 (1999).

13 Grama, A. *Introduction to Parallel Computing*. (ADDISON WESLEY Publishing Company Incorporated, 2003).

14 Barrett, B., Squyres, J. M., Lumsdaine, A., Graham, R. L. & Bosilca, G. Analysis of the component architecture overhead in open MPI. *Lect Notes Comput Sc* **3666**, 175-182 (2005).

15 M. Squyres, J. & Lumsdaine, A. in *Component Models and Systems for Grid Applications* (eds Vladimir Getov & Thilo Kielmann) Ch. 11, 167-185 (Springer US, 2005).

16 Palabos - Parallel Lattice Boltmann Solver (2009).

17 Stiebler, M., T, J., #246, lke & Krafczyk, M. Advection-diffusion Lattice-Boltzmann scheme for hierarchical grids. *Comput. Math. Appl.* **55**, 1576-1584, doi:10.1016/j.camwa.2007.08.024 (2008).

18 Stauffer, D. & Aharony, A. *Introduction to percolation theory*. 2nd edn, (Taylor & Francis, 1992).

19 Guo, Z. L., Shi, B. C. & Zheng, C. G. A coupled lattice BGK model for the Boussinesq equations. *Int J Numer Meth Fl* **39**, 325-342, doi:Doi 10.1002/Fld.337 (2002).